Theory of nuclear excitation by electron capture for heavy ions

Inaugural Dissertation
zur
Erlangung des Doktorgrades
der Naturwissenschaften
der Justus-Liebig-Universität Gießen
Fachbereich 07

vorgelegt von

Adriana Gagyi-Pálffy

aus Bukarest, Rumänien

Gießen 2006

Dekan: Prof. Dr. Volker Metag
1. Berichterstatter: Prof. Dr. Werner Scheid
2. Berichterstatter: Prof. Dr. Alfred Müller
Tag der mündlichen Prüfung:

Contents

Introduction

When Niels Bohr proposed in 1913 his first model of the atom, he depicted it as having a small and dense positively charged nucleus, surrounded by the orbiting electrons. The existence of the electron, a discrete unit of negative charge, had been proved in the cathode rays experiments performed by J. J. Thomson in 1897. However, it was the great interest attracted by radioactivity that engaged scientists in the quest for the microscopic world of the atom. The outcome of their scientific research established atomic and nuclear physics as new and interesting directions of study.

With the challenge of explaining theoretically the properties of nuclei and the increasing number of proposed models, nuclear and atomic physics developed further as separate fields. The investigation of the hyperfine structure of the atomic spectra has revealed several nuclear effects, such as the mass and field isotope shifts [Bre32, BK58], hyperfine splitting [GB29, Bre30] and nuclear polarization [PMGS89, PMGS91], which have been already subject of experimental and theoretical study for decades. In the same time, nuclear processes that actively involve atomic electrons such as β-decay and internal conversion have been encountered and investigated [GR58, Bla53]. However, atomic physics studies continue to be insensitive to the nuclear structure, up to the point that theoretical descriptions of atomic processes consider the nucleus as a point-like or extended positive charge without lacking in accuracy. The electrons in the atom have little regard for the internal structure of the nucleus. The nuclear transition energies are typically on the MeV scale, while the atomic processes take place at substantially lower energy values.

The question whether the match between the electronic and nuclear transition energies would allow for different interactions between the two systems has been inspiring physicists since the early 1970s. What if the nucleus and the electron would interact through the electromagnetic field and undergo transitions simultaneously? Such a process is already well-known in nuclear physics, as being sometimes the only decay channel for a nuclear excited state: the internal conversion (IC). An excited nucleus that for some reason cannot decay radiatively transfers its energy through the electromagnetic field to one of the atomic electrons which leaves the atom. The possible inverse mechanism in a laser-assisted environment was for the first time proposed in 1976 by Goldanskii and Namiot [GN76], who named it inverse internal electron conversion. However, in the following studies and publications this process was referred to as nuclear excitation by electron capture (NEEC). In the resonant process of NEEC, a free electron is captured into a bound shell of an ion with the simul-

taneous excitation of the nucleus. In terms of atomic physics, this process is the nuclear analogue of dielectronic recombination (DR), in which the place of the bound electron is taken by the nucleus. The excited nuclear state can in turn decay either by internal conversion, or by emitting a photon. The process of NEEC followed by the radiative decay of the nucleus is a rare electron recombination mechanism which competes with radiative recombination (RR) and DR. Although several attempts have been made [Mok89, Dau06], NEEC has not been observed experimentally yet.

Processes at the borderline between atomic and nuclear physics such as NEEC are of great interest, as they offer the possibility to explore the spectral properties of heavy nuclei through atomic physics experiments. Experimental techniques developed for scattering studies of electron recombination with atomic ions - for instance, with stored or trapped ions - can be applied to gain information about the nuclear structure of several nuclides, that is hardly accessible by nuclear scattering experiments. The high precision of atomic spectroscopy nowadays and the possibility of direct measurements are valuable considering the accuracy of present nuclear data. If confirmed experimentally, NEEC could allow the determination of nuclear transition energies, reduced nuclear transition probabilities and the study of atomic vacancy effects on nuclear lifetime and population mechanisms of excited nuclear levels.

The few theoretical studies concerning the magnitude of the NEEC cross sections were mainly focused on the cases of nuclear excitation in plasmas or in solid targets. The possible mechanisms of nuclear excitation in plasmas were the subject of a more recent work [HC99], which calculates the NEEC rates for the excitation of the nuclear isomeric state of $^{235}_{92}$U, using relativistic hydrogenic wave functions for the electrons. These estimates have been reconsidered in the study of non-radiative triggering of long-lived nuclear isomers [ZC02]. The possibility of NEEC occurring for bare ions channeling through single crystals has been investigated non-relativistically in several studies [CPR89, Cue89, KBC91, YK93]. In [CPR89, Cue89] the NEEC cross sections are estimated by scaling DR results, considering that the two processes differ only in the excitation part. The authors of Ref. [KBC91] apply a similar scaling procedure using experimental nuclear data rather than atomic data. None of these studies take into account the decay of the nuclear excited state following NEEC.

Aim and motivation of this thesis

It is the aim of this thesis to study the resonant process of NEEC theoretically and to provide candidate isotopes and transitions suitable for experimental observation in the near future. As the high-precision atomic spectroscopy has been experiencing much progress in the last years, similar processes that involve both the atomic shells and the nucleus, such as the nuclear excitation by electron transition (NEET) [KYS$^+$00] and bound internal conversion (BIC) [CHA$^+$00], have been experimentally confirmed in 2000. In the resonant process of NEET, an electron undergoes a transition between two bound states in an ion with the

simultaneous excitation of the nucleus. This rare nuclear excitation mechanism was proposed for the first time by Morita in 1973 [Mor73]. Its inverse process, the bound internal conversion, in which an excited nucleus decays with the simultaneous excitation of the electron to a bound orbital of the ion, has been suggested by the authors of [AAC$^+$95] in 1995 in order to explain a discrepancy in the experimental data while studying the influence of the electronic environment on nuclear decay processes. The experimental observation of both NEET and BIC has been source of much enthusiasm and brought these rare electron-nucleus interactions again into the interest of the community. Nevertheless, from the theoretical point of view NEEC lacks a proper relativistic description suitable for future experiments in storage rings or electron beam ion traps.

Another important motivating factor is the similarity between NEEC and DR, that has been one of the subjects of interest in the theoretical and experimental groups in Gießen in the last fifteen years. The theoretical formalism developed by Zimmerer [ZGS90, Zim92] and further by Zimmermann [ZGS97] for DR provides a good starting point for the study of NEEC. The presence of the nucleus has to be embedded into the formalism by using a nuclear model. Quantum interference between DR and RR has also been subject of theoretical investigation [ZGS97], offering the possibility to extend the approach for other resonant channels of photo recombination, such as NEEC. Other subjects related to DR such as the angular distribution of the emitted radiation [GGS98, Zak01], as well as the resonant electron scattering on the double-excited electronic state [Kol98] and the role of the electron-electron interaction [Har04] were considered. The effects of the nuclear charge distribution upon the total cross section of DR were theoretically investigated by the authors of [SHSG04], followed by the experimental isotope shifts measurements reported in [BKM$^+$06]. With the storage rings which opened the possibility for experiments with heavy highly-charged ions up to bare Uranium, the experimental group in Gießen was involved in several projects concerning DR in relativistic few-electron systems [SML$^+$92, BBH$^+$02, BKM$^+$03]. The DR resonances were also used for precise measurements of the Lamb shift in several Li-like ions, thus testing QED in strong fields.

Contents of this thesis

In this work we consider the process of NEEC followed by the radiative decay of the excited nucleus. Together with RR and DR, NEEC can be regarded as one of the resonant channels of photo recombination. In Chapter 1, we discuss the possible electron recombination mechanisms and derive the total cross section for the two-step process of NEEC. We present a Feshbach projection formalism that allows a clear separation of the direct and resonant contributions in the total cross section of photo recombination. The resonant part can be written in terms of the NEEC rate, that accounts for the nuclear excitation, and the radiative rate that characterizes the nuclear decay.

The evaluation of the NEEC rate requires the consideration of an adequate nuclear model. The collective model used, as well as the calculation of the

NEEC rates for electric and magnetic transitions are presented in Chapter 2. Numerically, we consider collision systems that involve electric $E2$ and magnetic $M1$ transitions. The studied nuclei have low-lying energy levels corresponding to the first nuclear excited state, that allow the nuclear excitation by electron capture into the K shell or L shell of the ion. Values for the NEEC transition rates and total cross sections are presented in Chapter 3, together with a discussion about the possible experimental observation of the process.

As the initial and final states of RR and NEEC followed by the radiative decay of the nuclear excited states are the same, the two processes are indistinguishable. Quantum interference may occur and the magnitude of this effect can be important for the observation of NEEC, particularly since RR acts a strong background in any recombination experiment. The theoretical calculation of the interference term in the total cross section, as well as numerical results for the studied collision systems are presented in Chapter 4. The study of the angular distribution of the emitted photons in the recombination process can provide additional means of discerning between RR and NEEC. In Chapter 5 we give a short review of the density matrix formalism used to calculate the asymmetry parameters and the angular distribution of the photons emitted in the radiative $E2$ decay of the nuclear state. Numerical results for the capture of the electron into the K shell of several bare ions are presented. The results of our study and an outlook over the possible future interests are discussed in the final Summary and Outlook.

Chapter 1

Theory of electron recombination

A free electron can be captured into the bound state of a highly-charged ion. When followed by the emission of a photon, this process is called photo recombination (PR) and can be split into non-resonant and resonant channels. The direct, non-resonant process is the radiative recombination of the electron, where a photon is subsequently emitted by the system. RR plays an important role in plasma physics, in particular for the spectroscopic analysis of fusion plasmas and also occurs as an important background in traps or in collisions involving highly-charged ions. As one of the basic processes in non-relativistic as well as relativistic collisions, RR has been the subject of many theoretical calculations, concerning both total cross sections for capture into bare ions [IE00] or few-electron ions [TN03], as well as angular differential cross sections of the emitted photons [FSS05]. Higher quantum electrodynamics (QED) corrections [SYBE00] and the role of electron-electron interactions [YSBE00] have also been investigated.

If the free electron is captured into an atomic shell in the presence of another bound electron, dielectronic recombination may occur. DR is a resonant channel of PR. The continuum electron is captured with the simultaneous excitation of the bound electron in the ion. In the second step the resulting double-excited state decays radiatively. This resonant recombination mechanism was first proposed by Massey and Bates in 1942 [MB42] and it is believed to be the dominant one in hot astrophysical plasmas. Since the beginning of the 1980s non-relativistic theories of DR have been developed [Hah85], followed by extensions for relativistic processes, that include the contribution of the Breit interaction to the capture rate [ZGS90, Zim92]. The quantum interference of the DR and RR channels and the interference of different resonant DR pathways [Sha94], as well as the role of electron-electron interaction [Har04] have been subject of theoretical investigation. The angular distribution of the emitted photons has also been considered by several authors [CS95, GGS98, Zak01].

Nuclear excitation by electron capture is the nuclear physics analogue of DR, in which the place of the bound electron is taken by the nucleus. If the electronic and nuclear energy levels match, the recombination can take place with the

simultaneous excitation of the nucleus, as shown schematically in Figure 1.1. The nuclear excited state decays then radiatively or can carry out an internal conversion. In contrast to DR, NEEC can also occur in bare ions, as the presence of a bound electron is not required.

Since it has been proposed for the first time in 1976, NEEC has been the subject of several theoretical studies involving recombination in plasmas [HC99] or in solid targets [CPR89, Cue89, KBC91, YK93]. When followed by the radiative decay of the nucleus, this rare recombination mechanism can be considered as another resonant channel of PR. The nuclear decay via internal conversion can also be interesting for studying resonant electron scattering on the nucleus. In the case of DR, resonant electron scattering on the double-excited electronic state has been considered in [Kol98].

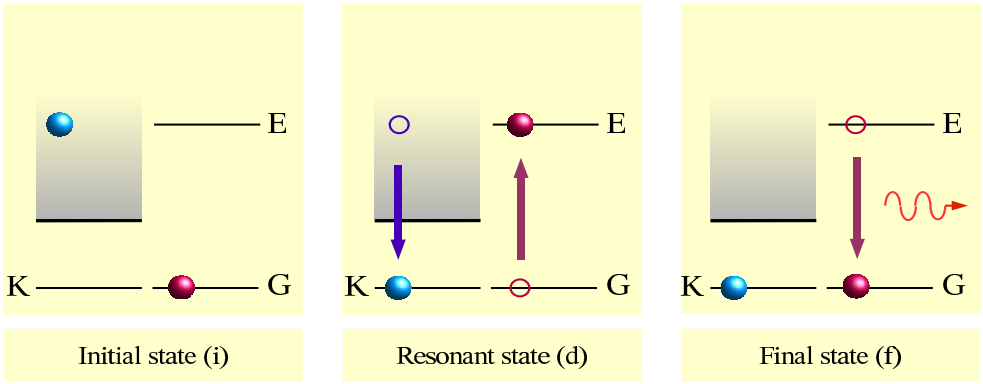

Figure 1.1: NEEC recombination mechanism of a continuum electron into the K shell of a bare ion, followed by the radiative decay of the nucleus. The left-hand side of each frame depicts the electronic transition. On the right-hand side the nucleus is schematically represented as undergoing the transition from the ground state (G) to the excited state (E) and then back to the ground state.

In this chapter we present a versatile formalism for describing theoretically the processes contributing to PR, including the NEEC recombination mechanism. We extend the formalism developed by Zimmerer [ZGS90, Zim92] for DR and RR, by taking into account the interaction of electronic and nuclear degrees of freedom. Zimmerer has used the perturbation expansion of the transition operator to treat the direct and resonant contributions of PR. The subspaces corresponding to the initial, intermediate and final states of the system were separated using a Feshbach projection operator formalism, used already by Haan and Jacobs [HJ89] for DR. This approach has been further developed by Zimmermann [ZGS97] to study interference effects between DR and RR. Considering the analogy between NEEC and DR, the projection formalism can be used to account for an intermediate excited state that concerns the nucleus instead of the bound electron. As in practice it is difficult to find a system in which DR and NEEC can occur simultaneously at the same energy, we focus in this work on the recombination process involving only the interference between RR and NEEC. For simplicity we consider that the electron is captured

into the bound state in the Coulomb field of a bare nucleus or of He-like ions with a closed-shell $1s^2$ configuration. We regard the capture into a closed-shell configuration as a one-electron problem, without the participation of the K-shell electrons. We also consider that the emitted photon corresponds to the radiative decay of the nuclear excited state. The perturbation expansion of the transition operator is used to derive the expression of the total PR cross section. Following the outline published in [PHS06], we focus in this chapter on the calculation of the NEEC transition amplitude, while the detailed study of the interference effects between NEEC and RR is presented separately in Chapter 4. Atomic units ($m_e = \hbar = e = 1$) are used throughout this work, unless otherwise specified.

1.1 Decomposition of the Fock space by means of projection operators

The initial state $|\Psi_i\rangle$ of the system consisting of the nucleus in its ground state, the free electron, and the vacuum state of the electromagnetic field can be written as a direct product of the nuclear, electronic, and photonic state vectors:

$$|\Psi_i\rangle = |NI_iM_i, \vec{p}m_s, 0\rangle \equiv |NI_iM_i\rangle \otimes |\vec{p}m_s\rangle \otimes |0\rangle \,. \tag{1.1}$$

Here, $\vec{p}$ is the asymptotic momentum of the electron and m_s its spin projection. As we consider only a one-electron problem, we omit describing the closed-shell configuration electrons in the case of electron capture into He-like ions. The nuclear ground state N is denoted by the total angular momentum I_i and its projection M_i. The state $|\Psi_d\rangle$ formed by the resonant capture has the form

$$|\Psi_d\rangle = |N^*I_dM_d, n_d\kappa_dm_d, 0\rangle \equiv |N^*I_dM_d\rangle \otimes |n_d\kappa_dm_d\rangle \otimes |0\rangle \,, \tag{1.2}$$

with n_d, κ_d, and m_d being the principal quantum number, Dirac angular momentum number, and magnetic quantum number of the bound one-electron state, respectively. The excited nuclear state is denoted by N^*. The final state $|\Psi_f\rangle$ of the NEEC process contains the emitted photon and the nucleus which is again in its ground state N. Rather than using the plane wave expansion for the electromagnetic field, it is more convenient in this case to consider photons of a given angular momentum and parity. The final state can be written as

$$|\Psi_f\rangle = |NI_fM_f, n_d\kappa_dm_d, \lambda kLM\rangle \equiv |NI_fM_f\rangle \otimes |n_d\kappa_dm_d\rangle \otimes |\lambda kLM\rangle \,. \tag{1.3}$$

The emitted photon has the wave number k, the total angular momentum L and its projection M. Furthermore, λ stands for electric (e) or magnetic (m) waves. The photonic state can be written as

$$|\lambda kLM\rangle = a^\dagger_{\lambda kLM}|0\rangle \,, \tag{1.4}$$

where $a^\dagger_{\lambda kLM}$ is the photon creation operator. The corresponding conjugate annihilation operator is denoted by $a_{\lambda kLM}$.

To clearly separate these states in the perturbative expansion of the transition operator, we introduce operators projecting onto the individual subspaces. Characterizing the state of the electron in the positive part of the continuous spectrum by the energy ε rather than the momentum of the free electron, we write the projector P belonging to the first type of subspace as

$$P = \int d\varepsilon \sum_{\alpha} |\alpha\varepsilon\rangle\langle\alpha\varepsilon| \ . \tag{1.5}$$

For brevity we introduce the multi-index α to stand for all discrete quantum numbers of the total system. The projection operator of the subspace spanned by intermediate states of the type (1.2) is written as

$$Q = \sum_{q} |q\rangle\langle q| \ , \tag{1.6}$$

with the cumulative index q introduced again to summarize all discrete quantum numbers describing the bound electron and the excited nucleus. The subspace of the state vectors containing one transverse photon is associated with the projection operator

$$R = \sum_{r} \sum_{\lambda kLM} a^{\dagger}_{\lambda kLM} |r\rangle\langle r| a_{\lambda kLM} \ , \tag{1.7}$$

where with r we denote the quantum numbers describing the nucleus in the final state and the bound electron. Assuming that the corrections due to two- or more-photon states [ZSG04] and due to the presence of the negative electronic continuum are negligible, we postulate the following completeness relation:

$$P + Q + R = \mathbf{1} \ , \tag{1.8}$$

where $\mathbf{1}$ is the unity operator of the Fock space.

1.2 The total Hamiltonian of the system

The total Hamiltonian operator for the system consisting of the nucleus, the electron, and the radiation field can be written as

$$H = H_n + H_e + H_r + H_{en} + H_{er} + H_{nr} \, . \tag{1.9}$$

We describe the nucleus using a suitable collective model. When considering nuclei with even numbers of protons and neutrons, the Hamiltonian of the nucleus H_n can be written in terms of creation and annihilation operators of the collective modes, $\beta^{\dagger}_{\ell m}$ and $\beta_{\ell m}$,

$$H_n = \sum_{\ell m} \omega_{\ell} \left(\beta^{\dagger}_{\ell m} \beta_{\ell m} + \frac{1}{2} \right) \ . \tag{1.10}$$

Here, ω_{ℓ} are the phonon frequencies. The applied nuclear collective model and the derivation of the nuclear Hamiltonian H_n are presented in Section 2.1. The Dirac Hamiltonian of the free electron is given by

$$H_e = c\vec{\alpha} \cdot \vec{p} + (\beta - 1)c^2 \ , \tag{1.11}$$

where $\vec{\alpha}$ is the vector of the Dirac α matrices $(\alpha_x, \alpha_y, \alpha_z)$ and $\vec{p}$ is the electron momentum. The pure quantized radiation field is described by

$$H_r = \sum_{\lambda kLM} \omega_k a^\dagger_{\lambda kLM} a_{\lambda kLM} \ . \tag{1.12}$$

Interactions between the three subsystems are given by the three remaining Hamiltonians in Eq. (1.9). We adopt the Coulomb gauge for the electron-nucleus interaction because it allows the separation of the dominant Coulomb attraction between the electronic and the nuclear degrees of freedom,

$$H_{en} = \int d^3 r_n \frac{\rho_n(\vec{r}_n)}{|\vec{r}_e - \vec{r}_n|} \ . \tag{1.13}$$

In the above equation $\rho_n(\vec{r}_n)$ is the nuclear charge density, $\vec{r}_n$ denotes the nuclear coordinate and $\vec{r}_e$ the electronic coordinate. The integration is performed over the whole nuclear volume. The interaction of the electron with the transverse photon field quantized in the volume of a sphere with radius R is given by

$$H_{er} = -\vec{\alpha} \cdot \vec{A} = \sum_{\lambda kLM} \left(a^\dagger_{\lambda kLM} \vec{\alpha} \cdot \vec{A}_{\lambda kLM}(\vec{r}) + \text{H.c.} \right) \ , \tag{1.14}$$

with the vector potential of the electromagnetic field [RS80]

$$\vec{A}(\vec{r}) = \sum_{\lambda kLM} \left(\vec{A}_{\lambda kLM}(\vec{r}) a^\dagger_{\lambda kLM} + \vec{A}^*_{\lambda kLM}(\vec{r}) a_{\lambda kLM} \right) \ . \tag{1.15}$$

Here, the two independent solutions of the wave equation for the $\vec{A}_{\lambda kLM}(\vec{r})$ are

$$\begin{aligned} \vec{A}_{(m)kLM}(\vec{r}) &= \sqrt{\frac{4\pi ck}{R}} j_L(kr) \vec{Y}^M_{LL}(\theta, \varphi) \\ \vec{A}_{(e)kLM}(\vec{r}) &= \frac{i}{k} \sqrt{\frac{4\pi ck}{R}} \nabla \times \left(j_L(kr) \vec{Y}^M_{LL}(\theta, \varphi) \right) \ , \end{aligned} \tag{1.16}$$

where the quantum number k is discretized by requiring the proper boundary conditions at a perfectly conducting sphere of radius R. The $\vec{Y}^M_{LL}(\theta, \varphi)$ denote the vector spherical harmonics defined as [Edm96]

$$\vec{Y}^M_{JL}(\theta, \varphi) = \sum_\nu \sum_q C(L\ 1\ J; \nu\ q\ M) Y_{L\nu}(\theta, \varphi) \vec{\epsilon}_q \ , \tag{1.17}$$

where $q = 0, \pm 1$ and the spherical vectors $\vec{\epsilon}_q$ are given by

$$\begin{aligned} \vec{\epsilon}_+ &= -\frac{1}{\sqrt{2}} (\vec{e}_x + i\vec{e}_y) \ , \\ \vec{\epsilon}_0 &= \vec{e}_z \ , \\ \vec{\epsilon}_- &= \frac{1}{\sqrt{2}} (\vec{e}_x - i\vec{e}_y) \ . \end{aligned} \tag{1.18}$$

Similarly, the interaction of the nucleus with the electromagnetic field is given by the Hamiltonian

$$H_{nr} = -\frac{1}{c} \sum_{\lambda kLM} \left(a^\dagger_{\lambda kLM} \int d^3 r_n \vec{j}_n(\vec{r}_n) \cdot \vec{A}_{\lambda kLM}(\vec{r}_n) + \text{H.c.} \right) \ , \tag{1.19}$$

where $\vec{j}_n(\vec{r}_n)$ is the nuclear current.

Using the projection operators we can separate the perturbation part in the Hamiltonian,

$$H = H_0 + V \tag{1.20}$$

with

$$H_0 = PHP + QHQ + RHR \ , \tag{1.21}$$

$$\begin{aligned} V \equiv H - H_0 \ &= \ PHQ + QHP + PHR + RHP \\ &\quad + RHQ + QHR . \end{aligned} \tag{1.22}$$

In this way the effect of the nuclear potential on bound and continuum electron states is included to all orders. The individual terms in the perturbation V describe transitions between the different subspaces. For example, PHQ describes the internal conversion and QHP accounts for its time-reversed process, the nuclear excitation by electron capture. PHR and RHP are the lowest-order operators for photo-ionization and radiative recombination, respectively. QHR and RHQ account for the radiative excitation of the nucleus and radiative decay of the nucleus or of the electron in a bound state.

1.3 Perturbation expansion of the transition operator

The transition operator is defined as

$$T(z) = V + VG(z)V \ , \tag{1.23}$$

where $G(z)$ is the Green operator of the system given by

$$G(z) = (z - H)^{-1} \ . \tag{1.24}$$

Here, z is a complex energy variable. The cross section for a process can be expressed by the transition operator, after summing over the final states and averaging over the initial states that are not resolved in the experiment as

$$\begin{aligned} \sigma_{i\to f}(E) \ &= \ \frac{2\pi}{F_i} \sum_{M_f m_d} \sum_{M} \frac{1}{2(2I_i+1)} \sum_{M_i m_s} \frac{1}{4\pi} \\ &\quad \times \int d\Omega_{\vec{p}} \lim_{\epsilon \to 0+} |\langle \Psi_f | T(E + i\epsilon) | \Psi_i \rangle|^2 \rho_f \ , \end{aligned} \tag{1.25}$$

with Ψ_f and Ψ_i as final and initial eigenstates of H_0 given in Eqs. (1.3) and (1.1), respectively. F_i denotes the flux of the incoming electrons, ρ_f the density of the final photonic states, and $\Omega_{\vec{p}}$ is the direction of the incoming free electron.

We use the Lippmann-Schwinger equation to write the perturbation series for $T(z)$ in powers of V with the Green function $G_0(z)$ of the unperturbed Hamiltonian H_0:

$$T(z) = V + VG_0(z)V + VG_0(z)VG_0(z)V + \dots \ . \tag{1.26}$$

Since the initial state of the PR process is by definition an eigenstate of P, and the final state is an eigenstate of R, we consider the projection RTP of the transition operator:

$$\begin{aligned} RTP &= RVP + RVG_0VP + RVG_0VG_0VP \\ &\quad + RVG_0VG_0VG_0VP + \ldots \end{aligned} \tag{1.27}$$

Here and in the following we omit the argument z. The first term in Eq. (1.27) accounts for the direct process of RR. The higher-order terms in the expansion have to be taken into consideration to describe the resonant process. By introducing the unity operator of the Fock space $\mathbf{1} = P + Q + R$ in the expression of the second term RVG_0VP we obtain

$$\begin{aligned} RVG_0VP &= RV(P+Q+R)G_0(P+Q+R)VP \\ &= RVQG_0QVP = RH_{nr}QG_0QH_{en}P \ . \end{aligned} \tag{1.28}$$

Inserting the spectral resolution (1.6) of Q and using the expression (1.24) for the Green function we arrive at

$$\langle \Psi_f | RTP | \Psi_i \rangle = \sum_q \frac{\langle \Psi_f | H_{nr} | q \rangle \langle q | H_{en} | \Psi_i \rangle}{z - E_q^0} \ . \tag{1.29}$$

The energy E_q^0 denotes the unperturbed eigenvalue of the state $|q\rangle$. If we continue analyzing the perturbation expansion (1.27), the third order term in V can be written as

$$\begin{aligned} RVG_0VG_0VP &= RH_{er}PG_0PH_{en}QG_0QH_{en}P \\ &\quad + RH_{er}PG_0PH_{er}RG_0RH_{er}P \\ &\quad + RHQG_0QHRG_0RH_{er}P \ . \end{aligned} \tag{1.30}$$

The first two terms do not contribute to the cross section of the considered NEEC process. The last term is decomposed as

$$\begin{aligned} RHQG_0QHRG_0RH_{er}P &= RH_{er}QG_0QH_{er}RG_0RH_{er}P \\ &\quad + RH_{er}QG_0QH_{nr}RG_0RH_{er}P \\ &\quad + RH_{nr}QG_0QH_{er}RG_0RH_{er}P \\ &\quad + RH_{nr}QG_0QH_{nr}RG_0RH_{er}P \ . \end{aligned} \tag{1.31}$$

Here, the first two terms are not considered, as they are a negligible correction to the transition amplitude of RR. While the interaction Hamiltonian H_{er} does not act on the subspace projected by Q, the process incorporated in the third term of (1.31) is not possible. From the remaining last term, the part $QH_{nr}RG_0RH_{er}P$ accounts for the capture of the free electron by exchanging a virtual transverse photon with the nucleus. Following the calculation presented in Appendix A, this term can be approximated by $QH_{magn}P$, where

$$H_{magn} = -\frac{1}{c}\vec{\alpha} \int d^3r_n \frac{\vec{j}_n(\vec{r}_n)}{|\vec{r} - \vec{r}_n|} = -\vec{\alpha} \cdot \vec{A}(\vec{r}) \tag{1.32}$$

is the magnetic interaction Hamiltonian. Here, $\vec{A}(\vec{r})$ is the vector potential of the magnetic field generated by the nuclear current.

We continue the expansion (1.27) of the T operator and consider only the terms that contain $QH_{en}P$ as the first step and $RH_{nr}Q$ as the final step. The contribution of order V^4 can be decomposed as

$$\begin{aligned} RVG_0VG_0VG_0VP = RH_{nr}QG_0QH_{ne}PG_0PH_{ne}QG_0QH_{ne}P \\ +RH_{nr}QG_0Q(H_{er}+H_{nr})RG_0R(H_{er}+H_{nr})QG_0QH_{ne}P \ . \end{aligned} \tag{1.33}$$

The first term can be rewritten as

$$\begin{aligned} &RH_{nr}QG_0QH_{ne}PG_0PH_{ne}QG_0QH_{ne}P = \\ &\sum_{q,q'} RH_{nr}QG_0|q\rangle\langle q|H_{ne}PG_0PH_{ne}|q'\rangle\langle q'|G_0QH_{ne}P \ . \end{aligned} \tag{1.34}$$

We adopt the so-called isolated resonance approximation by taking only the diagonal matrix elements into account. This approximation is valid if the distance between neighboring resonances is large with respect to their total natural widths, which is the case in all systems we study. The diagonal matrix element reads

$$\langle q|H_{ne}PG_0PH_{ne}|q\rangle = \int d\varepsilon \sum_\alpha \frac{\langle q|H_{ne}|\alpha\varepsilon\rangle\langle\alpha\varepsilon|H_{ne}|q\rangle}{z-E^0} \ , \tag{1.35}$$

with E^0 defined by $H_0|\alpha E^0\rangle = E^0|\alpha E^0\rangle$. Using the equality

$$\lim_{\epsilon\to 0_+} \frac{1}{x+i\epsilon} = \mathcal{P}\left(\frac{1}{x}\right) - i\pi\delta(x) \ , \tag{1.36}$$

it can be further decomposed into

$$\int d\varepsilon \sum_\alpha \frac{\langle q|H_{ne}|\alpha\varepsilon\rangle\langle\alpha\varepsilon|H_{ne}|q\rangle}{z-E^0} = \Delta E_q^{\rm NP} - \frac{i}{2}\Gamma_q^{\rm IC} \ , \tag{1.37}$$

with

$$\Delta E_q^{\rm NP} \equiv \mathcal{P}\int d\varepsilon \sum_\alpha \frac{\langle q|H_{ne}|\alpha\varepsilon\rangle\langle\alpha\varepsilon|H_{ne}|q\rangle}{z-E^0} \ , \tag{1.38}$$

$$\Gamma_q^{\rm IC} \equiv 2\pi \sum_\alpha \left|\langle q|H_{ne}|\alpha E^0\rangle\right|^2 \ . \tag{1.39}$$

The notation $\Delta E_q^{\rm NP}$ was introduced to denote the Coulomb nuclear polarization correction to the energy of the state q and $\Gamma_q^{\rm IC}$ for its internal conversion width. $\mathcal{P}$ denotes the principal value of the integral.

The second term of (1.33) can be analyzed in a similar manner. We can separate it into the following four parts:

$$\begin{aligned} &RH_{nr}QG_0Q(H_{er}+H_{nr})RG_0R(H_{er}+H_{nr})QG_0QH_{ne}P = \\ &RH_{nr}QG_0QH_{er}RG_0RH_{er}QG_0QH_{ne}P \\ &+RH_{nr}QG_0QH_{nr}RG_0RH_{nr}QG_0QH_{ne}P \\ &+RH_{nr}QG_0QH_{er}RG_0RH_{nr}QG_0QH_{ne}P \\ &+RH_{nr}QG_0QH_{nr}RG_0RH_{er}QG_0QH_{ne}P \ . \end{aligned} \tag{1.40}$$

The first term contains the emission and reabsorption of a photon by the electron recombined into the bound state. Its diagonal matrix element has a real and an imaginary part:

$$\langle q|H_{er}RG_0RH_{er}|q\rangle = \Delta E_q^{\mathrm{SE}} - \frac{i}{2}\Gamma_q^{\mathrm{e,rad}}\,. \tag{1.41}$$

ΔE_q^{SE} describes the one-loop self-energy correction to the bound state energy of the electron. The imaginary part which is the radiative decay rate of the electronic state vanishes in the case of electron capture into the ground state of the ion. The second term in (1.40) contains the emission and a subsequent reabsorption of a virtual photon by the nucleus, and its diagonal matrix element reads

$$\langle q|H_{nr}RG_0RH_{nr}|q\rangle = \Delta E_q^{\mathrm{NSE}} - \frac{i}{2}\Gamma_q^{\mathrm{n,rad}}\,. \tag{1.42}$$

Here, $\Delta E_q^{\mathrm{NSE}}$ is the nuclear self energy correction to the energy of the ion, and $\Gamma_q^{\mathrm{n,rad}}$ stands for the radiative decay width of the nucleus in the state q. The last two terms of (1.40) incorporate corrections to the intermediate state energy due to the exchange of a virtual transverse photon between the electronic and the nuclear currents. These corrections are neglected in our treatment as they are expected to be far less than the overall accuracy of experimental nuclear excitation energies.

Continuing the expansion (1.27) of the T operator, the matrix element of the intermediate state Green operator in fourth order contains terms of the form

$$\langle q|H_iG_0H_iG_0H_iG_0H_i|q\rangle = \sum_{q'}\frac{\langle q|H_iG_0H_i|q'\rangle\langle q'|H_iG_0H_i|q\rangle}{z-E_{q'}}\,, \tag{1.43}$$

where the label i stands for ne, er and nr. The isolated resonances approximation is equivalent to considering $q = q'$ in Eq. (1.43). Higher-order terms can be summed then as a geometric progression

$$\frac{1}{z-E_q^0}\sum_{k=0}^{\infty}x^k = \frac{1}{z-E_q^0}\frac{1}{1-x} \tag{1.44}$$

with the dimensionless quotient

$$x = \frac{1}{z-E_q^0}\Big(\langle q|H_{ne}PG_0PH_{ne}|q\rangle + \langle q|H_{er}RG_0RH_{er}|q\rangle + \langle q|H_{nr}RG_0RH_{nr}|q\rangle\Big) \tag{1.45}$$

resulting in

$$G(z) = \frac{1}{z-E_q^0-\Delta E_q^{\mathrm{NP}}-\Delta E_q^{\mathrm{SE}}-\Delta E_q^{\mathrm{NSE}}+\frac{i}{2}\Gamma_q^{\mathrm{IC}}+\frac{i}{2}\Gamma_q^{\mathrm{n,rad}}+\frac{i}{2}\Gamma_q^{\mathrm{e,rad}}}\,. \tag{1.46}$$

Thus, the infinite perturbation expansion introduces energy corrections and widths into the energy denominator of the lowest order amplitude (1.29). When

considering many-electron systems, corrections due to the Breit interaction between the electronic currents also come into play. The final expression for the transition amplitude of NEEC into the intermediate states d and followed by radiative nuclear decay is then

$$\langle \Psi_f | RT(z) P | \Psi_i \rangle = \sum_d \frac{\langle \Psi_f | H_{nr} | \Psi_d \rangle \langle \Psi_d | H_{en} + H_{magn} | \Psi_i \rangle}{z - E_d^0 - \Delta E_d + \frac{i}{2}\Gamma_d} \ . \tag{1.47}$$

Here we introduce the notation $\Delta E_d = \Delta E_d^{\rm NP} + \Delta E_d^{\rm SE} + \Delta E_d^{\rm NSE}$ for the energy correction and $\Gamma_d = \Gamma_d^{\rm IC} + \Gamma_d^{\rm n,rad} + \Gamma_d^{\rm e,rad}$ for the total natural width of the excited state $|d\rangle = |N^* I_d M_d, n_d \kappa_d m_d, 0\rangle$.

1.4 Total cross section for NEEC

Eq. (1.25) gives the total cross section in terms of the matrix element of the projected T-operator. Neglecting the interference of neighboring resonances, and taking into account only a single intermediate state d for NEEC, with the corresponding magnetic substates M_d, the cross section for the considered PR process is

$$\sigma_{i\to f}(E) = \frac{2\pi}{F_i} \sum_{M_f m_d} \sum_{M} \frac{1}{2(2I_i+1)} \sum_{M_i m_s} \frac{1}{4\pi} \int d\Omega_{\vec{p}} \tag{1.48}$$
$$\times \left| \sum_{M_d} \frac{\langle \Psi_f | H_{nr} | \Psi_d \rangle}{(E - E_d) + \frac{i}{2}\Gamma_d} \langle \Psi_d | H_{en} + H_{magn} | \Psi_i \rangle + \langle \Psi_f | H_{er} | \Psi_i \rangle \right|^2 \rho_f \ .$$

We denote the corrected energy of the intermediate state by

$$E_d = E_d^0 + \Delta E_d = E_d^0 + \Delta E_d^{\rm NP} + \Delta E_d^{\rm SE} + \Delta E_d^{\rm NSE} \ . \tag{1.49}$$

In the actual calculations we neglect the corrections $\Delta E_d^{\rm NP}$ and $\Delta E_d^{\rm NSE}$. The total cross section in Eq. (1.49) accounts for the recombination process consisting of RR and a given reaction pathway $i \to d \to f$ of NEEC. As the initial and the final states for the direct and resonant channels coincide, the total cross section includes also a third term accounting for quantum interference between the two processes. We investigate in the following the NEEC total cross section term, resuming the calculation of the RR and interference terms in Chapter 4. The NEEC total cross section can be written as

$$\sigma_{i\to d\to f}(E) = \frac{2\pi}{F_i} \sum_{M_f m_d} \sum_{M M_d} \frac{1}{2(2I_i+1)} \sum_{M_i m_s} \frac{1}{2I_d+1} \sum_{M_d'} \frac{1}{4\pi} \int d\Omega_{\vec{p}}$$
$$\times \frac{\left| \langle N I_f M_f, n_d \kappa_d m_d, \lambda k L M | H_{nr} | N^* I_d M_d, n_d \kappa_d m_d, 0 \rangle \right|^2}{(E - E_d)^2 + \frac{\Gamma_d^2}{4}}$$
$$\times \left| \langle N^* I_d M_d, n_d \kappa_d m_d, 0 | H_{en} + H_{magn} | N I_i M_i, \vec{p} m_s, 0 \rangle \right|^2 \rho_f \ . \tag{1.50}$$

We introduce the notations

$$Y_n^{i\to d} = \frac{2\pi}{2(2I_i+1)} \sum_{M_i m_s} \sum_{M_d m_d} \times \int d\Omega_{\vec{p}} \left| \langle N^* I_d M_d, n_d \kappa_d m_d, 0 | H_{en} + H_{magn} | N I_i M_i, \vec{p} m_s, 0 \rangle \right|^2 \rho_i \quad (1.51)$$

for the electron capture rate and

$$A_r^{d\to f} = \frac{2\pi}{2I_d+1} \sum_{M_f M} \sum_{M_d} \times \left| \langle N I_f M_f, n_d \kappa_d m_d, \lambda k L M | H_{nr} | N^* I_d M_d, n_d \kappa_d m_d, 0 \rangle \right|^2 \rho_f \quad (1.52)$$

for the radiative transition rate. Here, ρ_i is the density of the initial electronic continuum states. The product between the flux of the incoming electrons F_i and the density of the initial electronic states ρ_i does not depend on the normalization of the continuum wave functions [Zim92],

$$F_i \rho_i = \frac{p^2}{(2\pi)^3} \ . \quad (1.53)$$

Introducing the notation

$$L_d(E - E_d) = \frac{\Gamma_d / 2\pi}{(E-E_d)^2 + \frac{1}{4}\Gamma_d^2} \quad (1.54)$$

for the normalized Lorentz profile, the cross section formula can be written in the condensed form

$$\sigma_{i\to d\to f}(E) = \frac{2\pi^2}{p^2} \frac{A_r^{d\to f} Y_n^{i\to d}}{\Gamma_d} L_d(E - E_d) \, . \quad (1.55)$$

The integration of the cross section over the continuum electron energy gives the resonance strength S_d for a given recombined state d,

$$S_d = \int dE \ \frac{2\pi^2}{p^2} \frac{A_r^{d\to f} Y_n^{i\to d}}{\Gamma_d} L_d(E - E_d) \ . \quad (1.56)$$

The natural width Γ_d of the nuclear excited state is of the order of $10^{-5} - 10^{-8}$ eV. In this interval the value of the electron momentum p as well as of the NEEC rate $Y_n^{i\to d}$ can be considered constant. As the Lorentz profile is normalized to unity,

$$\int dE \ L_d(E - E_d) = 1 \ , \quad (1.57)$$

the resonance strength can be written as

$$S_d = \frac{2\pi^2}{p^2} \frac{A_r^{d\to f} Y_n^{i\to d}}{\Gamma_d} \ . \quad (1.58)$$

Determining the total cross section of the NEEC process requires the calculation of the transition rates $Y_n^{i\to d}$ and $A_r^{d\to f}$, and the initial and final state energies for the electronic and nuclear transitions. The derivation of the NEEC rates in the framework of nuclear collective models is presented in the following chapter.

Chapter 2

Theory of nuclear excitation by electron capture

In the resonant process of NEEC, the electron transfers its energy and momentum to the nucleus which undergoes a transition from the ground state to an excited state. The theoretical treatment of the nuclear transition mechanism transcends the field of atomic physics and requires the use of an appropriate nuclear model. In order to describe the nuclear states we use for simplicity a collective model which allows the separation of the electronic and nuclear parts in the expression of the NEEC rate. A short review of the nuclear collective model is presented in the first section of this chapter, followed by the calculation of the NEEC rates for electric and magnetic transitions in Sections 2.2 and 2.3, respectively.

2.1 Nuclear model

The phenomenological collective model of the nucleus has as underlying physical picture the classical charged liquid drop [RS80, GM96]. The liquid drop model was historically the first one proposed as an explanation of the different properties of the nucleus. In this approach the interior structure (i.e. the existence of the individual nucleons) is neglected in favor of the picture of a homogeneous fluid-like nuclear matter. Obviously, the model of the liquid drop is applicable only if the size of the nucleon can be neglected with respect to the size of the nucleus as a whole, as it happens in the case of heavy nuclei. For low-lying levels the compression of nuclear matter is not considered, as it requires higher excitation energy, and the thickness of the nuclear surface layer is also neglected. We consider therefore a liquid drop of constant density and with a sharp surface. Because of their simplicity, collective models are used to describe the intrinsic nuclear dynamics in atomic processes such as nuclear polarization [PMGS89, PMGS91, YHHI01].

The excitation spectra of the even-even nuclei in the energy range up to 2 MeV show characteristic band structures in the case of deformed nuclei that are interpreted as vibrations and rotations of the nuclear surface, or vibrational multiplets in the case of spherical nuclei. The even-even nuclei have usually a

low-lying 2^+ first excited state, which is characterized by a strong electric $E2$ transition to the ground state. We use the notation I^π to label the nuclear state, where π is the parity quantum number and I is the total angular momentum of the nucleus. The nuclear surface of such nuclei can be parameterized as

$$R(\theta,\varphi,t) = R_0\Big(1+\sum_{\ell=0}^{\infty}\sum_{m=-\ell}^{\ell}\alpha^*_{\ell m}(t)Y_{\ell m}(\theta,\varphi)\Big), \tag{2.1}$$

where the time-dependent amplitudes $\alpha_{\ell m}(t)$ describe the deviations of the nuclear surface with respect to the sphere of radius R_0 and thus serve as collective coordinates. The excitations of the spherical nucleus produce small oscillations around the spherical equilibrium shape. The shapes of the multipole deformations $\ell = 2,3,4$ of nuclei are illustrated in Figure 2.1.

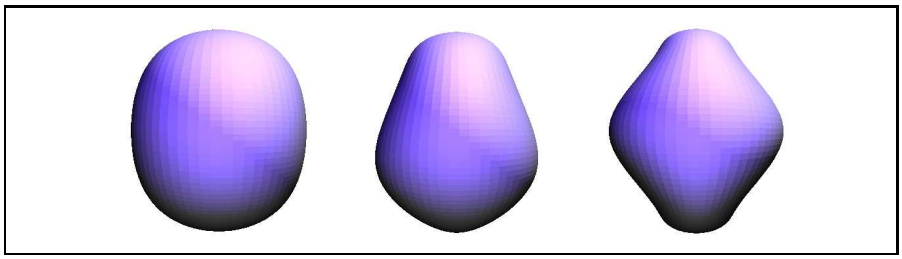

Figure 2.1: Quadrupole, octupole and hexadecupole deformations of a nucleus. The figures are not scaled correctly with respect to each other. The nuclear volume should be constant for all the cases.

The most important collective excitation of the nucleus is the quadrupole one. Indeed, the monopole deformation, for which ℓ=0, accounts for a change in radius of the nuclear sphere, as the spherical harmonic $Y_{00}(\theta,\varphi)$ is constant. The associated excitation is called the breathing-mode of the nucleus. Because of the large amount of energy needed for the compression of the nuclear matter, this mode is not in the energy range of NEEC. On the other hand, the dipole deformations correspond to a shift of the mass-center of the nucleus. This translation of the nucleus is disregarded for nuclear excitations.

In the harmonic approximation for the vibrations around the spherical equilibrium shape the collective dynamics of the nuclear surface is described by the Hamiltonian H_n [GM96]

$$H_n = T + V = \frac{1}{2}\sum_{\ell m}\frac{1}{B_\ell}|\pi_{\ell m}|^2 + \frac{1}{2}\sum_{\ell m}C_\ell|\alpha_{\ell m}|^2 \ , \tag{2.2}$$

where $\pi_{\ell m} = B_\ell\dot{\alpha}^\dagger_{\ell m}$ are the conjugate momenta to the collective coordinates α_{lm}. Here B_ℓ and C_ℓ stand for the inertia and the stiffness parameters, respectively. The dynamical evolution of the Heisenberg operators $\alpha_{\ell m}$ is given by

$$\begin{aligned}\alpha_{\ell m}(t) &= e^{iH_nt}\alpha_{\ell m}(0)e^{-iH_nt} \ , \\ \dot{\alpha}_{\ell m}(t) &= i[H_n,\alpha_{\ell m}(t)] \ ,\end{aligned} \tag{2.3}$$

which implies the time dependence

$$\alpha_{\ell m}(t) = \alpha_{\ell m}(0) e^{-i\omega_\ell t} \tag{2.4}$$

for the free shape oscillations. The frequency ω_ℓ of the nuclear collective modes, called *phonons* in analogy to the quanta of vibrations in solids, can be written in terms of the inertia and stiffness parameters,

$$\omega_\ell = \left(\frac{C_\ell}{B_\ell}\right)^{\frac{1}{2}} \ . \tag{2.5}$$

The operators $\alpha_{\ell m}$ and $\pi_{\ell m}$ are related to the phonon creation (annihilation) operators $\beta^\dagger_{\ell m}$ ($\beta_{\ell m}$) via a canonical transformation

$$\beta^\dagger_{\ell m} = \sqrt{\frac{\omega_\ell B_\ell}{2}} \left(\alpha_{\ell m} - \frac{i}{\omega_\ell B_\ell}\pi^\dagger_{\ell m}\right) \ . \tag{2.6}$$

The collective Hamiltonian H_n can then be written using the creation and annihilation operators for the collective modes,

$$H_n = \sum_{\ell m} \omega_\ell \left(\beta^\dagger_{\ell m}\beta_{\ell m} + \frac{1}{2}\right) \ , \tag{2.7}$$

yielding the expression that has already been introduced in Eq. (1.10).

The pure liquid drop has a stable equilibrium only for spherical surfaces. However, it can happen as a consequence of shell effects that the potential V in the collective Hamiltonian (2.2) has minima at finite non-vanishing values of $\alpha_{\ell m}$. In this case the nucleus has a stable ground state deformation. The nuclear excitations are described by rotations of the deformed nucleus. For nuclei that exhibit a static deformation, it is more convenient to introduce the variables describing the nuclear shape in the intrinsic frame, which together with the three Euler angles Ω are used as collective dynamical coordinates. For the quadrupole modes we have

$$\alpha_{2m} = D^2_{m0}(\Omega) a_{20} + \left(D^2_{m2}(\Omega) + D^2_{m-2}(\Omega)\right) a_{22} \ , \tag{2.8}$$

where a_{20} indicates the stretching of the z axis with respect to the x and y axes in the intrinsic frame and $a_{22} = a_{2-2}$ determines the difference in length between the x and y axes. The Euler angles Ω determine the orientation of the intrinsic frame with respect to the laboratory-fixed frame. The dynamical variables a_{20} and a_{22} can be replaced by the shape defining parameters β and γ, which correspond to something like polar coordinates in the space (a_{20},a_{22}), defined as [RS80]

$$\begin{aligned} a_{20} &= \beta\cos\gamma \ , \\ a_{22} &= \frac{1}{\sqrt{2}}\beta\sin\gamma \ . \end{aligned} \tag{2.9}$$

In terms on β, γ and the set of Euler angles Ω the collective Hamiltonian can be written as

$$\begin{aligned} H_{coll} &= -\frac{1}{2B_2}\left[\frac{1}{\beta^2}\frac{\partial}{\partial\beta}\left(\beta^4\frac{\partial}{\partial\beta}\right)+\frac{1}{\beta^2\sin 3\gamma}\frac{\partial}{\partial\gamma}\left(\sin 3\gamma\frac{\partial}{\partial\gamma}\right)\right] \\ &\quad +T_{rot}+V(\beta,\gamma)\ , \end{aligned} \tag{2.10}$$

where the rotational energy is

$$T_{rot}=\frac{I_1^2}{2\Im_1}+\frac{I_2^2}{2\Im_2}+\frac{I_3^2}{2\Im_3}\ . \tag{2.11}$$

The operators I_k are the projections of the total angular momentum $\vec{I}$ represented in the Euler angles onto the body-fixed axes. The quantities $\Im_k$ are functions of β and γ given by

$$\Im_k=4B_2\beta^2\sin^2\left(\gamma-\frac{2\pi}{3}k\right), \qquad k=1,2,3\ . \tag{2.12}$$

When the deformations β,γ are fixed, T_{rot} corresponds to the kinetic energy of a rotor with the moment of inertia $\Im_k$. The majority of deformed nuclei present well-pronounced minima of V for finite values $\beta_0\approx 0.2-0.3$ and $\gamma_0=0$. In this case the lowest 2^+ state is described only by the rotation Hamiltonian

$$T_{rot}=\frac{\vec{I}^2}{2\Im_0}\ , \tag{2.13}$$

where $\Im_0$ corresponds to the moment of inertia with respect to the first two axes, $\Im_0=\Im_1(\beta_0,0)=\Im_2(\beta_0,0)$. The energy eigenvalues corresponding to the above Hamiltonian are

$$E_{rot}=\frac{I(I+1)}{2\Im_0}\ , \tag{2.14}$$

which give the rotational bands in the spectrum of deformed nuclei.

The Coulomb interaction Hamiltonian H_{en} in Eq. (1.13), which accounts for the electric excitations of the nucleus by electron capture, depends on the nuclear charge density $\rho_n(\vec{r},t)$. A formula for $\rho_n(\vec{r},t)$ can be derived with the aid of the surface parameterization (2.1), requiring that the charge is always homogeneously distributed in the nucleus. The density operator can then be written as

$$\rho_n(\vec{r},t)=\rho_0\Theta\left(R(\theta,\varphi,t)-r\right)\ , \tag{2.15}$$

with the constant charge density of the undeformed nucleus given by $\rho_0=\frac{3Z}{4\pi R_0^3}$. By introducing the surface parameterization in the above equation and performing a Taylor expansion of the Heaviside function around R_0 we obtain

$$\rho_n(\vec{r})=\rho_0\Theta(R_0-r)+\rho_0\delta(R_0-r)R_0\sum_{\ell m}\alpha^*_{\ell m}Y_{\ell m}(\theta,\varphi)+\dots\ . \tag{2.16}$$

We omit here and in the following the time dependence of the collective coordinates. As the vibration amplitudes of the nuclear surface are supposed to be

small, we neglect the terms in a higher order in the collective coordinates $\alpha_{\ell m}$. The nuclear charge density can be written as a sum of two terms,

$$\rho_n(\vec{r}) = \rho_{\rm st}(\vec{r}) + \rho_{\rm exc}(\vec{r}) \ . \tag{2.17}$$

The first term $\rho_{\rm st} = \rho_0 \Theta(R_0 - r)$ in the above equation is the static one and corresponds to the nucleus in its ground state. The second term is characterizing the nuclear excitation and enters the expression of the interaction Hamiltonian H_{en} in Eq. (1.13),

$$\rho_{\rm exc}(\vec{r}) = \rho_0 \delta(R_0 - r) R_0 \sum_{\ell m} \alpha^*_{\ell m} Y_{\ell m}(\theta, \varphi) \ . \tag{2.18}$$

Taking into account the expression of the nuclear charge density above, the interaction Hamiltonian H_{en} can be written as

$$H_{en} = \rho_0 R_0 \sum_{\ell m} \alpha^*_{\ell m} \int d^3 r_n \frac{\delta(R_0 - r_n) Y_{\ell m}(\theta_n, \varphi_n)}{|\vec{r}_e - \vec{r}_n|} \ . \tag{2.19}$$

It is more convenient to express the collective coordinates $\alpha_{\ell m}$ in terms of the spherical components of the electric multipole transition moment $Q_{\ell m}$, defined as [RS80]

$$Q_{\ell m} = \int d^3 r r^\ell Y_{\ell m}(\theta, \varphi) \rho_{\rm exc}(\vec{r}) \ . \tag{2.20}$$

Introducing the nuclear charge density from Eq. (2.18) in the above expression we obtain a useful relation between the collective coordinates and the electric multipole transition moment,

$$Q_{\ell m} = \int d^3 r r^\ell Y_{\ell m}(\theta, \varphi) \rho_0 \delta(R_0 - r) R_0 \sum_{\lambda \mu} \alpha^*_{\lambda \mu} Y_{\lambda \mu}(\theta, \varphi) = \rho_0 R_0^{\ell+1} \alpha_{\ell m} \ . \tag{2.21}$$

The interaction Hamiltonian H_{en} that accounts for the electric transitions of the nucleus then yields

$$H_{en} = \sum_{\ell m} \frac{Q_{\ell m}}{R_0^\ell} \int d^3 r_n \frac{\delta(R_0 - r_n) Y^*_{\ell m}(\theta_n, \varphi_n)}{|\vec{r}_e - \vec{r}_n|} \ . \tag{2.22}$$

Starting from this expression, we derive in Section 2.2 the NEEC rates for electric $E2$ excitations of even-even vibrator nuclei.

The isoscalar dynamical shape oscillations described by the collective coordinates $\alpha_{\ell m}$ do not account for magnetic excitations of the nucleus. Indeed, even-even nuclei do not have low-lying levels which can be connected with the ground state by magnetic transitions. From the theoretical point of view, we show in Appendix B that the magnetic multipole moment is zero in the first order in the collective coordinates $\alpha_{\ell m}$. The magnetic transitions that occur between nuclear states with non-zero total angular momentum I are modeled by rotations of deformed shapes.

The interaction Hamiltonian H_{magn} that accounts for magnetic excitations of the nucleus due to electron capture is given by

$$H_{magn} = -\vec{\alpha} \cdot \vec{A}(\vec{r}) \ . \tag{2.23}$$

We choose for the vector potential the expression developed by Schwartz [Sch55] by means of the vector spherical harmonics, so that the interaction Hamiltonian can be written as

$$H_{magn} = -\vec{\alpha}\cdot\vec{A} = -\frac{1}{c}\sum_{LM}\frac{4\pi}{2L+1}\vec{\alpha}\cdot\vec{Y}^{M*}_{LL}(\theta_e,\varphi_e) \times\int d^3r_n\frac{r_<^L}{r_>^{L+1}}\vec{j}_n(\vec{r}_n)\cdot\vec{Y}^{M}_{LL}(\theta_n,\varphi_n)\ . \quad (2.24)$$

The notations $r_<$ and $r_>$ stand for the smaller and the larger of the two radii r_e and r_n, respectively. In order to avoid deriving the expression of the nuclear current $\vec{j}_n(\vec{r}_n)$ in the collective model, we consider in the following a simple assumption regarding the system composed from the nucleus and the electron. We make the approximation that the electron does not enter the nucleus, namely that the electronic radial coordinate $r_e > r_n$ is always larger than the nuclear radial coordinate. Although this is not an exact treatment of the system, the approximation is not expected to affect drastically the results of the considered transitions [ABH$^+$56, GR58, Sch55]. Assuming that the electron does not enter the nucleus is equivalent to considering $r_< = r_n$ and $r_> = r_e$. The interaction Hamiltonian is then

$$H_{magn} = -\frac{1}{c}\sum_{LM}\frac{4\pi}{2L+1}\vec{\alpha}\cdot\vec{Y}^{M*}_{LL}(\theta_e,\varphi_e)r_e^{-(L+1)} \times\int d^3r_n r_n^L\vec{j}_n(\vec{r}_n)\cdot\vec{Y}^{M}_{LL}(\theta_n,\varphi_n)\ . \quad (2.25)$$

The nuclear coordinate integral in the above formula occurs also in the expression of the magnetic multipole moment, as defined in [Sch55]

$$M_{\ell m} = -\frac{i}{c}\sqrt{\frac{\ell}{\ell+1}}\int d^3r_n r_n^\ell\vec{Y}^m_{\ell\ell}(\theta_n,\varphi_n)\cdot\vec{j}_n(\vec{r}_n)\ . \quad (2.26)$$

The nuclear part in the Hamiltonian H_{magn} can thus be written in terms of the magnetic multipole moment,

$$H_{magn} = -i\sum_{LM}\frac{4\pi}{2L+1}\sqrt{\frac{L+1}{L}}r_e^{-(L+1)}M_{LM}\vec{\alpha}\cdot\vec{Y}^{M*}_{LL}(\theta_e,\varphi_e)\ . \quad (2.27)$$

This form of the interaction Hamiltonian simplifies considerably the calculation of the NEEC rates for magnetic transitions, which is the subject of Section 2.3.

We have used the collective nuclear model to express the interaction Hamiltonians with the help of the nuclear multipole moments. The nuclear matrix elements that are needed in the calculation of the NEEC rates

$$\langle N^* I_d M_d|Q_{\ell m}(M_{\ell m})|NI_iM_i\rangle \quad (2.28)$$

can be expressed with the help of the reduced nuclear transition probabilities,

$$B(E(M)\ell, I_i\to I_d) = \frac{1}{2I_i+1}|\langle N^*I_d\|Q_\ell(M_\ell)\|NI_i\rangle|^2\ . \quad (2.29)$$

We avoid the further use of the nuclear collective model for constructing the nuclear wave functions by taking experimental values for the reduced transition probabilities. These values contain the information about the nuclear states. The calculation of the electronic and nuclear parts in the NEEC rates for electric and magnetic transitions is the subject of the next two sections.

2.2 NEEC rates for electric transitions

For NEEC involving electric transitions, the rate Y_n (see 1.51) of the process is related to the matrix element of the Coulomb interaction Hamiltonian (2.22),

$$Y_n^{i\to d} = \frac{2\pi}{2(2I_i+1)} \sum_{M_i m_s} \sum_{M_d m_d} \times \int d\Omega_p \left|\langle N^* I_d M_d, n_d \kappa_d m_d, 0 | H_{en} | N I_i M_i, \vec{p} m_s, 0\rangle\right|^2 \rho_i \ . \tag{2.30}$$

In the calculation of the matrix element, we use the multipole expansion

$$\frac{1}{|\vec{r}_e - \vec{r}_n|} = \sum_{L=0}^{\infty} \sum_{M=-L}^{L} \frac{4\pi}{2L+1} Y_{LM}(\theta_n, \varphi_n) Y^*_{LM}(\theta_e, \varphi_e) \frac{r_<^L}{r_>^{L+1}} \ . \tag{2.31}$$

The notations $r_<$ and $r_>$ stand again for the smaller and the larger of the two radii r_e and r_n, respectively. The integration over the angular nuclear coordinate brings us to the following expression for the Coulomb interaction Hamiltonian,

$$H_{en} = \sum_{LM} \frac{4\pi}{2L+1} \frac{Q_{LM}}{R_0^L} Y^*_{LM}(\theta_e, \varphi_e) \int_0^\infty dr_n r_n^2 \frac{r_<^L}{r_>^{L+1}} \delta(R_0 - r_n) \ . \tag{2.32}$$

The matrix element of the Hamiltonian reads

$$\begin{aligned} (H_{en})_{di} &= \frac{1}{R_0^L} \sum_{LM} \frac{4\pi}{2L+1} \langle N^* I_d M_d | Q_{LM} | N I_i M_i \rangle \\ &\quad \times \langle n_d \kappa_d m_d | Y^*_{LM}(\theta_e, \varphi_e) \int_0^\infty dr_n r_n^2 \frac{r_<^L}{r_>^{L+1}} \delta(R_0 - r_n) | \vec{p} m_s \rangle \ . \end{aligned} \tag{2.33}$$

We write the matrix element of the electron-nucleus interaction Hamiltonian as a product of the nuclear and electronic parts. It is more convenient to use the reduced matrix element of the electric multipole operator Q_{LM}, defined as [Edm96]

$$\begin{aligned} \langle N^* I_d M_d | Q_{LM} | N I_i M_i \rangle &= \frac{(-1)^{I_i - M_i}}{\sqrt{2L+1}} C(I_d \ I_i \ L; M_d \ -M_i \ M) \\ &\quad \times \langle N^* I_d \| Q_{LM} \| N I_i \rangle \ . \end{aligned} \tag{2.34}$$

Here $C(I_d \ I_i \ L; M_d \ -M_i \ M)$ stands for the Clebsch-Gordan coefficient. The modulus squared of the reduced nuclear matrix element of the electric multipole operator can be related to the reduced transition probability of a certain

multipolarity L,

$$B(EL, I_i \to I_d) = \frac{1}{2I_i + 1} |\langle N^* I_d \| Q_L \| N I_i \rangle|^2 \ , \tag{2.35}$$

whose value can be taken from experimental results. In order to evaluate the electronic matrix element we expand the initial continuum electronic wave function in partial waves [EM95],

$$|\vec{p} m_s\rangle = \sum_{\kappa m} i^l e^{i\Delta_\kappa} \sum_{m_l} Y^*_{l m_l}(\theta_{\vec{p}}, \varphi_{\vec{p}}) C \left(l \ \frac{1}{2} \ j; m_l \ m_s \ m \right) |\varepsilon \kappa m\rangle \ , \tag{2.36}$$

where ε is the energy of the continuum electron measured from the ionization threshold, $\varepsilon = \sqrt{p^2c^2 + c^4} - c^2$. The orbital and total angular momenta of the partial wave are denoted by l, with its corresponding magnetic quantum number m_l, and $j = |\kappa| - \frac{1}{2}$, respectively. The phases Δ_κ are chosen so that the continuum wave function fulfills the boundary conditions of an incoming plane wave and an outgoing spherical wave. With these specifications, we can write the NEEC rate for a given electric multipolarity L as

$$\begin{aligned} {Y_n^{(e)}}_L &= \frac{4\pi^2 \rho_i}{(2L+1)^2} R_0^{-2(L+2)} B(EL, I_i \to I_d)(2j_d + 1) \\ &\times \sum_\kappa \left| R^{(e)}_{L,\kappa_d,\kappa} \right|^2 \ C \left(j_d \ L \ j; \frac{1}{2} \ 0 \ \frac{1}{2} \right)^2 \ , \end{aligned} \tag{2.37}$$

with the electronic radial integral

$$\begin{aligned} R^{(e)}_{L,\kappa_d,\kappa} &= \frac{1}{R_0^{L-1}} \int_0^{R_0} dr_e r_e^{L+2} \Big(f_{n_d\kappa_d}(r_e) f_{\varepsilon\kappa}(r_e) + g_{n_d\kappa_d}(r_e) g_{\varepsilon\kappa}(r_e) \Big) \\ &+ R_0^{L+2} \int_{R_0}^{\infty} dr_e r_e^{-L+1} \Big(f_{n_d\kappa_d}(r_e) f_{\varepsilon\kappa}(r_e) + g_{n_d\kappa_d}(r_e) g_{\varepsilon\kappa}(r_e) \Big) \ . \end{aligned} \tag{2.38}$$

In the electronic radial integrals $g_{\varepsilon\kappa}(r)$ and $f_{\varepsilon\kappa}(r)$ are the large and small radial components of the relativistic continuum electron wave function

$$\Psi_{\varepsilon\kappa m}(\vec{r}) = \begin{pmatrix} g_{\varepsilon\kappa}(r) \Omega^m_\kappa(\theta, \varphi) \\ i f_{\varepsilon\kappa}(r) \Omega^m_{-\kappa}(\theta, \varphi) \end{pmatrix} \ , \tag{2.39}$$

and $g_{n_d\kappa_d}(r)$ and $f_{n_d\kappa_d}(r)$ are the components of the bound Dirac wave functions

$$\Psi_{n_d\kappa_d m_d}(\vec{r}) = \begin{pmatrix} g_{n_d\kappa_d}(r) \Omega^{m_d}_{\kappa_d}(\theta, \varphi) \\ i f_{n_d\kappa_d}(r) \Omega^{m_d}_{-\kappa_d}(\theta, \varphi) \end{pmatrix} \ , \tag{2.40}$$

with the spherical spinor functions Ω^m_κ. The radial integral $R^{(e)}_{L,\kappa_d,\kappa}$ has to be calculated numerically.

2.3 NEEC rates for magnetic transitions

Using the expression (2.27) for the interaction Hamiltonian H_{magn}, the matrix element that enters the formula of the NEEC rate for magnetic transitions can be written as

$$\begin{aligned}(H_{en})_{di} &= 4\pi i \sum_{LM} (-1)^M \sqrt{\frac{L+1}{L}} \frac{1}{2L+1} \langle N^* I_d M_d | M_{LM} | N I_i M_i \rangle \\ &\times \langle n_d \kappa_d m_d | r_e^{-(L+1)} \vec{\alpha} \cdot \vec{Y}_{LL}^{-M}(\theta_e, \varphi_e) | \vec{p} m_s \rangle \ . \end{aligned} \tag{2.41}$$

Here we have used the formula for the complex conjugate of the vector spherical harmonics [VMK88],

$$\vec{Y}_{JL}^{M*} = (-1)^{L+J+M+1} \vec{Y}_{JL}^{-M} \ . \tag{2.42}$$

The nuclear matrix element can be related to the reduced magnetic transition probability of a certain multipolarity L,

$$B(ML, I_i \to I_d) = \frac{1}{2I_i+1} |\langle N^* I_d \| M_L \| N I_i \rangle|^2 \ . \tag{2.43}$$

In order to evaluate the electronic matrix element we expand the initial continuum wave function $|\vec{p} m_s\rangle$ in partial waves with proper quantum numbers κ and m, as in Eq. (2.36). The whole calculation resumes to the evaluation of the electronic matrix element

$$\langle n_d \kappa_d m_d | r_e^{-(L+1)} \vec{\alpha} \cdot \vec{Y}_{LL}^{-M}(\theta_e, \varphi_e) | \varepsilon \kappa m \rangle \ . \tag{2.44}$$

One way to calculate this matrix element is to replace the vector spherical harmonics by their expression from Eq. (1.17) and to perform analytically the angular integration. This treatment delivers somewhat lengthy formulas and can be found in [PHS06]. An equivalent approach uses the properties of spherical tensors and provides a more elegant and compact formula for the matrix element of interest. We present this calculation in Appendix C. The electronic matrix element reads then

$$\begin{aligned}&\langle n_d \kappa_d m_d | r^{-(L+1)} \vec{\alpha} \cdot \vec{Y}_{LL}^{-M}(\theta_e, \varphi_e) | \varepsilon \kappa m \rangle = \\ &i(-1)^{j-L+\frac{1}{2}} \sqrt{\frac{(2j+1)(2L+1)}{4\pi L(L+1)}} C(j \ L \ j_d; m \ -M \ m_d) \begin{pmatrix} j_d & j & L \\ \frac{1}{2} & -\frac{1}{2} & 0 \end{pmatrix} \\ &\times (\kappa_d + \kappa) \int_0^\infty dr_e r_e^{-L+1} \Big(g_{n_d \kappa_d}(r_e) f_{\varepsilon\kappa}(r_e) + f_{n_d \kappa_d}(r_e) g_{\varepsilon\kappa}(r_e) \Big) \ , \end{aligned} \tag{2.45}$$

where the Wigner $3j$-symbol used in the above equation is related to the Clebsch-Gordan coefficients by

$$C(j_1 \ j_2 \ j; m_1 \ m_2 \ m) = (-1)^{m+j_1-j_2} \sqrt{2j+1} \begin{pmatrix} j_1 & j_2 & j \\ m_1 & m_2 & -m \end{pmatrix} \ . \tag{2.46}$$

The NEEC transition rate for a certain multipolarity L can then be written as

$$\begin{aligned} {Y_n^{(m)}}_L &= \frac{4\pi^2\rho_i}{L^2(2L+1)^2} B(ML, I_i \to I_d)(2j_d+1) \\ &\quad \times \sum_{\kappa} (2j+1)(\kappa_d+\kappa) \begin{pmatrix} j_d & j & L \\ \frac{1}{2} & -\frac{1}{2} & 0 \end{pmatrix}^2 \left| R^{(m)}_{L,\kappa_d,\kappa} \right|^2 , \end{aligned} \tag{2.47}$$

where we have introduced the notation

$$R^{(m)}_{L,\kappa_d,\kappa} = \int_0^\infty dr_e r_e^{-L+1} \Big(g_{n_d\kappa_d}(r_e) f_{\varepsilon\kappa}(r_e) + f_{n_d\kappa_d}(r_e) g_{\varepsilon\kappa}(r_e) \Big) \tag{2.48}$$

for the radial integral.

The calculation of the NEEC rates involves therefore the knowledge of the reduced nuclear transition probabilities $B(\lambda L, I_i \to I_d)$ and the numerical integration of $R^{\lambda}_{L,\kappa_d,\kappa}$, where λ stands for electric (e) or magnetic (m), correspondingly.

Chapter 3

Total cross sections for NEEC

In this chapter we present numerical results for the total cross section of NEEC followed by the radiative decay of the nuclear excited state for various collision systems. An earlier version of these results has been published in [PHS06]. As the magnitude of the NEEC resonance strengths makes the experimental observation of the process a challenge for atomic physics measurements, we focus on finding candidate isotopes suitable for future experiments. In the second part of this chapter we review previous experimental attempts aiming to observe the NEEC resonance. We analyze our theoretical results along with the present possibilities offered by storage rings or electron beam ion traps experiments.

3.1 Numerical results

We consider heavy ion collision systems involving electric $E2$ and magnetic $M1$ transitions in isotopes with low-lying nuclear levels that make the occurrence of NEEC possible. For the case of electric multipole transitions we envisage the $0^+ \to 2^+$ $E2$ transitions of $^{236}_{92}$U, $^{238}_{92}$U, $^{248}_{96}$Cm, $^{174}_{70}$Yb, $^{170}_{68}$Er, $^{154}_{64}$Gd, $^{156}_{64}$Gd, $^{162}_{66}$Dy and $^{164}_{66}$Dy. The reduced transition probability $B(E2, 0 \to 2)$ for these nuclei as well as the energies of the nuclear transitions are taken from [RNT01]. A further $E2$ $\frac{5}{2}^- \to \frac{7}{2}^-$ transition of the odd $^{163}_{66}$Dy nucleus is considered. In order to derive the NEEC rate for this case, we use the assumption that the electron does not enter the nucleus, which allows a convenient separation of the electronic and nuclear matrix elements. Following the outline presented in Chapter 2, the NEEC rate can be written as

$$\begin{aligned} Y_n^{(e)} &= \frac{4\pi^2 \rho_i}{(2L+1)^2} B\left(E2, \frac{5}{2} \to \frac{7}{2}\right)(2j_d+1) \\ &\times \sum_{\kappa} |\tilde{R}^{(e)}_{L,\kappa_d,\kappa}|^2 \, C\left(j_d \; L \; j; \frac{1}{2} \; 0 \; \frac{1}{2}\right)^2 , \end{aligned} \tag{3.1}$$

where the radial integral is given by

$$\tilde{R}^{(e)}_{L,\kappa_d,\kappa} = \int_0^\infty dr r^{-L+1} \Big(f_{n_d\kappa_d}(r) f_{\epsilon\kappa}(r) + g_{n_d\kappa_d}(r) g_{\epsilon\kappa}(r) \Big) . \tag{3.2}$$

The values of the reduced nuclear transition probability $B\left(E2, \frac{5}{2} \rightarrow \frac{7}{2}\right)$ and the energy of the excited state are taken from [Bur89].

The NEEC total cross section in Eq. (1.55) contains also the nuclear radiative rate $A_r^{d\rightarrow f}$. We consider the relation between the reduced transition probabilities and the nuclear radiative rate [RS80]

$$A_r^{d\rightarrow f}(\lambda, L) = \frac{8\pi(L+1)}{L((2L+1)!!)^2}\frac{E_n^{2L+1}}{c}B(\lambda L, I_d \rightarrow I_f) \ , \tag{3.3}$$

where λ stands for electric E or magnetic M transition, and E_n is the energy of the excited nuclear state. The reduced transition probabilities for the emission, respectively the absorption of a gamma ray are related through the formula

$$B(\lambda L, I_d \rightarrow I_f) = \frac{2I_f+1}{2I_d+1}B(\lambda L, I_f \rightarrow I_d) \ , \tag{3.4}$$

which is based on the principle of detailed balance. The intermediate nuclear state may decay radiatively, or, when possible, by internal conversion. The natural width of the nuclear excited state is then given in atomic units by the sum of the radiative and IC rates,

$$\Gamma_d = \sum_f \left(A_r^{d\rightarrow f} + A_{\mathrm{IC}}^{d\rightarrow f}\right) \ . \tag{3.5}$$

The ratio of these rates gives for a transition $d\rightarrow f$ the dimensionless IC coefficient,

$$\alpha = \frac{A_{\mathrm{IC}}^{d\rightarrow f}}{A_r^{d\rightarrow f}} \ . \tag{3.6}$$

The NEEC and IC rates of the intermediate state are also related through the principle of detailed balance,

$$A_{\mathrm{IC}}^{d\rightarrow f} = \frac{2(2I_i+1)}{(2I_d+1)(2j_d+1)}Y_n \ . \tag{3.7}$$

The IC rate can also be obtained from tabulated values for the IC coefficients and reduced transition probabilities B, using the radiative rate (3.3) and applying Eq. (3.6). The IC coefficients are, however, usually given in the literature for neutral atoms and take into account the exchange interaction between the electrons either statistically [RFAP78] or by using a self-consistent-field Dirac-Fock method [BT93, BTN$^+$02]. If an electronic subshell is not completely filled, the IC coefficient can be scaled to account for the actual number of electrons [RD00]. The other shells and subshells of the ion are nevertheless considered to be fully occupied. We avoid to use tabulated IC coefficients, even rescaled, as for NEEC we consider only bare or He-like ions. A comparison between rescaled IC coefficients from the tabulation in Ref. [RFAP78] and the ones calculated using our NEEC rates corresponding to H-like of Li-like ions reveals discrepancies of up to 40%. We use, therefore, Eqs. (3.7) and (3.5) to calculate the IC rate and the width of the nuclear excited state Γ_d, respectively.

The calculation of the NEEC rates involves the numerical integration of the radial expressions $R^{(e)}_{L,\kappa_d,\kappa}$ and $\tilde{R}^{(e)}_{L,\kappa_d,\kappa}$ that enter Eqs. (2.37) and (3.1). This requires the knowledge of the bound and continuum radial functions for the electron. For the continuum electron we use relativistic Coulomb-Dirac wave functions, applying the approximation that the nucleus is a point-like charge. We assume that the free electron, which is far away from the ion, is not sensitive to the internal structure or size of the nucleus. Once the electron is captured into the Coulomb field of the nucleus, we consider relativistic wave functions calculated with the GRASP92 package [PFFG96] for the bound state. The acronym GRASP stands for **G**eneral-purpose **R**elativistic **A**tomic **S**tructure **P**rogram and is a suite of FORTRAN codes developed from the 1980s for various calculations of relativistic atomic structure. The multiconfiguration Dirac-Fock (MCDF) approximation is used for the calculation of atomic stationary states and transitions among them [DGJ$^+$89]. GRASP92 is an improvement of the previous versions and includes approximate QED corrections for the electronic energy levels. The finite size of the nucleus, i.e., its radius R_0, is also considered in the GRASP92 wave functions and has a sensitive effect on the lower energy levels of the bound electron. The radial integrals $R^{(e)}_{L,\kappa_d,\kappa}$ and $\tilde{R}^{(e)}_{L,\kappa_d,\kappa}$ show however little difference between calculations considering an extended or a point nucleus for the bound radial wave functions. We therefore assume that the approximation made by using Coulomb-Dirac wave functions for the continuum electron does not affect much the accuracy of the results. The nuclear radius R_0 is calculated according to the semi-empirical formula [JS85]

$$R_0 = (1.0793\, A^{1/3} + 0.73587)\ \text{fm}\ , \tag{3.8}$$

where A is the atomic mass number. The first term in the sum of radial integrals in Eq. (2.38) is about 3 orders of magnitude smaller than the second one,

$$\begin{aligned} &\frac{1}{R_0^{L-1}} \int_0^{R_0} dr r^{L+2} \Big(f_{n_d\kappa_d}(r) f_{\varepsilon\kappa}(r) + g_{n_d\kappa_d}(r) g_{\varepsilon\kappa}(r) \Big) \\ \ll\ & R_0^{L+2} \int_{R_0}^{\infty} dr r^{-L+1} \Big(f_{n_d\kappa_d}(r) f_{\varepsilon\kappa}(r) + g_{n_d\kappa_d}(r) g_{\varepsilon\kappa}(r) \Big)\ . \end{aligned} \tag{3.9}$$

This observation allows us to approximate the expression of $R^{(e)}_{L,\kappa_d,\kappa}$ as

$$R^{(e)}_{L,\kappa_d,\kappa} \simeq R_0^{L+2} \int_0^{\infty} dr r^{-L+1} \Big(f_{n_d\kappa_d}(r) f_{\varepsilon\kappa}(r) + g_{n_d\kappa_d}(r) g_{\varepsilon\kappa}(r) \Big)\ . \tag{3.10}$$

At a closer look this is equivalent to considering that the probability density of the electron is negligible in the nuclear volume. Indeed, introducing $R^{(e)}_{L,\kappa_d,\kappa}$ from the equation above in the expression of the NEEC rate in Eq. (2.37) we obtain the formula (3.1), which was calculated by assuming that $r_e > r_p$. If we evaluate the total cross section for NEEC using the above approximate expression for the radial integral, we obtain results that deviate with a few percent from the total cross section rigorously calculated using the collective model, without making any assumption about the motion of the electron. The difference varies from less than 1% in the case of lighter isotopes up to 6% for the recombination of the

Table 3.1: NEEC rates Y_n and resonance strengths S for various heavy ion collision systems involving $E2$ nuclear transitions. E_n is the nuclear excitation energy, E_d is the energy of the continuum electron at the resonance and Γ_d is the width of the excited nuclear state. The notation nl_j is used for the orbital into which the electron recombines.

${}^{A}_{Z}\mathrm{X}$	E_n(keV)	E_d(keV)	nl_j	$Y_n(1/s)$	Γ_d(eV)	S(b eV)
${}^{164}_{66}\mathrm{Dy}$	73.392	10.318	$1s_{1/2}$	1.86×10^{8}	4.37×10^{-8}	3.88×10^{-2}
${}^{170}_{68}\mathrm{Er}$	78.591	11.350	$1s_{1/2}$	2.23×10^{8}	5.75×10^{-8}	4.70×10^{-2}
${}^{174}_{70}\mathrm{Yb}$	76.471	4.897	$1s_{1/2}$	1.79×10^{8}	4.85×10^{-8}	9.27×10^{-2}
${}^{154}_{64}\mathrm{Gd}$	123.071	64.005	$1s_{1/2}$	5.69×10^{8}	2.51×10^{-7}	2.91×10^{-2}
${}^{156}_{64}\mathrm{Gd}$	88.966	74.742	$2s_{1/2}$	3.35×10^{7}	1.21×10^{-7}	7.09×10^{-4}
${}^{156}_{64}\mathrm{Gd}$	88.966	74.896	$2p_{1/2}$	1.16×10^{8}	1.32×10^{-7}	2.25×10^{-3}
${}^{156}_{64}\mathrm{Gd}$	88.966	75.680	$2p_{3/2}$	1.59×10^{8}	1.27×10^{-7}	3.17×10^{-3}
${}^{162}_{66}\mathrm{Dy}$	80.660	65.432	$2s_{1/2}$	2.81×10^{7}	9.39×10^{-8}	6.25×10^{-4}
${}^{162}_{66}\mathrm{Dy}$	80.660	65.594	$2p_{1/2}$	1.59×10^{8}	1.11×10^{-7}	2.98×10^{-3}
${}^{162}_{66}\mathrm{Dy}$	80.660	66.492	$2p_{3/2}$	2.15×10^{8}	1.04×10^{-7}	4.24×10^{-2}
${}^{163}_{66}\mathrm{Dy}$	73.440	58.212	$2s_{1/2}$	9.18×10^{6}	1.06×10^{-7}	2.09×10^{-4}
${}^{163}_{66}\mathrm{Dy}$	73.440	58.374	$2p_{1/2}$	6.93×10^{7}	1.36×10^{-7}	1.23×10^{-3}
${}^{163}_{66}\mathrm{Dy}$	73.440	59.272	$2p_{3/2}$	9.44×10^{7}	1.25×10^{-7}	1.79×10^{-3}
${}^{236}_{92}\mathrm{U}$	45.242	12.404	$2s_{1/2}$	1.06×10^{8}	1.76×10^{-8}	8.47×10^{-3}
${}^{236}_{92}\mathrm{U}$	45.242	12.698	$2p_{1/2}$	3.02×10^{9}	4.01×10^{-7}	1.02×10^{-2}
${}^{236}_{92}\mathrm{U}$	45.242	16.871	$2p_{3/2}$	3.10×10^{9}	2.07×10^{-7}	1.52×10^{-2}
${}^{238}_{92}\mathrm{U}$	44.910	12.073	$2s_{1/2}$	1.11×10^{8}	1.81×10^{-8}	8.80×10^{-3}
${}^{238}_{92}\mathrm{U}$	44.910	12.356	$2p_{1/2}$	3.14×10^{9}	4.17×10^{-7}	1.06×10^{-2}
${}^{238}_{92}\mathrm{U}$	44.910	16.534	$2p_{3/2}$	3.23×10^{9}	2.16×10^{-7}	1.56×10^{-2}
${}^{248}_{96}\mathrm{Cm}$	43.380	6.888	$2s_{1/2}$	2.18×10^{8}	3.25×10^{-8}	1.78×10^{-2}
${}^{248}_{96}\mathrm{Cm}$	43.380	7.190	$2p_{1/2}$	5.47×10^{9}	7.24×10^{-7}	1.91×10^{-2}
${}^{248}_{96}\mathrm{Cm}$	43.380	12.356	$2p_{3/2}$	5.33×10^{9}	3.54×10^{-7}	2.20×10^{-2}

electron in the $1s$ orbital of ${}^{248}_{96}\mathrm{Cm}$. This is predictable, as Cm is the heaviest of the considered isotopes, and the electron wave function of the $1s$ orbital overlaps the nucleus considerably. The relatively small discrepancies justify the non-penetration approximation used in the case of the magnetic transitions.

For the cases of the U isotopes and for ${}^{248}_{96}\mathrm{Cm}$, the capture into the K shell is possible only with the excitation of higher energy states ($E_n \simeq 140$ keV). For these 3 isotopes, we consider recombination into the L shell of initially He-like ions, which is the most probable one. We regard the capture of the electron into a subshell outside a closed-shell configuration as a one-electron problem, without the participation of the K-shell electrons. Our calculation does not account for photons emitted in electron transitions to lower bound states that are possible when the capture occurs into the $2p_{1/2}$ or $2p_{3/2}$ orbitals of the ion. Given the high atomic number of the Uranium and Curium ions, we consider

Table 3.2: NEEC rates Y_n and resonance strengths S for various heavy ion collision systems involving $M1$ nuclear transitions. E_n is the nuclear excitation energy, E_d is the energy of the continuum electron at the resonance and Γ_d is the width of the excited nuclear state. The notation nl_j is used for the orbital into which the electron recombines.

${}^{A}_{Z}$X	E_n(keV)	E_d(keV)	nl_j	$Y_n(1/s)$	Γ_d(eV)	S(b eV)
${}^{165}_{67}$Ho	94.700	29.563	$1s_{1/2}$	1.28×10^{10}	1.17×10^{-5}	8.84×10^{-1}
${}^{173}_{70}$Yb	78.647	7.073	$1s_{1/2}$	7.32×10^{9}	4.80×10^{-6}	1.26
${}^{185}_{75}$Re	125.358	42.198	$1s_{1/2}$	2.62×10^{10}	2.36×10^{-5}	1.34
${}^{187}_{75}$Re	134.243	51.083	$1s_{1/2}$	2.50×10^{10}	2.47×10^{-5}	1.16
${}^{55}_{25}$Mn	125.949	117.378	$1s_{1/2}$	2.45×10^{7}	1.75×10^{-6}	9.22×10^{-4}
${}^{57}_{26}$Fe	14.412	5.135	$1s_{1/2}$	6.21×10^{6}	2.56×10^{-9}	1.19×10^{-3}
${}^{40}_{19}$K	29.829	24.896	$1s_{1/2}$	1.33×10^{7}	9.47×10^{-8}	2.27×10^{-3}
${}^{155}_{64}$Gd	60.008	45.784	$2s_{1/2}$	2.73×10^{8}	1.97×10^{-6}	3.18×10^{-3}
${}^{155}_{64}$Gd	60.008	45.938	$2p_{1/2}$	2.40×10^{7}	1.86×10^{-6}	2.94×10^{-4}
${}^{155}_{64}$Gd	60.008	46.722	$2p_{3/2}$	4.00×10^{6}	1.85×10^{-6}	4.84×10^{-5}
${}^{157}_{64}$Gd	54.533	40.309	$2s_{1/2}$	4.16×10^{8}	4.37×10^{-7}	2.86×10^{-2}
${}^{157}_{64}$Gd	54.533	40.463	$2p_{1/2}$	3.68×10^{7}	2.71×10^{-7}	4.07×10^{-3}
${}^{157}_{64}$Gd	54.533	41.247	$2p_{3/2}$	6.21×10^{6}	2.56×10^{-7}	7.12×10^{-4}

total screening for the continuum electron, $Z_{\rm eff} = Z - 2$. The interaction between the electrons is included in the bound radial wave functions calculated with GRASP92 and influences the results through the value of the bound energy and through the shape of the electronic radial wave functions in the vicinity of the nucleus. The change in the shape of the radial wave functions has a larger numerical contribution to the value of the NEEC rate than the change of the bound energy level due to the electron-electron interaction.

For the other cases of even-even nuclei, capture into the K shell is possible. For the ${}^{156}_{64}$Gd, ${}^{154}_{64}$Gd, ${}^{162}_{66}$Dy, and ${}^{163}_{66}$Dy isotopes we have also treated the capture into He-like ions. Total screening of the nucleus is again assumed for the continuum electron. For the considered He-like ions, the width of the nuclear state in Eq. (3.5) contains then an extra term which accounts for the possible IC of the K-shell electrons. This is again calculated using the principle of detailed balance in Eq. (3.7). The capture rate into the $2p$ orbitals is generally one order of magnitude larger than the one for the capture into the $2s$ orbital. The rates and resonance strengths for NEEC followed by the radiative decay of the nucleus for electric transitions are presented in Table 3.1.

For the magnetic multipole transitions we consider the $M1$ excitations of the odd isotopes ${}^{165}_{67}$Ho, ${}^{173}_{70}$Yb, ${}^{55}_{25}$Mn, ${}^{57}_{26}$Fe, ${}^{40}_{19}$K, ${}^{155}_{64}$Gd, ${}^{157}_{64}$Gd, ${}^{185}_{75}$Re and ${}^{187}_{75}$Re. In most of these cases the nuclear transitions between the ground and the first excited states are not pure $M1$, but mixtures of $M1$ and $E2$ multipolarities. The electric component represents however only few percent of the transition and is neglected in the calculation of the total NEEC cross section. Numerical

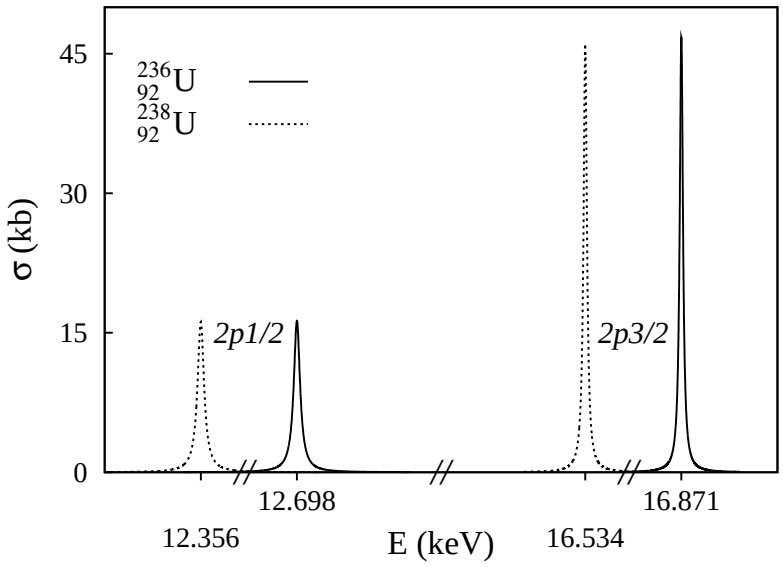

Figure 3.1: NEEC cross sections for Uranium isotopes $^{236}_{92}$U and $^{238}_{92}$U as a function of the continuum electron energy

results for these isotopes are given in Table 3.2. The electronic radial integrals are calculated numerically using the same type of wave functions for the bound and continuum electron as in the electric case. The reduced magnetic transition probabilities $B(M1, I_d \rightarrow I_f)$ and the energies of the nuclear levels are taken from Refs. [Fir91, Shi88, Pek92, Bro95, Huo91, Bha92, CS04, Rei94, Hel88]. Capture into the K shell is possible for all the chosen ions, except for the $^{157}_{64}$Gd isotope. The capture into higher shells is less probable, and already for the capture into the $2s$ orbital of $^{167}_{67}$Ho, the NEEC rate is one order of magnitude smaller. We present results for NEEC occuring in the He-like ions of $^{155}_{64}$Gd and $^{157}_{64}$Gd.

In Figure 3.1 we present the cross section for the capture of the continuum electron into the $2p_{1/2}$ and $2p_{3/2}$ orbitals of the two studied Uranium He-like ions. The cross sections for the capture into the $2p_{3/2}$ orbitals are larger than the ones into the $2p_{1/2}$ orbitals. Although the cross section values are in the order of thousands of barns, the width of the Lorentz profile is given by the natural width of the excited nuclear state, $\Gamma_d \sim 10^{-7} - 10^{-8}$ eV. This validates the use of the isolated resonance approximation in Section 1.3. In Figure 3.2 we present the total cross section for NEEC followed by the $M1$ radiative decay of the nucleus in the case of $^{185}_{75}$Re. The natural width of the excited nuclear state is $\Gamma_d = 2.36 \cdot 10^{-5}$ eV and the total cross section at the resonance energy is about 37 kb. This isotope has the largest NEEC resonance strength, namely S=1.34 b eV for the capture into the $1s$ orbital. This value is small in comparison with the DR resonance strengths observed experimentally in the past decades, which are in the order of 10^3 b eV. The lifetime of the resonant intermediate state in NEEC is several orders of magnitude larger than the one of the auto-ionizing electronic

state in DR. This makes NEEC a slow process in comparison to DR or RR, which involve only electronic transitions. Due to the very narrow width of the nuclear excited states, the observation of NEEC is an experimental challenge. In the following, we discuss several aspects of possible future NEEC experiments.

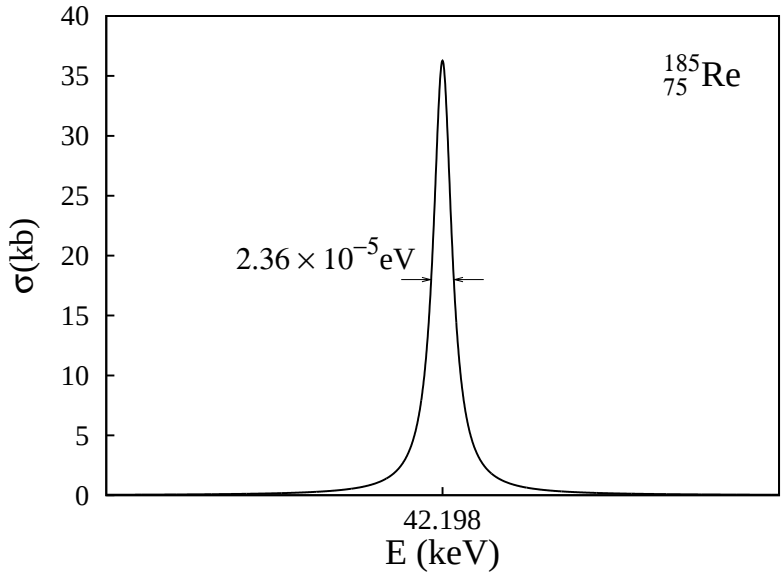

Figure 3.2: NEEC cross sections for $^{185}_{75}$Re as a function of the continuum electron energy

3.2 Possible experimental observation of NEEC

Highly-charged heavy ions are the most important ingredients required in any experiment concerning NEEC. Our theoretical calculations predict higher transition rates for the capture into the lower atomic shells. Furthermore, the presence of many electrons in the ion is expected to suppress the NEEC transition rates and consequently reduce the total cross section of the process. We have considered NEEC involving bare or He-like ions with the atomic number Z ranging from 19 up to 96. Such highly-charged ions can be produced nowadays in electron beam ion traps or in accelerators. We discuss in the following the possibilities of observing experimentally NEEC in these two types of facilities.

3.2.1 Electron Beam Ion Traps

The Electron Beam Ion Trap (EBIT) is a relatively compact device that creates and traps very highly charged ions by means of a monoenergetic, high current density electron beam [Cur03]. The ions are confined by a combination of electric and magnetic fields in the center of the so-called trap, under very high vacuum. The trap acts as a target for the powerful, highly focused

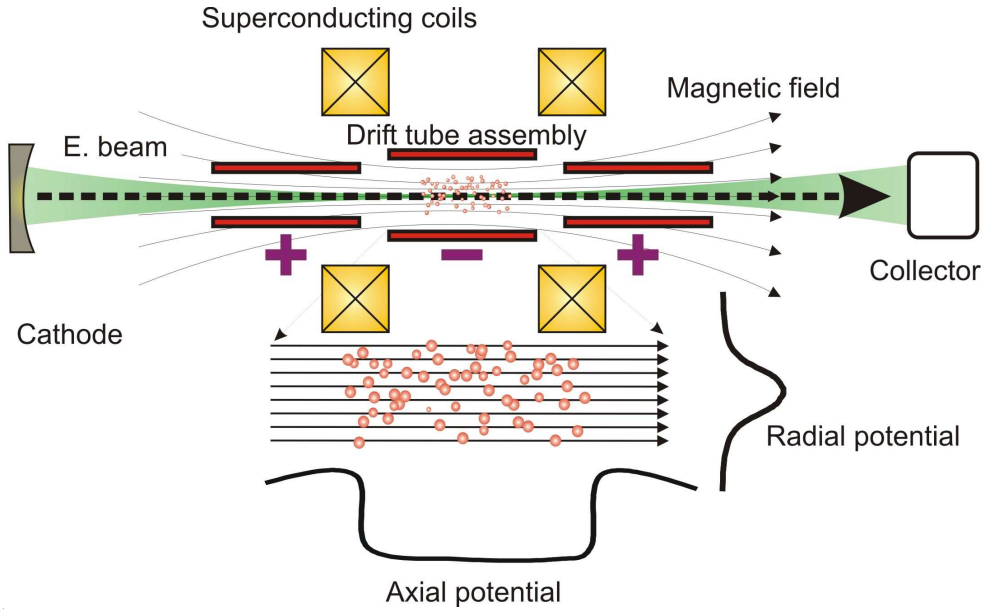

Figure 3.3: Schematic picture of the EBIT.

electron beam, which is compressed using a high magnetic field generated by a superconducting magnet. The electron beam has an electron density n_e of about 10^{13} electrons per cm^3 and an energy spread in the order of tens of eV. As long as the kinetic energy of the beam electrons is higher than the ionization energies of the bound electrons, the collisions strip electrons from the ions. The space charge of the dense electron beam traps the positive ions inside the beam in the radial direction, keeping them from leaving the trap. Along the electron beam axis, the motion of the trapped ions is constrained by three electrodes (drift tubes), two of them on both sides of the trap at positive potential, and the central drift tube, grounded or at negative potential, as shown in Fig. 3.3.

Due to the successive collisions with the beam electrons, the ions in the trap are heated up during the ionization and tend to escape it. To prevent them from leaving the trap, lighter ions are used for cooling. Through collisions, a large part of the kinetic energy of the heavier ions is taken by the lighter ones, which eventually evaporate from the trap. By injecting small amounts of Neon gas, for example, as an atomic beam, the cooled heavy ions can be kept trapped for a long period of time. This "evaporation" cooling technique also reduces the Doppler broadening of the radiation coming from the trapped ions. The highly charged ions can then be used for various measurements concerning dielectronic recombination [MLUB$^+$05, ZLUU03], high-precision lifetime measurements of forbidden transitions [LUBB$^+$05], electron correlation and QED effects [LJLU$^+$05], and surface modifications and analysis [SHH$^+$02].

If aiming to observe NEEC in an EBIT experiment, the electron beam is first used to produce the initial bare or He-like ions. At the SuperEBIT in the Lawrence Livermore National Laboratory, highly-charged ions up to bare Uranium U^{92+} have been produced. The Heidelberg EBIT in Germany, devel-

oped at the Freiburg University from 1998 to 2001, is designed to reach similar features. Its current achieved maximum electron beam energy is 100 keV. This value does not yet allow to produce bare Uranium, as the K-shell electrons for $Z = 92$ have the binding energy of around 132 keV, but is sufficient to work comfortably with He-like or even bare ions with lower atomic numbers. The available ionization data show that in order to produce most efficiently highly-charged ions, the electron impact energy E_e should be at least 2-3 times the binding energy $|E_b|$ of the ion, $E_e \approx (2-3)|E_b|$.

Once the highly-charged ions are produced and stored in the trap, the same electron beam can be used to achieve the nuclear excitation by electron capture. In this event the electron is recombined into a bound shell of the ion with the simultaneous excitations of the nucleus, at the resonance energy $E_e = E_d = E_n - |E_b|$. As the resonance condition for NEEC is critical, the electron beam energy has to be tuned from the ionization value needed to produce the highly-charged ions to the resonance energy E_d corresponding to the nuclear excitation. The success of a NEEC experiment relies strongly on finding an isotope that has close values for the ionization and nuclear excitation energies. The capture into bare Ytterbium, for instance, is not convenient as the binding energy of the $1s$ electrons is $|E_b|$ =71.574 keV, while the energy of the continuum electron corresponding to the nuclear excitation is E_c =4.897 keV for the case of $^{174}_{70}$Yb and E_c =7.073 keV for $^{173}_{70}$Yb. The captures into the L-shell of the He-like $^{155}_{64}$Gd and $^{157}_{64}$Gd ions have the best energy match between the ionization and nuclear excitation energies. The NEEC resonance strengths are however small, the largest being for the capture into the $2s$ orbital of $^{157}_{64}$Gd, S=2.86×10^{-2} b eV.

The NEEC total cross section has the shape of a very narrow Lorentzian peak with the width given by the natural width of the nuclear excited state. The nuclear excitation is supposed to occur only for the capture of free electrons with energies in the narrow interval of the width. The largest nuclear width $\Gamma_d = 2.47 \times 10^{-5}$ eV characterizes the $^{187}_{75}$Re isotope. As the electron energy resolution in the order of 10^{-5} eV or less cannot be presently achieved in an NEEC experiment, the theoretical total cross section should be convoluted with the energy distribution of the electrons to give an orientation for possible measurements in the EBIT. The energy distribution of the incoming electrons is assumed to be a Gaussian one with the width parameter s. The photon emitted in the decay of the nuclear excited state can be observed with semiconductor detectors. The spectrum of the detected photons would be however dominated by the continuous background of RR. In order to show the magnitude of the NEEC cross section $\sigma_{\rm NEEC}$ compared to that of RR, in Fig. 3.4 we present the ratio of the convoluted cross sections,

$$R(E,s) = \frac{\tilde{\sigma}_{\rm NEEC}(E,s)}{\tilde{\sigma}_{\rm RR}(E,s)} \tag{3.11}$$

for the case of $^{187}_{75}$Re as a function of the energy of the continuum electron for three different experimental width parameters, s = 10 eV, 1 eV and 0.5 eV. The values for the RR cross section $\sigma_{\rm RR}(E)$ were taken from Ref. [IE00]. While for a width parameter s = 0.5 eV and maybe also for s=1 eV the contributions of the NEEC and interference terms can be discerned from the RR background,

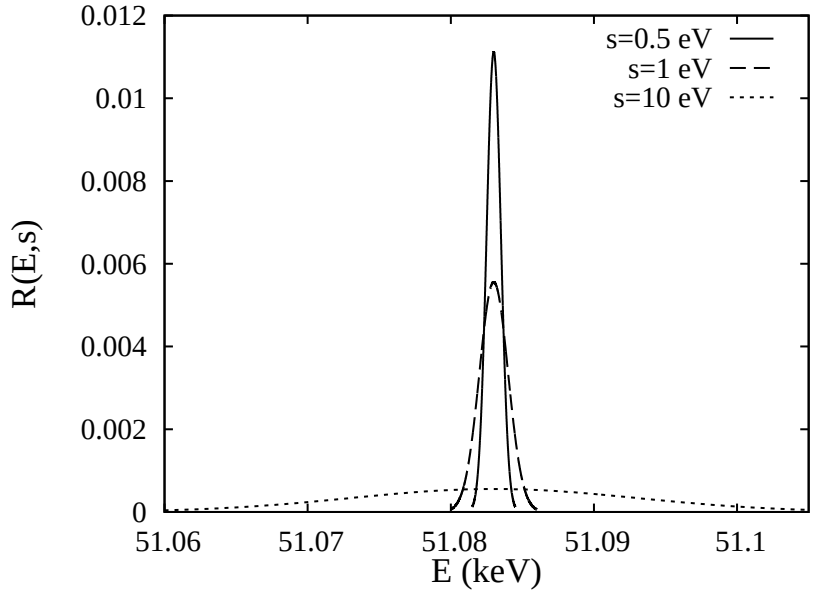

Figure 3.4: The ratio $R(E, s)$ in Eq. (3.11) for recombination into bare Rhenium as a function of the energy of the continuum electron for three different experimental electron energy width parameters s.

for more realistic widths in the order of tens of eV, the values of the ratio $\tilde{\sigma}_{\mathrm{NEEC}}/\tilde{\sigma}_{\mathrm{RR}}$ become too small to be observed experimentally.

The background could possibly be reduced by choosing an isotope with a cascade decay scheme. In this case the NEEC radiation would have a different energy than the RR photons and therefore a much better signal to background ratios would be expected. The extraction of the recombined ions from the EBIT in the case of nuclear excitation of isotopes with a longer lifetime could also reduce the RR background. In this case, if the excited nuclear state has a lifetime in the order of ms, the radiative decay would be delayed in comparison with the RR photons. Meanwhile the ions could be extracted from the EBIT and implanted into a semiconductor detector, where even weak signals would be accumulated practically background-free.

3.2.2 Ion Accelerators

Accelerator facilities offer multiple possibilities of research in atomic, plasma and nuclear physics, material sciences and biophysics, all involving the use of highly-charged ions. An accelerator can bring low-charged ions to high velocities near to the speed of light. The relativistic ion-beam is then shot through very thin foils (beam-foil method) or gas targets that act like strippers and remove a part of the ion's electrons. The remaining very fast highly-charged ions can be kept circling on a close orbit in a storage ring for a longer time. Such an ion beam is ideal to study atomic properties of the highly-charged heavy ions. High-precision experiments regarding recombination mechanisms

[WGL+00, MS01, WG03], laser spectroscopy with stored ions [KBE+94] or ions channeling through crystals [LAB+06, PDA+97] are performed at accelerator facilities such as GSI in Darmstadt, GANIL in Caen or TSR in Heidelberg.

The GSI heavy-ion accelerator complex in Darmstadt is presently the only facility in the world that can produce and store highly-charged ions up to bare Uranium U^{92+}. The system consists of a combination of a linear accelerator (UNILAC), a heavy-ion synchrotron (SIS) and the experimental storage ring (ESR) [BS03]. In the UNILAC the ions produced by a Penning ion source are resonantly accelerated by a strong high-frequency electric field. After a first radio-frequency quadrupole (RFQ) section the ions reach the energy of 1.4 MeV/u and go through a gas stripper that enhances their charge state. A further section with Alvarez and single-gap resonators accelerates the ions up to 11.4 MeV/u. The accelerated ions are then injected into the transfer channel to SIS, where they pass a foil stripper. The heavy-ion synchrotron SIS is a cyclic accelerator with a circumference of 216 m that can speed the ion beam to energies ranging up to 2 GeV/u. The guiding magnetic field in the synchrotron increases simultaneously with the energy and keeps the orbit of the ion beam stationary. The beam can be then injected into the Experimental Storage Ring (ESR), where highly-charged ions or even rare and radioactive nuclides produced in the Fragment Separator (FSR) can be stored. The ions circle periodically on a closed orbit of 108 m circumference with a typical frequency of 1 MHz. The number of ions in the beam is around $N_I = 10^8$ s^{-1}.

The atomic properties of the ions can be studied in collisions with interaction targets. ESR has two large straight drift sections with small ion dispersion, which are occupied by the internal gas jet target and the electron cooler (see Figure 3.5). The electron or gas targets represent tunable X-ray sources providing insight into the structure and dynamics of highly-charged few-electron systems. The straight sections are also suitable for collinear laser spectroscopy, which makes use of the superposition of a laser with the ion beam. The electron cooler consists of a monoenergetic electron beam that runs parallel to the ion beam with the same average velocity. The electrons cool the circulating ion beam through elastic scattering. After the interaction region of 2.5 m, the electrons are deflected from the ion orbit, decelerated and finally dumped into a collector. As the elastic cross sections are about two orders of magnitude larger than the recombination ones, only a small fraction of the ions recombine with the cooling electrons. The recombined ions, having a different charge than the main ion beam, are deviated from the storage ring.

The first experiment considering NEEC in axial channeling was planned at the GSI in 1989. Considering the theoretical calculations of Cue, Poizat and Remillieux [CPR89], the experimental proposal S003 [Mok89] aimed the observation of NEEC by tunneling accelerated highly-charged ions through a silicon crystal. The main advantage in using a crystal compared to gas targets or electron beams is the high electron density. While the electron beam in the cooler has a density of around $n_e = 10^8$ cm^{-3}, a gas cell of $n_e = 10^{16}$ cm^{-3} and a gas jet up to $n_e = 10^{14}$ cm^{-3}, the value in a solid target is substantially higher, namely $n_e = 10^{22} - 10^{23}$ cm^{-3} [Sch02]. The original plans were to produce in the SIS a 45-46 MeV/u bare or H-like $^{165}_{67}$Ho beam that would hit in

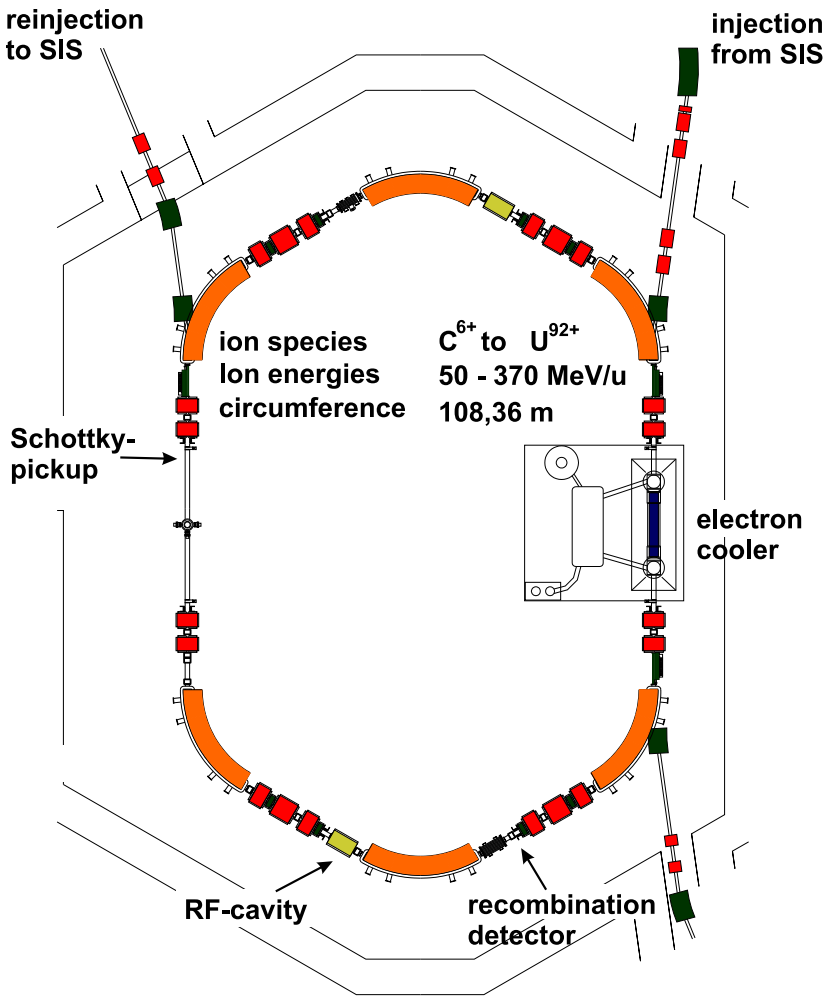

Figure 3.5: Outline of the Experimental Storage Ring (ESR) at GSI Darmstadt.

the FRS a Si single crystal oriented along the beam direction with its $< 110 >$ axis . Two high-resolution semiconductor detectors were to be used to record the emitted photons, in coincidence with the charge-selected and momentum-analyzed transmitted ions. The actual merged test-experiment for the S003 and S044 proposals, both involving channeling studies, took place in 1993, using a 300 MeV U^{73+} beam delivered by the SIS. The main objective was to study the charge state distribution of the U ions transmitted through a Si crystal with a thickness of h=100 μm along the $< 110 >$ directions, and the energy loss spectrum associated to each particular charge state, as development for a future NEEC experiment.

A further request for beam time for tests using an extracted beam from ESR was issued in 1994. The proposed scenario was that bare Ho^{67+} ions accelerated up to 200 MeV/u would be injected from the SIS into the ESR. There the beam was to be cooled and slowed down to about 55 MeV/u, which is the equivalent of a free electron energy of about 29 keV, needed for the nuclear excitation. The cooling would be interrupted during the deceleration process, and resumed afterwards. A cooled beam of H-like recombined ions was to be extracted and to hit the crystal target. The signature of a NEEC event would have been the detection of a 94.7 keV delayed photon in coincidence with a channeled He-like Holmium ion. As this was a rather sophisticated experiment in many aspects, the enumerated conditions were to be tested in preliminary channeling experiments with cooled and decelerated extracted beams. From such preliminary experiments, studies about ion deceleration in the ESR [PDA+97], charge exchange and superdensity effects in the crystal target [LAB+06] have been completed. The final NEEC experiment has never been performed, although important parts have been tested and the necessary knowledge has been acquired.

In September 2004 a NEEC experiment was performed at the LISE line of stripped ions in GANIL [Dau06]. The aim of the experiment was to observe the NEEC of the isomeric 14 keV state of Iron $^{57}_{26}$Fe. The bare Fe^{26+} ion beam was channeled through a 12 μm Si crystal. The recombined ions were deviated with a dipole in a 5.6 m straight section, where some ions lost the electrons due to internal conversion. A second dipole then selected the Fe^{26+} from the Fe^{25+} ions. By using two beams with different Iron isotopes, $^{57}_{26}$Fe and $^{56}_{26}$Fe, the NEEC contribution at the resonance energy of 9.4 MeV/u, corresponding to the energy $E_d = 5.135$ keV of the continuum electron, was supposed to be observed in the number of Fe^{26+} detected ions for the isotope with the isomeric state. The main source of background in this experiment was related to the ionizing collisions with residual particles in the experimental setup. The poor quality of the vacuum between the two dipoles in LISE jeopardized the experiment and NEEC was not observed. The possibility to improve the vacuum in the experimental setup is at present under evaluation at GANIL.

The experimental observation of NEEC remains an open challenge. Our theoretical results based on an ab initio calculation presented in the first part of this chapter are larger than the previous semi-empirical estimates [CPR89, Cue89, KBC91] and nonrelativistic calculations [YK93]. Considering one of the isotopes for which the calculated resonance strength is the largest, for instance

$^{173}_{70}$Yb, we can try to estimate the count rate in a NEEC experiment performed at GSI with an extracted beam from ESR channeling through a single crystal. By measuring in coincidence the emitted photons and the recombined ions, such an experiment at GSI has more chances of being successful than one in the EBIT or at LISE in GANIL, since the background is then substantially limited to RR photons. The count rate is directly proportional with the number of ions in the beam and the electron density, and also depends on the detector setup and efficiency [Cur03],

$$R = N_I \cdot n_e \cdot h \cdot \sigma_{\mathrm{NEEC}}(E_d) \cdot \frac{\Gamma_d}{\Gamma_\mathrm{e}} \cdot \tau_f \cdot \epsilon_f \ , \tag{3.12}$$

where $\Gamma_d/\Gamma_\mathrm{e}$ represents the ratio between the width of the nuclear excited state and the actual energy width of the electrons. Here ϵ_f represents the efficiency of the detectors, which is around $2 \cdot 10^{-3}$ and τ_f is the fraction of the photons which come into the detector. This depends on the geometry of the experimental setup and can be roughly estimated to 0.5. We assume the number of ions in the extracted beam to be $N_I = 10^5$ s^{-1}. The values for the thickness of the Si crystal and its electron density are taken h=100 μm and $n_e = 10^{23}$ cm^{-3}, respectively. The NEEC total cross section at the resonance energy E_d is $\sigma_{\mathrm{NEEC}}(E_d) = 1.67 \cdot 10^5$ b in the case of $^{173}_{70}$Yb. In order to estimate the energy width of the electrons in the crystal we study the width of the incident ion beam. The ratio $\Delta E_I/E_I$ for the decelerated ions in the ESR is about 10^{-5}. We assume the same value for the ions in the extracted beam, although it has never been confirmed experimentally. This would correspond to approximately 0.07 eV width of the electrons in the crystal. The value of the count rate is then

$$R = 10^5\mathrm{s}^{-1} \cdot 10^{21}\mathrm{cm}^{-2} \cdot 1.67 \cdot 10^{-19}\mathrm{cm}^2 \cdot 6.8 \cdot 10^{-5} \cdot 0.5 \cdot 2 \cdot 10^{-3} \approx 1 \ \mathrm{s}^{-1} \ . \tag{3.13}$$

Such a count rate is measurable. Taking into account all the work that has been already invested in the idea of measuring NEEC at the ESR in GSI and the high-precision equipment that the facility offers, it is reasonable to believe that the process will be observed experimentally in the near future.

Chapter 4

Quantum interference between NEEC and RR

In Chapter 1 we have introduced RR and NEEC as possible recombination mechanisms of a free electron into an ion. If the initial and final states for NEEC and RR are the same, quantum interference between the two processes occurs. Such an effect is very interesting as it involves two very different pathways: while in RR only the electronic part plays a role, NEEC has a resonant state in which the nucleus is excited. In Figure 4.1 we present schematically the two interfering channels. As the photons resulting from the recombination process are indistinguishable, RR is expected to be a strong background in any experiment concerning NEEC. The magnitude of the interference effect can therefore play an important role in the experimental observation of NEEC.

In this chapter we investigate theoretically the quantum interference between NEEC and RR, focusing our interest on collision systems with suitable excitation energies that could be candidates for experimental observation. The total cross section for this photo recombination process can be written as a sum of the RR, NEEC and interference terms. As the radiative decay of the nucleus involves photons with a certain multipolarity and parity, we use the spherical wave expansion of the radiation field to calculate RR matrix elements and cross sections. The latter are compared with other theoretical results [IE00] in order to check the numerical accuracy of our calculations. Numerical results for the interference cross sections are presented in the last section of this chapter.

4.1 Interference term in the total cross section

In Chapter 2 we have presented a versatile formalism that allows us to write the total cross section for the photo recombination process involving RR and NEEC using the perturbation expansion of the transition operator T,

$$\begin{aligned}\sigma_{i\to f}(E) &= \frac{2\pi}{F_i}\sum_{M_f m_d}\sum_{M}\frac{1}{2(2I_i+1)}\sum_{M_i m_s}\frac{1}{4\pi} \\ &\times \int d\Omega_{\vec{p}}\lim_{\epsilon\to 0+}|\langle\Psi_f|T(E+i\epsilon)|\Psi_i\rangle|^2\rho_f\ . \end{aligned} \tag{4.1}$$

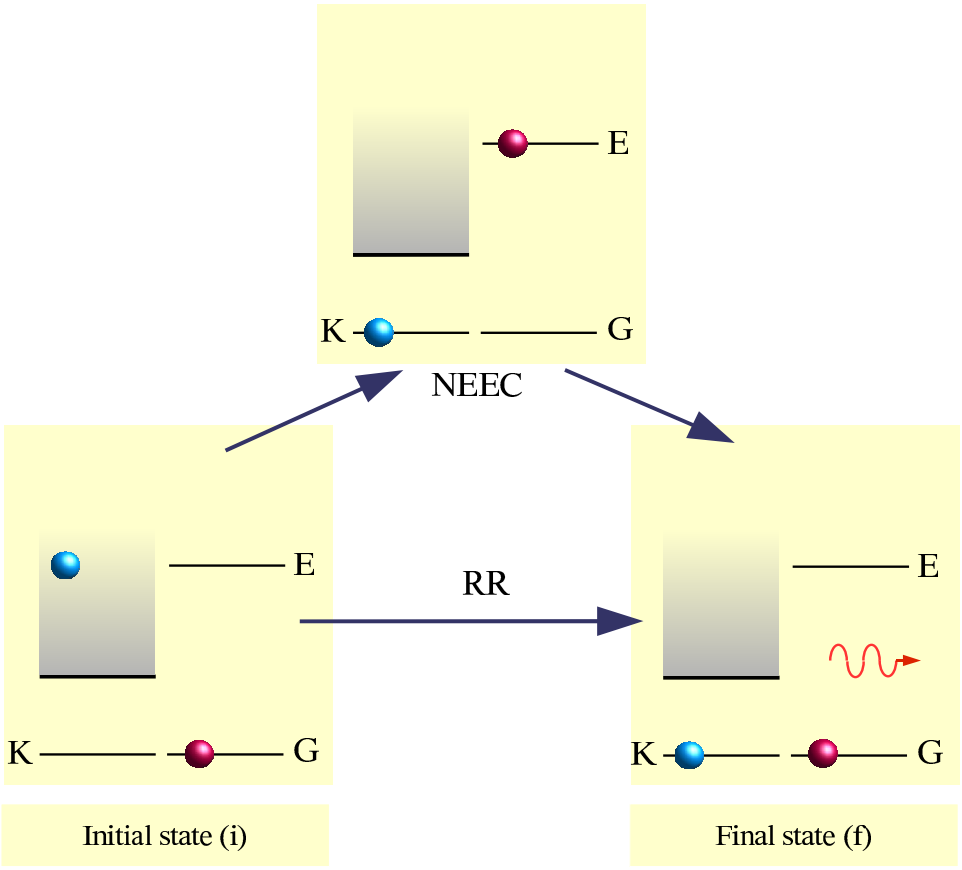

Figure 4.1: NEEC and RR recombination mechanisms of a continuum electron into the K shell of a bare ion. The nucleus is schematically represented as undergoing the transition from the ground state (G) to the excited state (E) and then again to the ground state.

Here we average over the initial states and sum over the final states that cannot be discerned in an experiment. As it was shown in Section 1.3, the matrix element of the transition operator for the considered process can be written as

$$\begin{aligned}\langle\Psi_f|T(z)|\Psi_i\rangle = \quad & \langle\Psi_f|H_{er}|\Psi_i\rangle + \\ & \frac{\langle\Psi_f|H_{nr}|\Psi_d\rangle\langle\Psi_d|H_{en}+H_{magn}|\Psi_i\rangle}{z-E_d+\frac{i}{2}\Gamma_d} \ . \end{aligned} \tag{4.2}$$

With this expression for the transition operator we can write the total cross section of the photo recombination process in Eq. (4.1) as

$$\begin{aligned}\sigma_{i\to f}(E) \ = \ & \frac{2\pi}{F_i}\sum_{M_f m_d}\sum_{M}\frac{\rho_f}{2(2I_i+1)}\sum_{M_i m_s}\frac{1}{4\pi}\int d\Omega_{\vec{p}} \\ \times \ & \Bigg|\sum_{M_d}\frac{\langle NI_fM_f,n_d\kappa_d m_d,\lambda kLM|H_{nr}|N^*I_dM_d,n_d\kappa_d m_d,0\rangle}{(E-E_d)+\frac{i}{2}\Gamma_d} \\ & \times\langle N^*I_dM_d,n_d\kappa_d m_d,0|H_{en}+H_{magn}|NI_iM_i,\vec{p}m_s,0\rangle \\ & +\langle NI_fM_f,n_d\kappa_d m_d,\lambda kLM|H_{er}|NI_iM_i,\vec{p}m_s,0\rangle\Bigg|^2 \ , \end{aligned} \tag{4.3}$$

where the first term in the modulus squared accounts for NEEC and the second one for RR. The total cross section can be separated in three terms,

$$\sigma_{i\to f}(E)=\sigma_{\rm NEEC}(E)+\sigma_{\rm RR}(E)+\sigma_{\rm int}(E) \ . \tag{4.4}$$

The RR and NEEC terms are given by

$$\begin{aligned}\sigma_{\rm RR}(E) \ = \ & \frac{2\pi}{F_i}\sum_{M_f m_d}\sum_{M}\frac{\rho_f}{2(2I_i+1)}\sum_{M_i m_s}\frac{1}{4\pi}\int d\Omega_{\vec{p}} \\ & \times|\langle NI_fM_f,n_d\kappa_d m_d,\lambda kLM|H_{er}|NI_iM_i,\vec{p}m_s,0\rangle|^2 \ , \end{aligned} \tag{4.5}$$

and

$$\begin{aligned}\sigma_{\rm NEEC}(E) = & \frac{2\pi}{F_i}\sum_{M_f m_d}\sum_{MM_d}\frac{\rho_f}{2(2I_i+1)}\sum_{M_i m_s}\frac{1}{4\pi}\int d\Omega_{\vec{p}} \\ & \times\frac{\Big|\langle NI_fM_f,n_d\kappa_d m_d,\lambda kLM|H_{nr}|N^*I_dM_d,n_d\kappa_d m_d,0\rangle\Big|^2}{(E-E_d)^2+\frac{\Gamma_d^2}{4}} \\ & \times\Big|\langle N^*I_dM_d,n_d\kappa_d m_d,0|H_{en}+H_{magn}|NI_iM_i,\vec{p}m_s,0\rangle\Big|^2 \ . \end{aligned} \tag{4.6}$$

The interference term between RR and NEEC can be written as

$$\begin{aligned}\sigma_{\rm int}(E) &= \frac{2\pi}{F_i}\sum_{M_f m_d}\sum_{M M_d}\frac{\rho_f}{2(2I_i+1)}\sum_{M_i m_s}\frac{1}{4\pi}\int d\Omega_{\vec{p}} \\ &\times \left(\frac{\langle NI_fM_f, n_d\kappa_d m_d, \lambda kLM|H_{nr}|N^*I_dM_d, n_d\kappa_d m_d, 0\rangle}{(E-E_d)+\frac{i}{2}\Gamma_d}\right. \\ &\times\langle N^*I_dM_d, n_d\kappa_d m_d, 0|H_{en}+H_{magn}|NI_iM_i, \vec{p}m_s, 0\rangle \\ &\left.\times\langle NI_fM_f, n_d\kappa_d m_d, \lambda kLM|H_{er}|NI_iM_i, \vec{p}m_s, 0\rangle^* + \text{H.c.}\right) .\end{aligned} \tag{4.7}$$

In the following we consider the interference term $\sigma_{\rm int}$ in the total cross section. As the electron-radiation interaction Hamiltonian H_{er} does not affect the nucleus, the initial and the final nuclear total angular momenta as well as their projections have to coincide in its matrix element,

$$\begin{aligned}&\langle NI_fM_f, n_d\kappa_d m_d, \lambda kLM|H_{er}|NI_iM_i, \vec{p}m_s, 0\rangle = \\ &\delta_{I_iI_f}\delta_{M_fM_i}\langle n_d\kappa_d m_d, \lambda kLM|H_{er}|\vec{p}m_s, 0\rangle \ .\end{aligned} \tag{4.8}$$

We also simplify the notations of the other two matrix elements,

$$\begin{aligned}&\langle NI_fM_f, n_d\kappa_d m_d, \lambda kLM|H_{nr}|N^*I_dM_d, n_d\kappa_d m_d, 0\rangle = \\ &\langle NI_fM_f, \lambda kLM|H_{nr}|N^*I_dM_d, 0\rangle\end{aligned} \tag{4.9}$$

and

$$\begin{aligned}&\langle N^*I_dM_d, n_d\kappa_d m_d, 0|H_{en}+H_{magn}|NI_iM_i, \vec{p}m_s, 0\rangle = \\ &\langle N^*I_dM_d, n_d\kappa_d m_d|H_{en}+H_{magn}|NI_iM_i, \vec{p}m_s\rangle \ .\end{aligned} \tag{4.10}$$

Using the partial wave expansion in Eq. (2.36) for the initial state continuum electronic wave function we can write the interference cross section as

$$\begin{aligned}\sigma_{\rm int}(E) &= \frac{2\pi}{F_i}\sum_{M_dM_i}\sum_{M m_d}\frac{\rho_f}{2(2I_i+1)}\sum_{\kappa m}\frac{1}{4\pi} \\ &\times \left(\frac{\langle NI_iM_i, \lambda kLM|H_{nr}|N^*I_dM_d, 0\rangle}{(E-E_d)+\frac{i}{2}\Gamma_d}\right. \\ &\times\langle N^*I_dM_d, n_d\kappa_d m_d|H_{en}+H_{magn}|NI_iM_i, \varepsilon\kappa m\rangle \\ &\left.\times\langle n_d\kappa_d m_d, \lambda kLM|H_{er}|\varepsilon\kappa m, 0\rangle^* + \text{H.c.}\right) .\end{aligned} \tag{4.11}$$

The bracket in the above expression can be written as twice the real part of the matrix element product. It is also useful to eliminate the complex denominator,

so that the interference cross section reads

$$\begin{aligned}\sigma_{\rm int}(E) &= \frac{2\pi}{F_i}\sum_{M_dM_i}\sum_{Mm_d}\frac{\rho_f}{2I_i+1}\sum_{\kappa m}\frac{1}{4\pi}\frac{2\pi}{\Gamma_d}L_d(E-E_d)\\ &\times \mathrm{Re}\Bigg[\left((E-E_d)-\frac{i\Gamma_d}{2}\right)\langle NI_iM_i,\lambda kLM|H_{nr}|N^*I_dM_d,0\rangle\\ &\quad\times\langle N^*I_dM_d,n_d\kappa_dm_d|H_{en}+H_{magn}|NI_iM_i,\varepsilon\kappa m\rangle\\ &\quad\times\langle n_d\kappa_dm_d,\lambda kLM|H_{er}|\varepsilon\kappa m,0\rangle^*\Bigg]\,, \end{aligned}\tag{4.12}$$

with the Lorentz profile defined in Eq. (1.54). From Eq. (1.55) we can express $L_d(E-E_d)$ with the help of the NEEC total cross section, so that the interference term reads

$$\begin{aligned}\sigma_{\rm int}(E) &= \frac{p^2}{2\pi F_i}\sum_{M_dM_i}\sum_{Mm_d}\frac{\rho_f}{2I_i+1}\sum_{\kappa m}\frac{\sigma_{\rm NEEC}(E)}{A_r^{d\to f}Y_n^{i\to d}}\\ &\times \mathrm{Re}\Bigg[\left((E-E_d)-\frac{i\Gamma_d}{2}\right)\langle NI_iM_i,\lambda kLM|H_{nr}|N^*I_dM_d,0\rangle\\ &\quad\times\langle N^*I_dM_d,n_d\kappa_dm_d|H_{en}+H_{magn}|NI_iM_i,\varepsilon\kappa m\rangle\\ &\quad\times\langle n_d\kappa_dm_d,\lambda kLM|H_{er}|\varepsilon\kappa m,0\rangle^*\Bigg]\,, \end{aligned}\tag{4.13}$$

where $Y_n^{i\to d}$ is the NEEC rate in Eq. (1.51) and $A_r^{d\to f}$ is the nuclear radiative rate in Eq. (1.52). Following the outline from [Fan61], we introduce the generalized dimensionless Fano profile parameter Q_f, whose inverse is defined as

$$\begin{aligned}\frac{1}{Q_f} &= \pi\rho_i\sum_{M_dM_i}\sum_{Mm_d}\sum_{\kappa m}\langle N^*I_dM_d,n_d\kappa_dm_d|H_{en}+H_{magn}|NI_iM_i,\varepsilon\kappa m\rangle\\ &\times\ \langle n_d\kappa_dm_d,\lambda kLM|H_{er}|\varepsilon\kappa m,0\rangle^*\\ &\times\ \frac{\langle NI_iM_i,\lambda kLM|H_{nr}|N^*I_dM_d,0\rangle}{\sum_{M_i'M'}\sum_{M_d'}\left|\langle NI_iM_i',k\lambda LM'|H_{nr}|N^*I_dM_d',0\rangle\right|^2}\,. \end{aligned}\tag{4.14}$$

The nuclear radiative rate has been written explicitly and prime indices have been used for the summation in order to avoid any confusion. The interference cross section can then be written as

$$\sigma_{\rm int}(E)=\sigma_{\rm NEEC}(E)\frac{\Gamma_d}{Y_n^{i\to d}}\frac{2I_d+1}{2I_i+1}\left(2\frac{E-E_d}{\Gamma_d}\mathrm{Re}\left(\frac{1}{Q_f}\right)+\mathrm{Im}\left(\frac{1}{Q_f}\right)\right)\,.\tag{4.15}$$

With the further observation that the Fano profile parameter $1/Q_f$ is for both electric and magnetic cases real, the interference cross section yields

$$\sigma_{\rm int}(E)=\sigma_{\rm NEEC}(E)\frac{2(E-E_d)}{Y_n^{i\to d}}\frac{2I_d+1}{2I_i+1}\frac{1}{Q_f}\,.\tag{4.16}$$

In the following two sections the expression of the Fano profile parameter is calculated for electric and magnetic transitions.

The most conspicuous manifestation of the interference between RR and NEEC is expected to be the asymmetric energy profile of the total cross section of the recombination process. Behar and co-workers [BJO$^+$00] have introduced a parameter that reflects the degree of asymmetry in the total PR process involving RR and DR. Considering the parallel between DR and NEEC, we introduce the profile asymmetry parameter $R^{\rm int}$ defined as

$$R^{\rm int} = \left| \frac{\sigma_{\rm int}(\varepsilon_{\pm 1/2})}{\sigma_{\rm NEEC}(\varepsilon_{\pm 1/2})} \right| = \frac{\Gamma_d}{Y_n^{i\to d}} \frac{2I_d+1}{2I_i+1} \frac{1}{|Q_f|} \ , \tag{4.17}$$

where the interference and NEEC contributions have been evaluated at the two energies

$$\varepsilon_{\pm 1/2} = E_d \pm \frac{\Gamma_d}{2} \ . \tag{4.18}$$

At these values the interference contribution has an extremum due to a single isolated resonance d, and the Lorentzian function describing the energy dependence of the NEEC cross section attains one half of its maximum. The numerical values of the Fano and asymmetry profile parameters for the considered systems are presented in Section 4.4.

4.2 Electric transitions

In the following we consider the interference between NEEC and RR for electric transitions of the nucleus and derive the expression of the Fano profile parameter. This calculation involves the matrix elements of the interaction Hamiltonians H_{en}, H_{er} and H_{nr}.

In the case of the electric transitions, the matrix element corresponding to the NEEC process for a given partial wave component and a given multipolarity L can then be written as

$$\begin{aligned}
&\langle N^* I_d M_d, n_d \kappa_d m_d | H_{en} | N I_i M_i, \varepsilon \kappa m \rangle = \\
&\sum_{\mu=-L}^{L} (-1)^{I_d+M_i+L+\mu+m+3j_d} R_0^{-(L+2)} R^{(e)}_{L,\kappa_d,\kappa} \langle N^* I_d \| Q_L \| N I_i \rangle \\
&\times \sqrt{2j_d+1} \sqrt{\frac{4\pi}{(2L+1)^3}} \ C(I \ I_d \ L; -M_i \ M_d \ \mu) \\
&\times \ C(j \ j_d \ L; -m \ m_d \ -\mu) \ C\left(j_d \ L \ j; \frac{1}{2} \ 0 \ \frac{1}{2}\right) \ ,
\end{aligned} \tag{4.19}$$

with the electronic radial integral $R^{(e)}_{L,\kappa_d,\kappa}$ given in Eq. (2.38). For the matrix element of the interaction Hamiltonian between the nucleus and the radiation field H_{nr}, we follow the outline in [RS80], considering that the wavelength of the radiation is large compared to the nuclear radius, $kR_q \ll 1$, so that the Bessel functions can be approximated in the first order in kr as

$$j_L(kr) \simeq \frac{(kr)^L}{(2L+1)!!} \ . \tag{4.20}$$

In this case the electric solution of the wave equation can be written as

$$\vec{A}_{(e)kLM}(\vec{r}) = -\sqrt{\frac{4\pi ck}{R}}\frac{\sqrt{(L+1)(2L+1)}}{(2L+1)!!}(kr)^{L-1}\vec{Y}^M_{LL-1}(\theta,\varphi)\ . \tag{4.21}$$

The matrix element of the nucleus-radiation interaction Hamiltonian then reads

$$\begin{aligned}\langle NIM_f,(e)kLM|H_{nr}|N^*I_dM_d,0\rangle &= \sqrt{\frac{4\pi k}{cR}}\frac{\sqrt{(L+1)(2L+1)}}{(2L+1)!!}\\ \times\langle NIM_f|\int d^3r(kr)^{L-1}\vec{j}_n(\vec{r})\cdot\vec{Y}^M_{LL-1}(\theta,\varphi)|N^*I_dM_d\rangle\ .&\end{aligned} \tag{4.22}$$

In order to evaluate the integral over the nuclear coordinate in the matrix element we further make use of the properties of the vector spherical harmonics and write $\vec{Y}^M_{LL-1}$ as [BEG85]

$$\vec{Y}^M_{LL-1}(\theta,\varphi) = \sqrt{\frac{L}{2L+1}}Y_{LM}(\theta,\varphi)\vec{e}_r + \frac{1}{\sqrt{L(2L+1)}}\,r\,\nabla Y_{LM}(\theta,\varphi)\ , \tag{4.23}$$

where $\vec{e}_r$ stands for the radial unit vector. After integrating by parts and using the continuity equation for the nuclear current $\vec{j}_n$ the matrix element yields

$$\begin{aligned}&\langle NI_iM_i,(e)kLM|H_{nr}|N^*I_dM_d,0\rangle =\\ &(-1)^{I_d-M_d+1}\sqrt{\frac{4\pi ck}{R}}C\,(I_i\ I_d\ L;M_i\ -M_d\ M)\\ &\times\frac{\sqrt{L+1}}{\sqrt{L(2L+1)}}\frac{ik^L}{(2L+1)!!}\langle NI_i\|Q_L\|N^*I_d\rangle\ .\end{aligned} \tag{4.24}$$

The remaining matrix element of H_{er} can be evaluated by writing the electric solution of the wave equation in a more suitable form

$$\begin{aligned}\vec{A}_{(e)kLM}(\vec{r}) \;=\; &\sqrt{\frac{4\pi ck}{R}}\left(\sqrt{\frac{L}{2L+1}}j_{L+1}(kr)\vec{Y}^M_{LL+1}(\theta,\varphi)\right.\\ &\left.-\sqrt{\frac{L+1}{2L+1}}j_{L-1}(kr)\vec{Y}^M_{LL-1}(\theta,\varphi)\right)\ .\end{aligned} \tag{4.25}$$

The electron-radiation interaction matrix element then yields

$$\begin{aligned}&\langle n_d\kappa_dm_d,(e)kLM|H_{er}|\varepsilon\kappa m,0\rangle = -\sqrt{\frac{4\pi ck}{R}}\\ &\times\left(\sqrt{\frac{L}{2L+1}}\langle n_d\kappa_dm_d|j_{L+1}(kr)\vec{\alpha}\cdot\vec{Y}^M_{LL+1}(\theta,\varphi)|\varepsilon\kappa m\rangle\right.\\ &\left.-\sqrt{\frac{L+1}{2L+1}}\langle n_d\kappa_dm_d|j_{L-1}(kr)\vec{\alpha}\cdot\vec{Y}^M_{LL-1}(\theta,\varphi)|\varepsilon\kappa m\rangle\right)\ .\end{aligned} \tag{4.26}$$

The matrix elements containing the product of the Bessel spherical functions, the Dirac α matrix and the vector spherical harmonics can be expressed in an

elegant way using the properties of the spherical tensor operators (the complete calculation is given in Appendix C). The expression in the above equation becomes

$$\begin{aligned}
&\langle n_d\kappa_d m_d,(e)kLM|H_{er}|\varepsilon\kappa m,0\rangle = \\
&i(-1)^{j-L+\frac{1}{2}}\sqrt{\frac{4\pi ck}{R}}\,C(j\ L\ j_d;m\ M\ m_d)\sqrt{\frac{2j+1}{4\pi}}\begin{pmatrix} j_d & j & L \\ \frac{1}{2} & -\frac{1}{2} & 0\end{pmatrix} \\
&\times\left[\sqrt{\frac{L+1}{L(2L+1)}}(LI^-_{L-1}-(\kappa_d-\kappa)I^+_{L-1})\right. \\
&\left.+\sqrt{\frac{L}{(L+1)(2l+1)}}((L+1)I^-_{L+1}+(\kappa_d-\kappa)I^+_{L+1})\right]\ , \qquad (4.27)
\end{aligned}$$

with the radial integrals

$$I^{\pm}_L=\int_0^\infty drr^2 j_L(kr)\left(g_{\kappa_d}(r)f_{\varepsilon\kappa}(r)\pm g_{\varepsilon\kappa}(r)f_{\kappa_d}(r)\right)\ . \qquad (4.28)$$

Collecting the formulas of the three matrix elements from Eqs. (4.19), (4.24) and (4.27) in the expression of the Fano profile parameter and using the summation properties of the Clebsch-Gordan coefficients we obtain

$$\begin{aligned}
\frac{1}{Q_f} \;=\;& \pi\rho_i(-1)^{I_i-I_d+1}R_0^{-(L+2)}(2j_d+1)\sqrt{\frac{L}{(L+1)(2L+1)^3}} \\
&\times k^{-L}(2L+1)!!\sum_\kappa R_{L,\kappa_d,\kappa}(2j+1)\begin{pmatrix} j_d & j & L \\ \frac{1}{2} & -\frac{1}{2} & 0\end{pmatrix}^2 \\
&\times\left[\sqrt{\frac{L+1}{L(2L+1)}}(LI^-_{L-1}-(\kappa_d-\kappa)I^+_{L-1})\right. \\
&\left.+\sqrt{\frac{L}{(L+1)(2L+1)}}((L+1)I^-_{L+1}+(\kappa_d-\kappa)I^+_{L+1})\right]\ . \qquad (4.29)
\end{aligned}$$

4.3 Magnetic transitions

In the case of interference involving magnetic transitions, the expression of the Fano profile parameter involves the matrix elements of the interaction Hamiltonians H_{magn}, H_{er} and H_{nr}. The NEEC matrix element for the magnetic transition for a given partial wave and a given multipolarity can be written as

$$\begin{aligned}
&\langle N^*I_dM_d,n_d\kappa_dm_d|H_{magn}|NI_iM_i,\varepsilon\kappa m\rangle = \\
&4\pi i\sqrt{\frac{L+1}{L(2L+1)^3}}\sum_\mu(-1)^{I_i-M_i+\mu+1}\,C(I_d\ I\ L;M_d\ -M_i\ \mu) \qquad (4.30)\\
&\times\langle N^*I_d||M_L||NI\rangle\langle n_d\kappa_dm_d|r^{-(L+1)}\vec{\alpha}\cdot\vec{Y}^{-\mu}_{LL}(\theta,\varphi)|\varepsilon\kappa m\rangle\ ,
\end{aligned}$$

as shown in Section 2.3. The electronic matrix element can be evaluated using the properties of the spherical tensors as shown in Appendix C to yield

$$\begin{aligned}&\langle n_d\kappa_d m_d|r^{-(L+1)}\vec{\alpha}\cdot\vec{Y}_{LL}^{-\mu}(\theta,\varphi)|\varepsilon\kappa m\rangle = \\ &i(-1)^{j-L+\frac{1}{2}}\sqrt{\frac{(2j+1)(2L+1)}{4\pi L(L+1)}}\,C(j\ L\ j_d;m\ -\mu\ m_d)(\kappa_d+\kappa) \\ &\times\begin{pmatrix} j_d & j & L \\ \frac{1}{2} & -\frac{1}{2} & 0\end{pmatrix}\int_0^\infty dr r^{-L+1}\left(g_{\kappa_d}(r)f_{\varepsilon\kappa}(r)+f_{\kappa_d}(r)g_{\varepsilon\kappa}(r)\right)\ .\end{aligned} \tag{4.31}$$

The matrix element corresponding to RR has, up to the presence of the spherical Bessel functions, a similar expression,

$$\langle n_d\kappa_d m_d,(m)kLM|H_{er}|\varepsilon\kappa m,0\rangle = -\sqrt{\frac{4\pi ck}{R}}\langle n_d\kappa_d m_d|j_L(kr)\vec{\alpha}\cdot\vec{Y}_{LL}^{M}(\theta,\varphi)|\varepsilon\kappa m\rangle\ . \tag{4.32}$$

Using the properties of the spherical tensor operators, we can write the RR matrix element as

$$\begin{aligned}&\langle n_d\kappa_d m_d,(m)kLM|H_{er}|\varepsilon\kappa m,0\rangle = \\ &\sqrt{\frac{4\pi ck}{R}}i(-1)^{j-L-\frac{1}{2}}\sqrt{\frac{(2j+1)(2L+1)}{4\pi L(L+1)}}\,C(j\ L\ j_d;m\ M\ m_d)(\kappa_d+\kappa) \\ &\times\begin{pmatrix} j_d & j & L \\ \frac{1}{2} & -\frac{1}{2} & 0\end{pmatrix}\int_0^\infty dr j_L(kr)\left(g_{\kappa_d}(r)f_{\varepsilon\kappa}(r)+f_{\kappa_d}(r)g_{\varepsilon\kappa}(r)\right)\ .\end{aligned} \tag{4.33}$$

The remaining matrix element involved in the expression of the Fano profile parameter Q_f is the one of the interaction between the nucleus and the radiation field. We make use again of the long-wavelength approximation, so that the spherical Bessel functions are written as in Eq. (4.20). With this approximation and using the properties of the vector spherical harmonics the magnetic solution of the wave equation has the expression

$$\vec{A}_{(m)kLM}(\vec{r}) = \sqrt{\frac{4\pi ck}{R}}\frac{k^L}{i\sqrt{L(L+1)}}\frac{1}{(2L+1)!!}(\vec{r}\times\nabla)(r^L Y_{LM}(\theta,\varphi))\ . \tag{4.34}$$

Rewriting the Hamiltonian H_{nr} we obtain

$$\begin{aligned}H_{nr} &= i\sqrt{\frac{4\pi ck}{R}}\sqrt{\frac{L+1}{L}}\frac{k^L}{(2L+1)!!}\frac{1}{c(L+1)} \\ &\quad\times\int d^3r_n(\vec{r}_n\times\vec{j}_n(\vec{r}_n))\cdot\nabla(r_n^L Y_{LM}(\theta_n,\varphi_n))\ .\end{aligned} \tag{4.35}$$

The integral over the nuclear coordinate can be related to the magnetic multipole operator M_{LM}, defined as [RS80]

$$M_{LM} = \frac{1}{c(L+1)}\int d^3r_n(\vec{r}_n\times\vec{j}_n(\vec{r}_n))\cdot\nabla(r_n^L Y_{LM}(\theta_n,\varphi_n))\ . \tag{4.36}$$

The matrix element of the interaction Hamiltonian between the radiation field and the nucleus yields

$$\begin{aligned}
&\langle NI_iM_i,(m)kLM|H_{nr}|N^*I_dM_d,0\rangle = \\
&i\sqrt{\frac{4\pi ck}{R}}\frac{k^L}{\sqrt{L}}\frac{\sqrt{L+1}}{(2L+1)!!}\langle NI_iM_i|M_{LM}|N^*I_dM_d\rangle \\
&= (-1)^{I_d-M_d}i\sqrt{\frac{4\pi ck}{R}}\frac{k^L}{(2L+1)!!}\sqrt{\frac{L+1}{L(2L+1)}} \\
&\times C\left(I_d\ I_i\ L; M_d\ -M_i\ -M\right)\langle NI_i\|M_L\|N^*I_d\rangle\ . \qquad (4.37)
\end{aligned}$$

We combine the results from Eqs. (4.31), (4.33) and (4.37) and use the summation properties of the Clebsch-Gordan coefficients in order to obtain the expression of the inverse of the dimensionless Fano profile parameter Q_f,

$$\begin{aligned}
\frac{1}{Q_f} &= \frac{\pi\rho_i(-1)^{I_i-I_d+1}(2j_d+1)}{L(2L+1)(L+1)}k^{-L}(2L+1)!!\sum_\kappa(2j+1)(\kappa_d+\kappa)^2 \\
&\times\begin{pmatrix} j_d & j & L \\ \frac{1}{2} & -\frac{1}{2} & 0\end{pmatrix}^2\int_0^\infty dr r^{-L+1}\left(g_{\kappa_d}(r)f_{\varepsilon\kappa}(r)+f_{\kappa_d}(r)g_{\varepsilon\kappa}(r)\right) \\
&\times\int_0^\infty dr j_L(kr)\left(g_{\kappa_d}(r)f_{\varepsilon\kappa}(r)+f_{\kappa_d}(r)g_{\varepsilon\kappa}(r)\right)\ . \qquad (4.38)
\end{aligned}$$

4.4 Numerical results

We have calculated the Fano profile parameters and the profile asymmetry parameters for the collision systems involving electric $E2$ and magnetic $M1$ transitions considered in Chapter 3. The capture of the electron occurs either into the K shell of a bare ion or into the L shell of an ion with a closed $1s^2$ configuration. For the calculation of the radial integrals corresponding to the NEEC and RR matrix elements, we have used the same Coulomb-Dirac wave functions for the continuum electron and GRASP92 radial wave functions considering a homogeneously charged nucleus to describe the bound state. Values of the Fano and asymmetry profile parameters, the NEEC rate and the natural width of the nuclear excited state are presented in Table 4.1 for the electric $E2$ transitions and in Table 4.2 for the magnetic $M1$ transitions. The cases with the largest profile asymmetry parameter $R^{\rm int}$ are the ones that display the most obvious interference effect. This are the capture into the $1s$ orbital of $^{174}_{70}$Yb in the case of the electric transitions and the capture into the $2p_{3/2}$ of $^{155}_{64}$Gd among the magnetic transitions. However, due to the small resonance strength of the NEEC cross section for $^{155}_{64}$Gd, the interference effect in this case is not likely to be observed experimentally with the present techniques.

A possibility to cross-check our accuracy is given by the matrix element of the interaction Hamiltonian H_{er}, which enters the expression of the Fano profile parameter. We can calculate the total cross section for RR for a given energy, that is in the spherical wave approach

$$\sigma_{\rm RR} = \frac{2\pi}{F_i}\frac{1}{2}\sum_{m_s}\frac{1}{4\pi}\int d\Omega_{\vec{p}}\sum_{m_d}\sum_{\lambda LM}|\langle n_d\kappa_d m_d,\lambda kLM|H_{er}|\vec{p}m_s,0\rangle|^2\rho_f\ . \quad (4.39)$$

Table 4.1: The Fano and asymmetry profile parameters and the NEEC rates for various heavy ion collision systems which involve electric $E2$ multipole transitions. E_d is the energy of the continuum electron at the resonance and Γ_d is the width of the excited nuclear state. The notation nl_j is used for the capture orbital.

${}^{A}_{Z}\mathrm{X}$	E_d(keV)	nl_j	$Y_n(1/s)$	Γ_d(eV)	$1/Q_f$	R^{int}
${}^{164}_{66}$Dy	10.318	$1s_{1/2}$	1.86×10^{8}	4.37×10^{-8}	-2.11×10^{-3}	3.67×10^{-3}
${}^{170}_{68}$Er	11.350	$1s_{1/2}$	2.23×10^{8}	5.75×10^{-8}	-2.07×10^{-3}	4.05×10^{-3}
${}^{174}_{70}$Yb	4.897	$1s_{1/2}$	1.79×10^{8}	4.85×10^{-8}	-2.09×10^{-3}	4.30×10^{-3}
${}^{154}_{64}$Gd	64.005	$1s_{1/2}$	5.69×10^{8}	2.51×10^{-7}	-2.61×10^{-4}	8.77×10^{-4}
${}^{156}_{64}$Gd	74.742	$2s_{1/2}$	3.35×10^{7}	1.21×10^{-7}	-6.10×10^{-5}	1.67×10^{-3}
${}^{156}_{64}$Gd	74.896	$2p_{1/2}$	1.16×10^{8}	1.32×10^{-7}	- 1.16×10^{-5}	1.00×10^{-4}
${}^{156}_{64}$Gd	75.680	$2p_{3/2}$	1.59×10^{8}	1.27×10^{-7}	3.06×10^{-4}	1.86×10^{-3}
${}^{162}_{66}$Dy	65.432	$2s_{1/2}$	2.81×10^{7}	9.39×10^{-8}	-1.28×10^{-4}	3.26×10^{-3}
${}^{162}_{66}$Dy	65.594	$2p_{1/2}$	1.59×10^{8}	1.11×10^{-7}	-5.78×10^{-5}	3.06×10^{-4}
${}^{162}_{66}$Dy	66.492	$2p_{3/2}$	2.15×10^{8}	1.04×10^{-7}	3.56×10^{-4}	1.31×10^{-3}
${}^{236}_{92}$U	12.404	$2s_{1/2}$	1.06×10^{8}	1.76×10^{-8}	1.60×10^{-3}	2.00×10^{-3}
${}^{236}_{92}$U	12.698	$2p_{1/2}$	3.02×10^{9}	4.01×10^{-7}	-1.26×10^{-3}	1.27×10^{-3}
${}^{236}_{92}$U	16.871	$2p_{3/2}$	3.10×10^{9}	2.07×10^{-7}	-9.86×10^{-4}	5.01×10^{-4}
${}^{238}_{92}$U	12.073	$2s_{1/2}$	1.11×10^{8}	1.81×10^{-8}	1.61×10^{-3}	2.01×10^{-3}
${}^{238}_{92}$U	12.356	$2p_{1/2}$	3.14×10^{9}	4.17×10^{-7}	-1.24×10^{-3}	1.25×10^{-3}
${}^{238}_{92}$U	16.534	$2p_{3/2}$	3.23×10^{9}	2.16×10^{-7}	-9.97×10^{-4}	5.07×10^{-4}
${}^{248}_{96}$Cm	6.888	$2s_{1/2}$	2.18×10^{8}	3.25×10^{-8}	1.92×10^{-3}	2.16×10^{-3}
${}^{248}_{96}$Cm	7.190	$2p_{1/2}$	5.47×10^{9}	7.24×10^{-7}	-5.96×10^{-4}	5.99×10^{-4}
${}^{248}_{96}$Cm	12.356	$2p_{3/2}$	5.33×10^{9}	3.54×10^{-7}	-1.43×10^{-3}	7.24×10^{-4}

Table 4.2: The Fano and asymmetry profile parameters and NEEC rates for various heavy ion collision systems which involve magnetic $M1$ transitions. E_d is the energy of the continuum electron at the resonance and Γ_d is the width of the excited nuclear state. The notation nl_j is used for the capture orbital.

${}^{A}_{Z}$X	E_d(keV)	nl_j	$Y_n(1/s)$	Γ_d(eV)	$1/Q_f$	$R^{\rm int}$
${}^{165}_{67}$Ho	29.563	$1s_{1/2}$	1.28×10^{10}	1.17×10^{-5}	-1.67×10^{-3}	2.90×10^{-3}
${}^{173}_{70}$Yb	7.073	$1s_{1/2}$	7.32×10^{9}	4.80×10^{-6}	-2.24×10^{-3}	2.98×10^{-3}
${}^{185}_{75}$Re	42.198	$1s_{1/2}$	2.62×10^{10}	2.36×10^{-5}	-2.58×10^{-3}	4.71×10^{-3}
${}^{187}_{75}$Re	51.083	$1s_{1/2}$	2.50×10^{10}	2.47×10^{-5}	-2.50×10^{-3}	5.00×10^{-3}
${}^{55}_{25}$Mn	117.378	$1s_{1/2}$	2.45×10^{7}	1.75×10^{-6}	-2.14×10^{-5}	3.10×10^{-3}
${}^{57}_{26}$Fe	5.135	$1s_{1/2}$	6.21×10^{6}	2.56×10^{-9}	-6.73×10^{-5}	8.42×10^{-5}
${}^{40}_{19}$K	24.896	$1s_{1/2}$	1.33×10^{7}	9.47×10^{-8}	-1.46×10^{-5}	1.22×10^{-4}
${}^{155}_{64}$Gd	45.784	$2s_{1/2}$	2.73×10^{8}	1.97×10^{-6}	-1.25×10^{-4}	2.06×10^{-3}
${}^{155}_{64}$Gd	45.938	$2p_{1/2}$	2.40×10^{7}	1.86×10^{-6}	-1.85×10^{-5}	3.27×10^{-3}
${}^{155}_{64}$Gd	46.722	$2p_{3/2}$	4.00×10^{6}	1.85×10^{-6}	-1.81×10^{-5}	1.91×10^{-2}
${}^{157}_{64}$Gd	40.309	$2s_{1/2}$	4.16×10^{8}	4.37×10^{-7}	-2.86×10^{-2}	3.00×10^{-4}
${}^{157}_{64}$Gd	40.463	$2p_{1/2}$	3.68×10^{7}	2.71×10^{-7}	-2.00×10^{-5}	3.36×10^{-4}
${}^{157}_{64}$Gd	41.247	$2p_{3/2}$	6.21×10^{6}	2.56×10^{-7}	-1.94×10^{-5}	1.82×10^{-3}

The expressions of the considered matrix elements are given in Eqs. (4.27) and (4.33) for electric and magnetic multipoles, respectively. The RR cross section is an infinite sum of both electric and magnetic multipoles. In practice, since the contribution of the higher terms is very small, we have only used the multipoles up to L=6. We compare in Table 4.3 the RR cross section for the studied systems involving capture into the bare ion at the resonance electron energy calculated with Eq. (4.39), with the tabulations from [IE00]. Eichler and Ichihara [IE00] have used the plane wave expansion of the electromagnetic field for a precise relativistic calculation of RR in bare ions. Their extensive tabulation of the RR cross section as a function of the electron energy with respect to the ion represents a benchmark in the field. We find our results for the RR cross section to be in very good agreement with the values in [IE00], which proves the accuracy of our electronic radial wave functions.

In Figure 4.2 we present plots of the interference and scaled NEEC cross section terms as a function of the continuum electron energy for the $M1$ transition of ${}^{185}_{75}$Re and $E2$ transition of ${}^{174}_{70}$Yb, respectively. These are the isotopes with the largest NEEC resonance strengths for the magnetic and electric multipole transitions, respectively. The NEEC cross section has the shape of a very narrow Lorentzian, with the width given by the natural width of the excited nuclear state, about $2.36\cdot10^{-5}$ eV for the case of ${}^{185}_{75}$Re and $4.85\cdot10^{-8}$ eV for the case of ${}^{174}_{70}$Yb. The interference term $\sigma_{\rm int}$ for both electric and magnetic cases is more than two orders of magnitude smaller that the NEEC terms $\sigma_{\rm NEEC}$. This is not unexpected as the NEEC total cross section at the resonance energy has much larger values than the RR background. For instance, in the case of

Table 4.3: RR total cross sections for the NEEC resonance energy E_d of the continuum electron, compared with results from [IE00]. For all cases the free electron is captured into the K-shell of a bare ion X^{q+}. The values from [IE00] are numerically interpolated by a spline routine to obtain the RR cross section for the resonance energy E_d.

		σ_{RR}(b)	
X^{q+}	E_d(keV)	this work	[IE00]
K^{19+}	24.896	6.64	6.55
Mn^{25+}	117.378	0.8653	0.8492
Fe^{26+}	5.135	216.75	216.71
Gd^{64+}	64.005	79.12	79.55
Dy^{66+}	10.318	832.00	832.36
Ho^{67+}	29.563	252.64	252.46
Er^{68+}	11.350	797.82	795.63
Yb^{70+}	4.897	2080.39	2083.66
Yb^{70+}	7.073	1413.14	1412.02
Re^{75+}	42.198	212.14	212.28
Re^{75+}	51.083	166.51	166.79

$^{174}_{70}$Yb, the peak NEEC cross section $\sigma_{\mathrm{NEEC}}(E_d) = 1.21 \cdot 10^6$ b, while the RR cross section, as shown in Table 4.3, is only about 2080 b. Furthermore, the magnitude of the interference term can be explained by investigating the contributions of the multipolarities that enter in the RR cross section σ_{RR}. While σ_{RR} consists of an infinite sum of multipolarities, in the interference process only the RR photon with the precise multipolarity of the nuclear transition participates. The main contribution to the RR cross section comes from the electric monopole $E1$ photon. The cross sections corresponding to the $M1$ and $E2$ photons are considerably smaller. In the case of $^{174}_{70}$Yb, the $E2$ photon accounts only for 121 b in the RR total cross section of 2080 b, while the $M1$ photon for $^{185}_{75}$Re only brings 0.5 b of the 212 b RR total cross section.

The interference cross sections are not large enough to undoubtedly play a role in the experimental observation of NEEC. This can be also qualitatively explained by the different time scales that characterize the two interfering processes. While RR is a fast process, the resonant channel of NEEC involves an intermediate state with a relatively long lifetime, given by the lifetime of the nuclear excited state. The shortest lifetime considered is in the order of tens of ps, which is still 'long' from the atomic physics point of view.

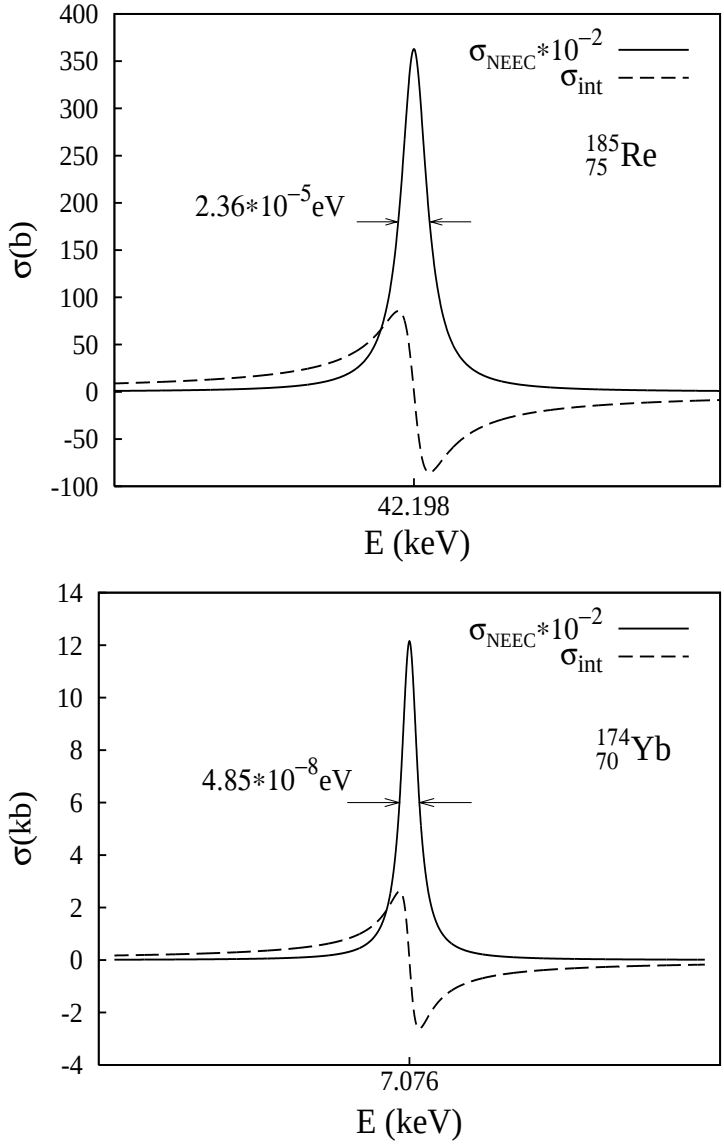

Figure 4.2: Interference and NEEC terms of the cross section for capture into bare Re^{75+} ions (top) and Yb^{70+} ions (bottom) as a function of the continuum electron energy. The NEEC term is scaled in both cases by a factor of 10^{-2}.

Chapter 5

Angular distribution of radiation emitted in NEEC

In the total cross section for recombination the photons emitted in the direct and resonant channels are indistinguishable. RR is expected to be a strong background in a NEEC experiment aiming to detect the photons emitted in the radiative decay of the nucleus. Together with the narrow natural width of the nuclear excited state, the competing RR is a major hindrance in the experimental observation of NEEC. The angular differential cross sections of the emitted photons can provide additional information on their origin and can act as a signature for the occurrence of NEEC.

In this chapter we investigate the angular distribution of the $E2$ radiation following the capture into the $1s$ orbital of several bare ions. We use the same density matrix formalism used for RR [FSS05] to calculate the angular distribution of the photons emitted in the radiative decay of the nucleus. Since its introduction in 1927 by von Neumann and Landau, the density matrix approach has been found to be a useful and elegant tool in many fields of modern physics. For applications in atomic physics, and combined in particular with the concept of spherical tensors, this approach has been developed by Fano [Fan57] in the late fifties. The density matrix theory has been used successfully ever since in a large number of case studies on atomic collisions, the excitation of atomic autoionizing states, the polarization effects in the radiative and Auger decay or even lifetime interferences in resonantly excited atoms.

Because the radiation properties are closely related to the alignment of the excited nuclear states, we first investigate their population as it arises due to the electron capture process. The reorientation of the nuclear axis caused by the electric field of a charged particle that excites the nucleus (reorientation effect) is a well-studied process in nuclear physics. The change in the nuclear spin directions following the Coulomb excitation of the nucleus by collisions with low-energy charged particles affects the angular distribution of the emitted γ rays [BGR56]. In the case of the electric radiative transitions, NEEC can be regarded as a Coulomb excitation with free electrons that are in the end captured by the bare ion.

In Section 5.3 we present numerical results for the photons emitted in the

radiative $E2$ decay of the nuclear state following the capture of the electron into the K-shell of several bare ions. The collision systems involving $M1$ transitions of the nucleus are not considered as they are expected to have a very similar angular pattern with RR. Furthermore, $M1$ transitions are often accompanied by strong $E2$ nuclear decays, which makes the interpretation of angular distribution data more intricate.

5.1 Alignment of the excited nuclear state

In NEEC the initial state of the combined system is given by the electron with the well-defined asymptotic momentum $\vec{p}$ and spin projection m_s, and the nucleus with the total angular momentum I_i and its projection M_i. Assuming that these two subsystems are uncorrelated, the overall initial density operator is given as the direct product of the initial density operators of the two subsystems :

$$\hat{\rho}_i = \hat{\rho}_{ion} \otimes \hat{\rho}_e \ . \tag{5.1}$$

If neither the electrons nor the ions are initially polarized, the tensor product can be written as

$$\hat{\rho}_i = \frac{1}{2}\frac{1}{2I_i+1} \sum_{m_s M_i} |NI_iM_i\rangle|\vec{p}m_s\rangle\langle\vec{p}m_s|\langle NI_iM_i| \ . \tag{5.2}$$

In the intermediate state following the capture of the electron, the statistical operators must describe both the electron in some bound ionic state $|n_d\kappa_d m_d\rangle$ and the excited nucleus $|N^*I_dM_d\rangle$. As known from the density matrix theory, the statistical operators of the initial and the (subsequent) intermediate states of the system are simply connected by [Blu81]

$$\hat{\rho}_d = \hat{T}\hat{\rho}_i\hat{T}^\dagger \, , \tag{5.3}$$

where $\hat{T}$ is the transition operator for the Coulomb interaction which causes the excitation of the nucleus, namely the Hamiltonian H_{en} given in Eq. (1.13),

$$H_{en} = \int d^3r_n \frac{\rho_n(\vec{r}_n)}{|\vec{r}_e - \vec{r}_n|} \ . \tag{5.4}$$

Assuming that the incident electrons and ions are initially unpolarized, we write conveniently the statistical operators in a matrix representation as

$$\begin{aligned}
&\langle N^*I_dM_d, n_d\kappa_d m_d|\hat{\rho}_d|N^*I_dM'_d, n_d\kappa_d m'_d,\rangle = \\
&\frac{1}{2}\frac{1}{2I_i+1} \sum_{m_s M_i} \langle N^*I_dM_d, n_d\kappa_d m_d|H_{en}|NI_iM_i, \vec{p}m_s\rangle \\
&\times\langle N^*I_dM'_d, n_d\kappa_d m'_d|H_{en}|NI_iM_i, \vec{p}m_s\rangle^* \ ,
\end{aligned} \tag{5.5}$$

The intermediate-state density matrix in the above equation still contains the complete information about the NEEC process and, thus, can be used to derive all the properties of the bound electron and the excited nucleus. For instance, by

assuming that the magnetic states m_d of the bound electron remain unobserved in the experiment, we may characterize the sublevel population of the excited nucleus $|N^*I_d\rangle$ in terms of the nuclear density matrix

$$\begin{aligned}&\langle N^*I_dM_d|\hat{\rho}_d^{ion}|N^*I_dM_d'\rangle = \\ &\frac{1}{2}\frac{1}{2I_i+1}\sum_{m_sM_im_d}\langle N^*I_dM_d,n_d\kappa_dm_d|H_{en}|NI_iM_i,\vec{p}m_s\rangle \\ &\times\langle N^*I_dM_d',n_d\kappa_dm_d|H_{en}|NI_iM_i,\vec{p}m_s\rangle^* \ . \end{aligned} \tag{5.6}$$

Here we have considered the trace over the quantum number m_d of the electron.

As seen from Eq. (5.6), the information about the states of the excited nucleus produced by the electron capture into the bare ions is now contained in the transition matrix elements $\langle N^*I_dM_d,n_d\kappa_dm_d|H_{en}|NI_iM_i,\vec{p}m_s\rangle$. These matrix elements contain the wave function $|\vec{p}m_s\rangle$ of a free electron with a definite asymptotic momentum. We consider the partial wave expansion of the continuum electron wave function choosing the direction of the electron momentum $\vec{p}$ as quantization axis [EM95],

$$|\vec{p}m_s\rangle = \sum_\kappa i^l e^{i\Delta_\kappa}\sqrt{4\pi(2l+1)}\,C\left(l\ \frac{1}{2}\ j;0\ m_s\ m_s\right)|\varepsilon\kappa m_s\rangle \ . \tag{5.7}$$

The Coulomb phases for the capture into the bare ion can be calculated as [EM95]

$$\Delta_\kappa = \frac{1}{2}arg\left(\frac{-\kappa+i\nu/W}{s+i\nu}\right) - arg(\Gamma(s+i\nu)) + \frac{\pi(l+1-s)}{2} \ , \tag{5.8}$$

where $W = E\alpha^2$, $\nu = \alpha ZW/\sqrt{W^2-1}$, $s = \sqrt{\kappa^2-(\alpha Z)^2}$. Here α is the fine structure constant, Z is the nuclear charge and E is the total electron energy. In the case of capture into ions with an initial closed shell – i.e., He-like – configuration, the phases can be approximated by using an effective nuclear charge of $Z_{\text{eff}} = Z - N_b$ in Eq. (5.8), with N_b being the number of bound electrons in the ion. The sufficiency of this approximation is confirmed by calculating the electrostatic potential induced by the screening electrons in the Dirac-Fock approximation and numerically determining the phases for the combined nuclear and screening potentials.

The intermediate nuclear density matrix (5.6) can be rewritten in the form

$$\begin{aligned}&\langle N^*I_dM_d|\hat{\rho}_d^{ion}|N^*I_dM_d'\rangle = \\ &\frac{1}{2}\frac{4\pi}{2I_i+1}\sum_{m_sM_im_d}\sum_{\kappa\kappa'} i^{l-l'}\,e^{i(\Delta_\kappa-\Delta_{\kappa'})}\sqrt{(2l+1)(2l'+1)} \\ &\times C\left(l\ \frac{1}{2}\ j;0\ m_s\ m_s\right)\langle N^*I_dM_d,n_d\kappa_dm_d|H_{en}|NI_iM_i,\varepsilon\kappa m_s\rangle \\ &\times C\left(l'\ \frac{1}{2}\ j';0\ m_s\ m_s\right)\langle N^*I_dM_d',n_d\kappa_dm_d|H_{en}|NI_iM_i,\varepsilon\kappa' m_s\rangle^* \ . \end{aligned} \tag{5.9}$$

This expression represents the most general form of the intermediate nuclear density matrix which allows us to study the properties of the excited nucleus.

However, for the analysis of the radiative deexcitation of the nucleus it is more convenient to represent the intermediate state in terms of the so-called statistical tensors [Blu81]

$$\begin{aligned}\rho_{kq}(N^*I_d) &= \sum_{M_d M'_d} (-1)^{I_d - M'_d} C(I_d\ I_d\ k; M_d\ -M'_d\ q) \\ &\times \langle N^* I_d M_d | \hat{\rho}_d^{ion} | N^* I_d M'_d \rangle \end{aligned} \tag{5.10}$$

that transform like spherical harmonics of rank k under a rotation of the coordinates. Although the density matrix (5.9) and the statistical tensors (5.10) are equivalent expressions, the latter enables us to exploit the rotational symmetry of free atoms and ions. The statistical tensors of the intermediate nucleus can be written as

$$\begin{aligned}\rho_{kq}(N^*I_d) &= \frac{4\pi}{2(2I_i+1)} \sum_{m_s\, M_i\, m_d} \sum_{\kappa\,\kappa'} \sum_{M_d\, M'_d} i^{l-l'}\, \mathrm{e}^{i(\Delta_\kappa - \Delta_{\kappa'})} (-1)^{I_d - M'_d} \\ &\times \sqrt{(2l+1)(2l'+1)}\, C(I_d\ I_d\ k; M_d\ -M'_d\ q) \\ &\times C\left(l\ \frac{1}{2}\ j; 0\ m_s\ m_s\right)\ C\left(l'\ \frac{1}{2}\ j'; 0\ m_s\ m_s\right) \\ &\times \langle N^* I_d M_d, n_d \kappa_d m_d | H_{en} | N I_i M_i, \varepsilon \kappa m_s \rangle \\ &\times \langle N^* I_d M'_d, n_d \kappa_d m_d | H_{en} | N I_i M_i, \varepsilon \kappa' m_s \rangle^* \ . \end{aligned} \tag{5.11}$$

The spin state of the excited nucleus is described by the reduced statistical tensors or alignment parameters

$$\mathcal{A}_k(N^*I_d) = \frac{\rho_{k0}(N^*I_d)}{\rho_{00}(N^*I_d)}\ , \tag{5.12}$$

which are directly related to the cross sections $\sigma_{i\to d}(E, N^*)$ for the population of the different nuclear magnetic sublevels $|N^*I_dM_d\rangle$.

5.2 Radiative decay of the excited nuclear state

The final state of the system consists of the electron in the same bound state $|n_d\kappa_d m_d\rangle$, the ground-state nucleus $|NI_fM_f\rangle$ and the photon emitted in the nuclear radiative decay. As we are interested in the direction of the emitted radiation, we characterize the photons by the wave number $\vec{k}$ and the polarization λ. The final-state density matrix can be written as

$$\hat{\rho}_f = \hat{T}\hat{\rho}_d\hat{T}^\dagger\ , \tag{5.13}$$

where T is now the transition operator for the interaction between the nucleus and the electromagnetic field H_{nr}. In the plane-wave expansion of the radiation field, the Hamiltonian H_{nr} has the form

$$H_{nr} = -\sum_{\vec{k}\lambda} \int d^3 r_n \vec{j}_n(\vec{r}_n) \sqrt{\frac{2\pi}{\omega_k V}} \left(\vec{\epsilon}_{\vec{k}\lambda} e^{i\vec{k}\cdot\vec{r}_n} a_{\vec{k}\lambda} + \text{H.c.} \right)\ , \tag{5.14}$$

which is equivalent to the expression in Eq. (1.19). Here $\vec{\epsilon}_{\vec{k}\lambda}$ is the polarization vector of the photon, V is the quantization volume and $a_{\vec{k}\lambda}$ is the photon annihilation operator. The corresponding conjugate creation operator for a photon of wave number $\vec{k}$ and polarization λ is $a^{\dagger}_{\vec{k}\lambda}$. The observable properties are extracted from the density matrix by using detector operators that determine the probability for an event. For the angular distribution of the emitted photons, measured with a detector which is sensitive to the energies but not to the polarization of the photons, the detector operator is

$$\hat{P}_{\vec{k}} = \sum_{\lambda M_f} |\vec{k}\lambda\rangle|NI_fM_f\rangle\langle NI_fM_f|\langle\vec{k}\lambda| \ . \tag{5.15}$$

The angular differential cross section of the emitted photons is then proportional to the trace over the product of this operator with the final-state density matrix, $\mathrm{Tr}(\hat{P}_{\vec{k}}\hat{\rho}_f)$.

As we have assumed for the incoming electrons the z direction, the system has azimuthal symmetry. The angle θ of the emitted photon is defined with respect to the z-axis. The polarization and the angular distribution of the radiative decay are closely related to the sublevel population of the excited nuclear state and hence to the alignment parameters $\mathcal{A}_k$. The angular distribution of the characteristic photons emitted in the $|N^*I_dM_d\rangle \rightarrow |NI_fM_f\rangle + \gamma$ radiative decay is given by

$$\frac{d\sigma_{\mathrm{NEEC}}}{d\Omega}(\theta) = \frac{\sigma_{\mathrm{NEEC}}}{4\pi}\left(1 + \sum_{k=2,4,\ldots} f_k(N^*I_d, NI_f)\mathcal{A}_k(N^*I_d)P_k(\cos\theta)\right) \ , \tag{5.16}$$

where $f_k(N^*I_d, NI_f)$ are anisotropy parameters that do not depend on the nuclear excitation process. Furthermore, $P_k(\cos\theta)$ denote the Legendre polynomials. Accounting for all the different multipolarities L in the expansion of the radiation-nucleus interaction, the anisotropy parameter of kth order is given by [SJSF06]

$$\begin{aligned} f_k(N^*I_d, NI_f) &= \frac{\sqrt{2I_d+1}}{2}\sum_{LL'\pi\pi'} i^{L'+\pi'-L-\pi}(-1)^{I_f+I_d+k+1} \\ &\times \sqrt{(2L+1)(2L'+1)}\,C(L\ L'\ k;1\ -1\ 0) \\ &\times \left(1+(-1)^{L+p+L'+\pi'-k}\right)\left\{\begin{array}{ccc} L & L' & k \\ I_d & I_d & I_f \end{array}\right\} \\ &\times \frac{\langle N^*I_d\|H_{nr}(L,\pi)\|NI_f\rangle^*\langle N^*I_d\|H_{nr}(L',\pi')\|NI_f\rangle}{\sum_{L,\pi}|\langle N^*I_d\|H_{nr}(L,\pi)\|NI_f\rangle|^2} \ . \end{aligned} \tag{5.17}$$

Here, π denotes the parity $\pi = 1$ for electric and $\pi = 0$ for magnetic multipoles of the radiation field. In the particular case of the $2^+ \rightarrow 0^+$ $E2$ radiative transition of the nucleus that presents no multipole mixing, the angular differential cross section for the emitted photons is given by

$$\frac{d\sigma_{\mathrm{NEEC}}}{d\Omega}(\theta) = \frac{\sigma_{\mathrm{NEEC}}}{4\pi}\left(1 - \frac{\sqrt{70}}{14}\mathcal{A}_2P_2(\cos\theta) - \frac{2\sqrt{14}}{7}\mathcal{A}_4P_4(\cos\theta)\right) \ . \tag{5.18}$$

The calculation of the angular distributions of the emitted photons

$$W(\theta) = 1 - \frac{\sqrt{70}}{14}\mathcal{A}_2 P_2(\cos\theta) - \frac{2\sqrt{14}}{7}\mathcal{A}_4 P_4(\cos\theta) \tag{5.19}$$

involves therefore the alignment parameters $\mathcal{A}_2$ and $\mathcal{A}_4$, and further the statistical tensors ρ_{00}, ρ_{20} and ρ_{40}. The calculation of the transition amplitudes

$$\langle N^* I_d M_d, n_d \kappa_d m_d | H_{en} | N I_i M_i, \varepsilon \kappa m_s \rangle \tag{5.20}$$

for the electric transitions $0^+ \rightarrow 2^+$ occuring in Eq. (5.11) has been presented in Section 2.2. For a given multipolarity L of the nuclear transition the matrix element can be written as

$$\begin{aligned}
&\langle N^* I_d M_d, n_d \kappa_d m_d | H_{en} | N I_i M_i, \varepsilon \kappa m_s \rangle = \\
&\sum_{\mu=-L}^{L} (-1)^{I_d + M_i + L + \mu + m_s + 3j_d} R_0^{-(L+2)} R^{(e)}_{L,\kappa_d,\kappa} \langle N^* I_d \| Q_L \| N I_i \rangle \\
&\times \sqrt{2j_d+1} \sqrt{\frac{4\pi}{(2L+1)^3}}\; C(I\ I_d\ L; -M_i\ M_d\ \mu) \\
&\times\ C(j\ j_d\ L; -m_s\ m_d\ -\mu)\ C\left(j_d\ L\ j; \frac{1}{2}\ 0\ \frac{1}{2}\right)\ ,
\end{aligned} \tag{5.21}$$

with the electronic radial integral $R^{(e)}_{L,\kappa_d,\kappa}$ given in Eq. (2.38). For the particular case of the $0^+ \rightarrow 2^+$ $E2$ transitions the transition amplitude reads

$$\begin{aligned}
&\langle N^* 2 M_d, n_d \kappa_d m_d | H_{en} | N 00, \varepsilon \kappa m_s \rangle = \frac{\sqrt{4\pi}}{\sqrt{125}} R_0^{-4} (-1)^{M_d + m_s + 3j_d} \sqrt{2j_d+1} \\
&\times \langle 2 \| Q_2 \| 0 \rangle\ C(j\ j_d\ 2; -m_s\ m_d\ -M_d)\ C\left(j_d\ 2\ j; \frac{1}{2}\ 0\ \frac{1}{2}\right) R^{(e)}_{2,\kappa_d,\kappa}\ .
\end{aligned} \tag{5.22}$$

The Clebsch-Gordan coefficient $C(j\ j_d\ 2; -m_s\ m_d\ -M_d)$ imposes that $M_d = m_s - m_d$, therefore $M_d = M'_d$ and $q = 0$ in Eq. (5.11), as one may expect also from symmetry reasons. The expression of the statistical tensors becomes

$$\begin{aligned}
&\rho_{k0}(N^*2) = \frac{8\pi^2}{125} |\langle 2 \| Q_2 \| 0 \rangle|^2 R_0^{-8} (2j_d+1) \sum_{m_s m_d} \sum_{M_d} \\
&\times (-1)^{2-M_d}\ C(2\ 2\ k; M_d\ -M_d\ 0) \\
&\times \left| \sum_{\kappa} i^l e^{i\Delta_\kappa} \sqrt{2l+1}\ C\left(l\ \frac{1}{2}\ j; 0\ m_s\ m_s\right) \right. \\
&\left. \times\ C(j\ j_d\ 2; -m_s\ m_d\ -M_d)\ C\left(j_d\ 2\ j; \frac{1}{2}\ 0\ \frac{1}{2}\right) R^{(e)}_{2,\kappa_d,\kappa} \right|^2 ,
\end{aligned} \tag{5.23}$$

where we have replaced the double sum over κ and κ' by a simple sum in the modulus squared. As the calculation of the alignment parameters $\mathcal{A}_2$ and $\mathcal{A}_4$ involves the ratios of the statistical tensors ρ_{00}, ρ_{20} and ρ_{40}, the constant factor

$$C = \frac{8\pi^2}{125} |\langle 2 \| Q_2 \| 0 \rangle|^2 R_0^{-8} (2j_d+1)\ , \tag{5.24}$$

does not play a role in the angular distribution of the emitted photons. In the case of RR, the quantity equivalent to ρ_{00} has a special meaning and corresponds to the radiative recombination total cross section up to a factor which depends on the electronic state [FSS05]. In that case, due to the normalization of the density matrix,

$$\rho_{00}^{\mathrm{RR}} \propto \frac{1}{\sqrt{2J_f+1}}\sigma_{\mathrm{RR}} \ , \tag{5.25}$$

where J_f stands for the total angular momentum of the final state. Analogously, one expects that the statistical tensor ρ_{00} in Eq. (5.11) corresponds to the NEEC rate up to a factor depending on the electronic state. The statistical tensors of higher rank ρ_{k0} with k=2,4 refer to the population of the various substates relative to each other, representing the orientation and alignment of the nucleus.

5.3 Numerical results

In this section we present the alignment parameters and the angular distribution of the emitted photons that follow the nuclear excitation by electron capture into the $1s$ orbitals of bare ions. We consider the even-even nuclei $^{174}_{70}$Yb, $^{170}_{68}$Er, $^{154}_{64}$Gd and $^{162}_{66}$Dy for which the electron capture into the K-shell has been investigated in Chapter 3. The calculation of the statistical tensors involves the numerical integration of $R^{(e)}_{L,\kappa_d,\kappa}$. We consider, just as in the case of the total cross section, Coulomb-Dirac wave functions for the continuum electron. The Coulomb phases calculated according to Eq. (5.8) do not include the effect of the finite nuclear size, which is expected to be negligible. For the bound electron we have used GRASP92 wave functions that consider a homogeneously charged nucleus of radius R_0.

In order to check the proportionality between the statistical tensor ρ_{00} and the NEEC rate, we investigate also the capture into the $2s$ orbital of the He-like ions Yb^{68+}, Er^{66+}, Gd^{62+} and Dy^{64+}. In this case we consider screening for the continuum wave functions. The Coulomb phases of the continuum wave functions were calculated by considering the Dirac-Fock (DF) approximation of the ground state $1s^2$ seen by the free electron. The difference between such a calculation and the $Z_{\mathrm{eff}} = Z-2$ full screening approximation is very small in the Coulomb phase, of about 0.01 rad and has a negligible effect on the alignment parameters. In Table 5.1 we present the Coulomb phases for the capture into the $1s$ orbital and $2s$ orbitals of the considered ions, the latter calculated using both approximations. As the $1s$ and $2s$ orbitals are characterized by the same total angular momentum $j_d = 1/2$, we calculate the ratios $\rho_{00}(1s)/\rho_{00}(2s)$ of the rank-zero statistical tensors for the captures into the same ion. These are compared to the ratios of the NEEC rates for the capture into the same orbitals in Table 5.2, showing a very good agreement.

The values of the alignment parameters $\mathcal{A}_2$ and $\mathcal{A}_4$ of the 2^+ excited nuclear states are presented in Table 5.3. Both captures into the $1s$ and $2s$ orbitals are considered. The alignment of the excited nuclear state characterized by these parameters gives in the second step of NEEC the orientation of the emitted radiation. In Figures 5.1, 5.2, 5.3 and 5.4 we present the angular distribution

Table 5.1: Coulomb phases for capture into bare ($Z_{\rm eff}$=Z) and He-like ions. $Z_{\rm eff}$=Z-2 stands for total screening and DF for the Dirac-Fock approximations.

		Δ_κ		
${}^{A}_{Z}$X	κ	$Z_{\rm eff}$=Z	$Z_{\rm eff}$=Z-2	DF
${}^{154}_{64}$Gd	2	2.31266	2.52420	2.52871
	-3	-0.91336	-0.70944	-0.70648
${}^{162}_{66}$Dy	2	0.74727	2.27025	2.27293
	-3	-2.46145	-0.95393	-0.95220
${}^{170}_{68}$Er	2	0.80549	2.27741	2.28010
	-3	-2.40769	-0.95222	-0.95053
${}^{174}_{70}$Yb	2	5.29313	2.22876	2.23117
	-3	2.07904	-1.00408	-1.00259

Table 5.2: Comparison between the ratios of the NEEC rates and the statistical tensors ρ_{00} for captures into $1s$ and $2s$ orbitals

${}^{A}_{Z}$X	$\frac{\rho_{00}(1s)}{\rho_{00}(2s)}$	$\frac{Y_n(1s)}{Y_n(2s)}$
${}^{154}_{64}$Gd	8.83467	8.83467
${}^{164}_{66}$Dy	8.48401	8.48401
${}^{170}_{68}$Er	8.35099	8.35099
${}^{174}_{70}$Yb	7.61649	7.61649

Table 5.3: Alignment parameters for the 2^+ excited nuclear state after NEEC. We denote the capture orbital by nl_j and E_d is the energy of the continuum electron at the resonance.

${}^{A}_{Z}$X	E_d(keV)	nl_j	$\mathcal{A}_2$	$\mathcal{A}_4$
${}^{154}_{64}$Gd	64.005	$1s_{1/2}$	-1.18259	1.54706
${}^{164}_{66}$Dy	10.318	$1s_{1/2}$	-1.18471	1.55655
${}^{170}_{68}$Er	11.350	$1s_{1/2}$	-1.18276	1.54782
${}^{174}_{70}$Yb	4.897	$1s_{1/2}$	-1.18136	1.54157
${}^{154}_{64}$Gd	108.847	$2s_{1/2}$	-1.14584	1.38272
${}^{164}_{66}$Dy	58.164	$2s_{1/2}$	-1.09043	1.13493
${}^{170}_{68}$Er	62.317	$2s_{1/2}$	-1.07270	1.05562
${}^{174}_{70}$Yb	59.106	$2s_{1/2}$	-1.02923	0.86122

$W(\theta)$ given in Eq. (5.19) for the capture into the $1s$ and $2s$ shells of ${}^{154}_{64}$Gd, ${}^{162}_{66}$Dy, ${}^{170}_{68}$Er and ${}^{174}_{70}$Yb, respectively. The angular patterns are similar for all the four ions, as they all involve $E2$ transitions of nuclei with close mass and atomic numbers. Both radiations following the capture into the $1s$ and $2s$ orbitals of the ion present maxima at $\theta = 45°$ and $\theta = 135°$, pattern which differs from that of RR. While for the capture into the $1s$ orbitals there are no photons emitted at $\theta = 0°, 90°, 180°$, the pattern for the capture into $2s$ displays non-zero minima at these angles. In contrast to NEEC, the radiative capture of the free electron is dominated by the $E1$ transition and has therefore a $\sin^2\theta$-like angular distribution with a maximum at $\theta = 90°$.

As the RR and NEEC angular distributions of the emitted photons have maxima at different values of θ, we estimate the ratio between the two angular differential cross sections for different emission angles,

$$R(E) = \left(\frac{d\sigma_{\mathrm{NEEC}}}{d\Omega}(E,\theta) \Big/ \frac{d\sigma_{\mathrm{RR}}}{d\Omega}(E,\theta) \right) \Bigg|_{\theta=\theta_{max}} \tag{5.26}$$

for the case of electron capture into bare Ytterbium. We consider here the maximum values $\theta_{max} = 45°, 90°, 135°$ that correspond to the NEEC and RR radiation angular distributions. The NEEC total cross section is convoluted with the energy distribution of the continuum electrons assuming a Gaussian width parameter of s=0.1 eV. The RR angular differential cross section is calculated with the aid of the density matrix formalism following the outline in [FSS05]. We assume that the RR and NEEC alignment parameters are constant on the studied energy interval of approximately 1 eV.

We envisage the scenario of a possible NEEC experiment in a storage ring, in which the radiation is emitted by the nucleus of the Yb^{69+} ion moving relativistically with respect to the laboratory frame. A Lorentz transformation of the NEEC and RR angular differential cross sections in the center-of-mass frame is therefore required in order to obtain the quantities in the laboratory system. The angular differential cross section in the laboratory system can be

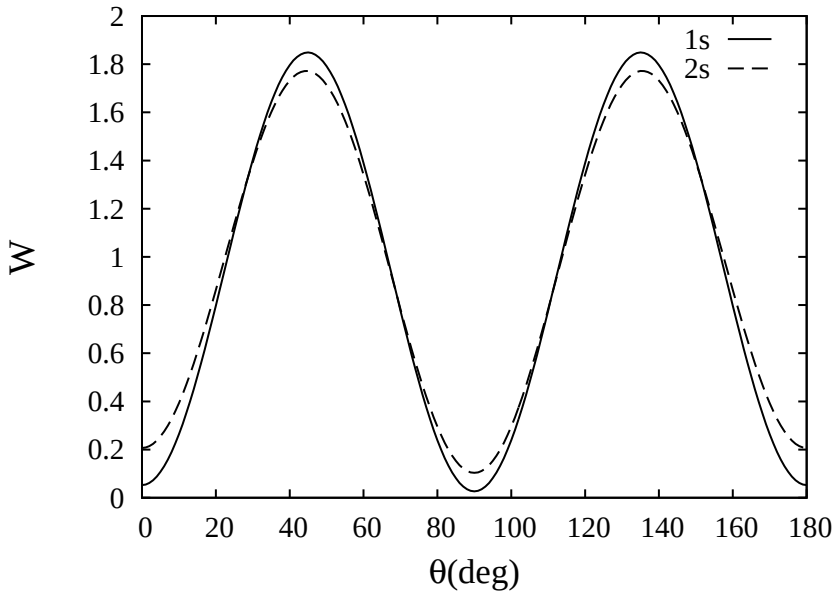

Figure 5.1: Angular distribution of the photons emitted in the radiative decay of the 2^+ excited state of $^{154}_{64}$Gd following the NEEC into $1s$ and $2s$ orbitals.

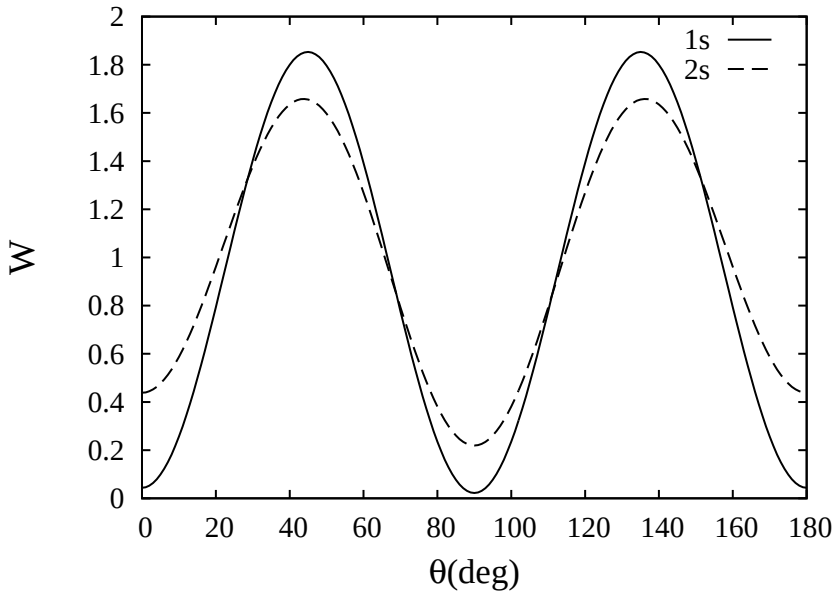

Figure 5.2: Angular distribution of the photons emitted in the radiative decay of the 2^+ excited state of $^{164}_{66}$Dy following the NEEC into $1s$ and $2s$ orbitals.

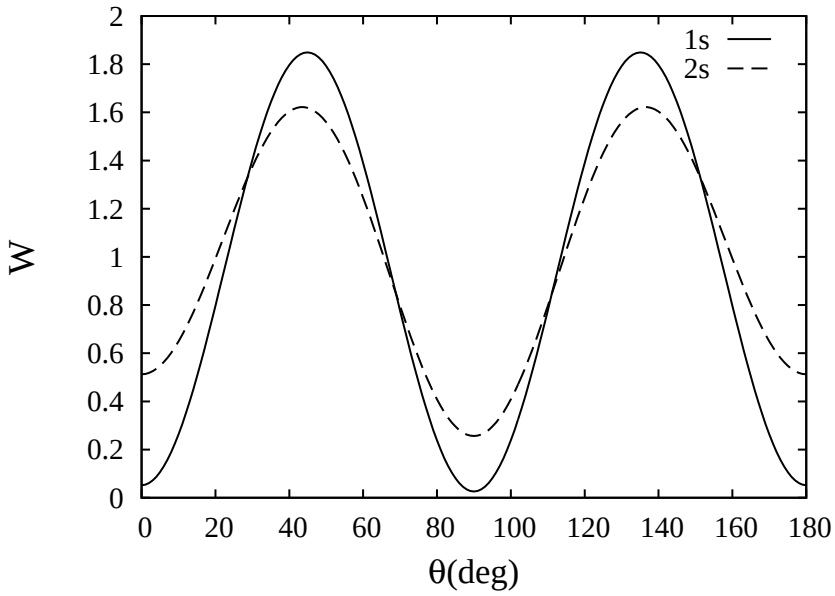

Figure 5.3: Angular distribution of the photons emitted in the radiative decay of the 2^+ excited state of $^{170}_{68}$Er following the NEEC into $1s$ and $2s$ orbitals.

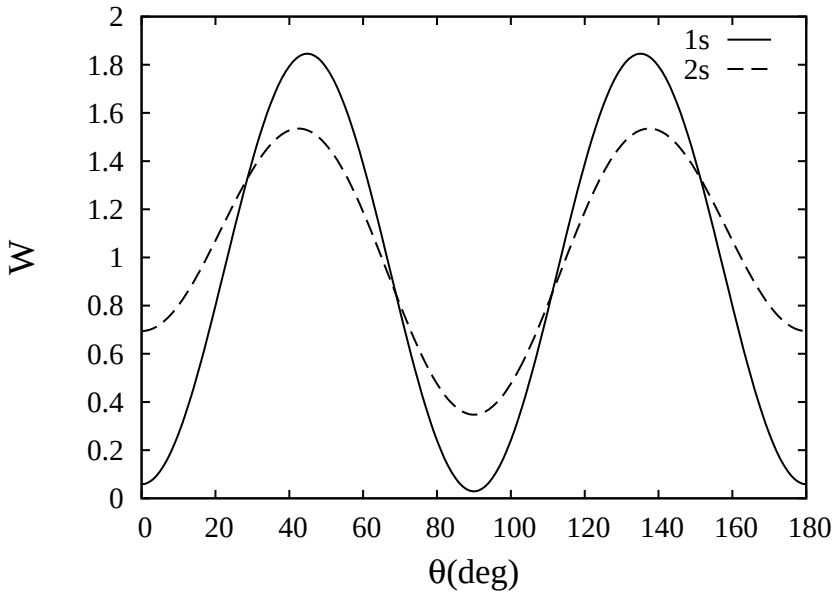

Figure 5.4: Angular distribution of the photons emitted in the radiative decay of the 2^+ excited state of $^{174}_{70}$Yb following the NEEC into $1s$ and $2s$ orbitals.

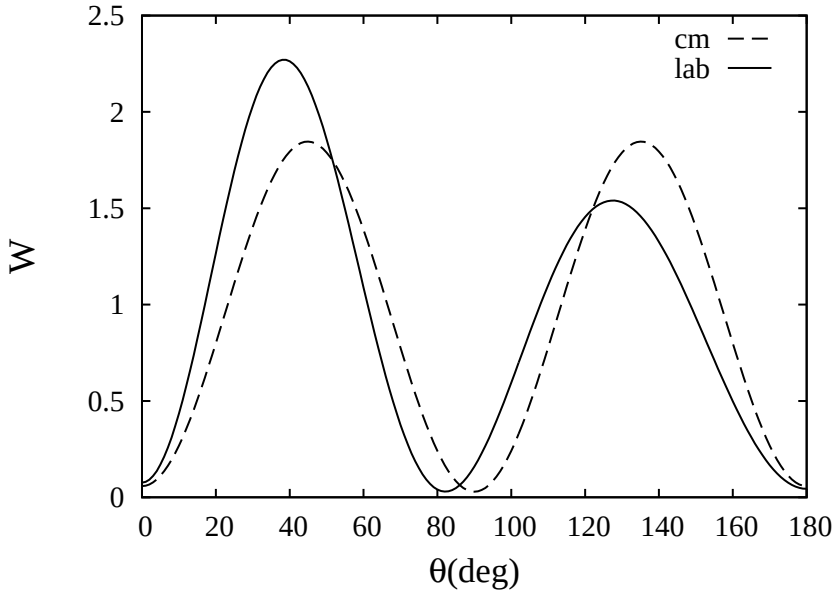

Figure 5.5: Angular distribution of the photons with respect to the laboratory and center-of-mass systems for the case of NEEC into the $1s$ orbital of Yb^{70+}.

written as [EM95]

$$\frac{d\sigma(\theta)}{d\Omega} = \frac{1}{\gamma^2(1-\beta\cos\theta)^2}\frac{d\sigma'(\theta')}{d\Omega'} \ , \tag{5.27}$$

where $\sigma'(\theta')/d\Omega'$ is the differential cross section in the center-of-mass system. In our case the reduced velocity β is 0.138 and the Lorentz factor is $\gamma = 1.009$. The angle of the photons in the laboratory frame θ is related to the one in the ion-fixed frame θ' by

$$\cos\theta' = \frac{\cos\theta - \beta}{1-\beta\cos\theta} \ . \tag{5.28}$$

As the system has azimuthal symmetry, $\varphi' = \varphi$. The angular distribution of the photons with respect to the laboratory system for the case of Ytterbium is presented in Figure 5.5.

In Figure 5.6 we present the ratio in Eq. (5.26) as a function of the continuum electron energy for the three values of the photon emission angle θ for which $\sigma(\theta)_{\mathrm{NEEC}}/d\Omega$ or $\sigma(\theta)_{\mathrm{RR}}/d\Omega$ have a maximum. In the laboratory frame, the NEEC angular distribution has maxima at $\theta = 40°$ and 129°, while in the case of RR the peak is at approximately $\theta = 86°$. The ratio of the NEEC and RR angular differential cross sections is more than one order of magnitude larger for $\theta = 40°$ and 129° than in the case of $\theta = 86°$. If the photons emitted perpendicular to the direction of the incoming electron are measured in an experiment, it is most likely that just the RR background will be detected, as NEEC has a minimum for $\theta = 82°$. For the emission angles $\theta = 40°$ and $\theta = 129°$ the RR contribution is lowered with more than 50% in comparison

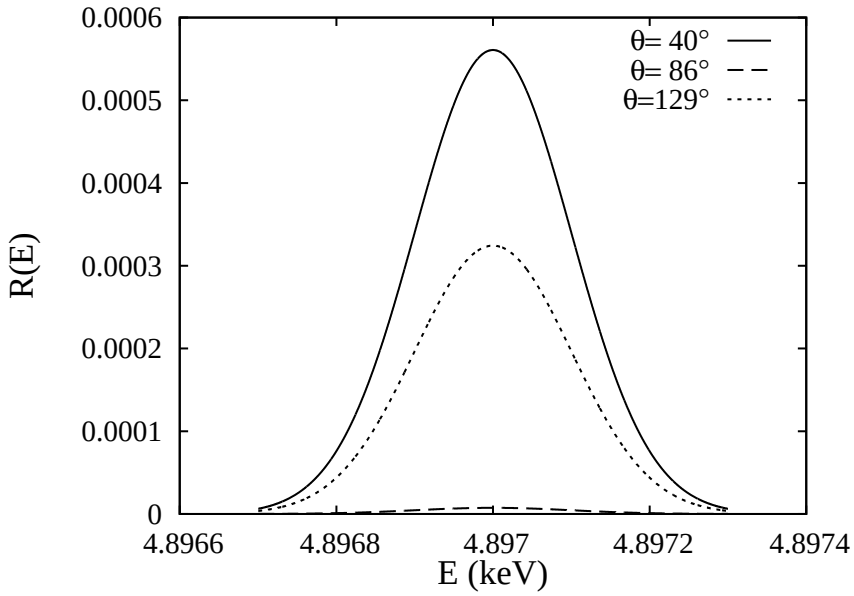

Figure 5.6: The NEEC and RR angular differential cross sections ratio for the case of $^{174}_{70}$Yb as a function of the continuum electron energy for three different photon emission angles. The NEEC total cross section was convoluted with a Gaussian electron energy distribution with the width parameter s=0.1 eV.

with considering the total cross sections of the recombination process,

$$\left(\frac{d\sigma_{\rm NEEC}}{d\Omega}(E_d,\theta)\Big/\frac{d\sigma_{\rm RR}}{d\Omega}(E_d,\theta)\right)\Big|_{\theta=40^\circ} \simeq 3\,\frac{\sigma_{\rm NEEC}(E_d)}{\sigma_{\rm RR}(E_d)}\,, \qquad (5.29)$$

$$\left(\frac{d\sigma_{\rm NEEC}}{d\Omega}(E_d,\theta)\Big/\frac{d\sigma_{\rm RR}}{d\Omega}(E_d,\theta)\right)\Big|_{\theta=129^\circ} \simeq 2\,\frac{\sigma_{\rm NEEC}(E_d)}{\sigma_{\rm RR}(E_d)}\,. \qquad (5.30)$$

As the ratio of the NEEC and RR angular differential cross sections is small, the experimental observation of the NEEC signature is challenging for the present measurement precision. Nevertheless, knowing the angular pattern of NEEC is important as it provides means of suppressing the RR background. Storage ring experiments focused on detecting the photons emitted in photo recombination at $\theta = 40^\circ$ angle have the best chances to observe the NEEC resonance for the case of pure $E2$ transitions of the $^{174}_{70}$Yb nucleus.

Summary and outlook

Summary

In this thesis we have investigated theoretically the resonant process of nuclear excitation by electron capture (NEEC) in collisions involving highly-charged ions. NEEC is a rare recombination process in which a free electron is captured into a bound shell of an ion with the simultaneous excitation of the nucleus. The excited nuclear state can then decay either radiatively or by internal conversion. When followed by the radiative decay of the nucleus, NEEC can be considered, next to dielectronic recombination (DR), as one of the resonant channels of photo recombination. NEEC can interfere with the direct radiative recombination (RR) channel, and also with DR, provided that the electronic and nuclear transition energies match.

NEEC offers many possibilities of theoretical study. The literature in this field is scarce and up to our knowledge, we have presented the first relativistic calculation of NEEC for highly-charged, heavy ions in scattering processes. However, as the small amplitudes of NEEC did not allow the experimental observation of the process until now, the utility of any theoretical study on this subject is related to the possibility of measuring the effect. Our aim was therefore to find suitable candidate isotopes for possible future measurements. Following this outline we have studied several aspects of recombination processes considering this rare nuclear excitation channel.

In the first place we have calculated total cross sections for NEEC followed by the radiative decay of the excited nucleus in various collision systems. We have considered the electron capture into the K or L shells of the K^{19+}, Fe^{26+}, Mn^{25+}, $Gd^{62+,64+}$, $Dy^{64+,66+}$, Ho^{67+}, Er^{68+}, Yb^{70+}, Re^{75+}, U^{90+} and Cm^{94+} ions, corresponding to electric $E2$ and magnetic $M1$ transitions of the nucleus. The dynamics of the electrons was described by the Dirac equation as required in the case of high-Z elements. For the description of the nuclear states, we have considered a phenomenological collective model and used experimental values for the reduced nuclear transition probabilities. Our theoretical values obtained from ab initio calculations are larger than earlier semi-empirical predictions, but still small in comparison with the equivalent results for DR. The total cross sections have the shape of a very narrow Lorentzian, with the width given by the natural width of the nuclear excited state, in the order of $10^{-5} - 10^{-8}$ eV and resonance strengths of about 1 b eV or less. The possibility to observe NEEC in scattering experiments with trapped or stored ions was discussed focusing on the cases with the largest calculated resonance strength. We estimated that an

experimental energy resolution of less than 1 eV is required for the continuum electron in order to observe the NEEC effect.

As the photons emitted in the different channels of the electron recombination process are indistinguishable in the total cross section, RR acts as an omnipresent background in any possible NEEC experiment. We have investigated the role of RR in the NEEC recombination mechanism and presented theoretical estimates for the magnitude of the interference between the two processes. Due to the very narrow width of the nuclear excited state, the interference effect turned out to be small in comparison with the RR and NEEC contributions to the total cross sections.

The presence of the RR background combined with the small magnitude of the NEEC effect make the experimental observation of NEEC challenging for the present measurement precision. The angular distribution of the emitted photons in the recombination process provides means of discerning NEEC from RR. We calculated angular differential cross sections for the photons emitted in the $E2$ radiative decay of the nucleus following NEEC. While in the case of RR the dominating $E1$ transitions determine the $\sin^2\theta$ distribution of the emitted photons, the $E2$ radiative nuclear decay has a quadrupole pattern that presents maxima at 45° and 135°. The angular distribution of the emitted photons in the radiative decay can be therefore used to suppress the RR background. We have estimated the ratio of the NEEC and RR angular differential cross sections for various emission angles.

The discussion of the present experimental possibilities regarding the observation of NEEC has focused on the accelerator and electron beam ion trap facilities. Highly-charged ions and a good electron energy resolution are compulsory for any experiment concerning NEEC. Since in an EBIT the necessary small energy resolution of the electron beam cannot be achieved at present, scenarios for measuring NEEC involve some new methods to reduce the RR background and make the effect observable. In the ion accelerator facility in GSI the present measurement precision allows, according to our count rate estimate, for the experimental observation of NEEC.

Outlook

NEEC offers many possibilities to continue our theoretical study and to improve the present calculations. A main direction of interest would be the study of NEEC occuring in many-electron systems. Until now we have mainly considered the capture into the $1s$ orbitals of bare ions. In the cases where the capture into the L-shell of the ion is interesting from the experimental point of view, we have considered the K-shell as a closed configuration, without taking into account the electron-electron interaction explicitly. Furthermore, a possible electron transition between the capture orbital and another free bound state, like in the case of recombination into the $2p$ orbitals of a He-like ion, was not considered. In order to study the resonant capture into the L-shell of He-like, Li-like or Be-like ions the Feshbach projection operator formalism has to be extended to include for the electron-electron interaction and electronic

transitions between bound states. The electron-electron interaction also plays a role on the shape of the bound and continuum wave functions of the captured electron. While the GRASP92 package provides bound radial wave functions that include the correlation between electrons, for the continuum electron this interaction has to be considered. An enhanced precision for NEEC occuring in many-electron systems is important as these cases are often convenient in envisaging experimental observation.

We have until now always considered NEEC followed by the radiative decay of the excited nucleus. In this case, we have calculated the total and angular cross section for the emitted photons. However, the nucleus can decay also by internal conversion (IC). As the IC rate is for some nuclei up to two orders of magnitude larger than the radiative decay rate, it would be interesting to consider NEEC followed by the emission of the conversion electron. The Feshbach projection operator formalism can be adjusted in this case to account for final states characterized by the presence of the conversion electron. The angular distribution of the emitted electrons in IC could act as a signature for the occurrence of the process. One has, however, to take into account that the electron spectroscopy nowadays is less precise compared to the photon detection possibilities. The conversion electron cross sections might turn out to be still too small for experimental observation.

Finally, we would like to mention the possibility to investigate NEEC occuring in a laser-assisted environment and to study the dynamics of a electron-nucleus-laser system. It was the original idea of Goldanskii and Namiot [GN76], the authors which first proposed the NEEC mechanism, to induce the excitation of isomeric nuclear levels by laser radiation through inverse internal electron conversion. The study of laser-nucleus interactions usually involves secondary particles such as electrons in a plasma or in solid targets, as the direct matrix elements are small. A recent study [BEK06] shows that nuclei can also interact with super-intense laser fields. The effects of laser fields on atomic electrons which in turn produce nuclear excitation have been the subject of several studies until now [BGM88, KKR99]. The theoretical study of nuclear excitation occuring in atomic systems interacting with lasers is a very interesting research topic today, as it is expected to confirm the realization of the gamma-ray laser.

Deutschsprachige Zusammenfassung

In dieser Dissertation wurde von theoretischer Seite ein seltener Elektron-Rekombinationsmechanismus mit Kernanregung untersucht. Kernanregung durch Elektroneinfang, in Englisch *Nuclear Excitation by Electron Capture (NEEC)*, wurde ursprünglich von Goldanskii und Namiot im Jahre 1976 [GN76] als Umkehrprozeß der internen Konversion beschrieben. In dem NEEC-Resonanzprozeß wird ein freies Elektron in eine gebundene Schale eines Ions unter gleichzeitiger Anregung des Kerns eingefangen. Dies stellt das kernphysikalische Analogon zur *dielektronischen Rekombination (DR)* der Atomphysik dar, wobei die Rolle des gebundenen Elektrons vom Atomkern übernommen wird. Der angeregte Kernzustand zerfällt anschliessend entweder durch interne Konversion oder durch Emission eines Photons. NEEC mit anschliessender Photonemission ist ein seltener Elektron-Rekombinationsmechanismus, der mit *radiativer Rekombination (RR)* und DR in Konkurrenz steht. Trotz mehrfacher experimenteller Anstrengungen [Mok89, Dau06] konnte NEEC bis heute nicht beobachtet werden.

Der NEEC Prozess stellt eine Brücke zwischen der Atom- und Kernphysik dar. Solche Prozesse sind sehr interessant; denn sie bieten die Möglichkeit, die spektralen Eigenschaften schwerer Kerne mittels atomphysikalischer Experimente zu untersuchen. Hierbei können experimentelle Methoden angewandt werden, welche für Streuexperimente zur Elektronenrekombination von Ionen entwickelt wurden. Damit kann man Informationen über die Kernstruktur von Nukliden erhalten, die ansonsten in Kernstreuexperimenten unzugänglich wären. Die hohe Präzession der modernen Atomspektroskopie und die Möglichkeit der direkten Messung von NEEC sind angesichts des derzeitigen Kenntnisstands von nuklearen Daten sehr vielversprechend. Durch die Vermessung des NEEC-Effekts könnte man sowohl Kern-Übergangsenergien als auch reduzierte Kern-Übergangswahrscheinlichkeiten bestimmen. Ausserdem würde dies dazu beitragen, den Effekt von Elektronenvakanzen auf die Lebensdauer und den Populationsmechanismus von angeregten Kernzuständen zu studieren.

NEEC bietet vielfältige Möglichkeiten für theoretische Studien, allerdings ist die Literatur auf diesem Gebiet gering. Gemäß unseres Wissens haben wir die erste relativistische Rechnung für NEEC in Streuprozessen von Elektronen mit hochgeladenen Schwerionen in dieser Arbeit ausgeführt. Da die kleinen Amplituden des NEEC-Prozesses die experimentelle Beobachtung bis heute

unmöglich machte, muß sich jede neue theoretische Studie an ihrer experimentellen Umsetzbarkeit orientieren. Darum war es unser Ziel, für zukünftige Experimente messbare Isotope zu ermitteln. Mit diesem Hintergrund wurden von uns mehrere Aspekte dieses seltenen Kernanregungprozesses untersucht.

Wir haben zuerst die totalen Wirkungsquerschnitte für NEEC für mehrere Kollisionssysteme berechnet. Dabei haben wir uns auf Prozesse mit radiativem Zerfall des angeregten Kerns konzentriert. Ausgehend von den theoretischen Methoden aus [ZGS90, Zim92] für DR, haben wir einen Feshbach-Projektor-Formalismus entwickelt, welcher eine klare Separierung der direkten und resonanten Beiträge zum totalen Photorekombinationsquerschnitt erlaubt. Der resonante Anteil kann als Produkt der NEEC-Rate und der radiativen Rate beschrieben werden. Erstere beschreibt die Kernanregung und letztere den Zerfall des angeregten Zustands. Für die Kernzustände nutzen wir ein phänomenologisches kollektives Modell. Im Rahmen dieses Modell kann man die elektronischen und nuklearen Anteile in den Ausdrücken der NEEC-Rate separieren.

Wir haben den Elektroneinfang in die K- und L-Schalen von K^{19+}, Fe^{26+}, Mn^{25+}, $Gd^{62+,64+}$, $Dy^{64+,66+}$, Ho^{67+}, Er^{68+}, Yb^{70+}, Re^{75+}, U^{90+} und Cm^{94+} Ionen untersucht. Der Atomkern führt dabei einen elektrischen $E2$- oder magnetischen $M1$-Übergang aus. Für hohe Ladungszustände des Ions wird das Problem relativistisch und die Elektronendynamik muß durch die Dirac-Gleichung beschrieben werden. Der Kontinuumszustand des Elektrons wird durch eine relativistische Coulomb-Dirac Wellenfunktion beschrieben. Wir berechnen die Wellenfunktion des gebundenen Zustands mit Hilfe des GRASP92 Pakets [DGJ+89], welches die endliche Ausdehnung des Kerns berücksichtigt. Die theoretischen Resultate unserer ab-initio Rechnungen für die Wirkungsquerschnitte sind größer als vorherige halbempirische Vorhersagen [CPR89, Cue89, KBC91, YK93], aber dennoch klein im Vergleich zu entsprechenden Ergebnissen für DR. Die Energieabhängigkeit des totalen Wirkungsquerschnitts entspricht einer Lorentz-Verteilung. Die Breite der Verteilung, welche durch die natürliche Breite des angeregten Kernzustands gegeben ist, beträgt etwa $10^{-5} - 10^{-8}$ eV und die Resonanzstärke errechnet sich zu etwa 1 b eV oder weniger. Wir diskutierten die Möglichkeit zur Messung des NEEC Prozesses in Streuprozessen von Elektronen mit Ionen in Speicherringen und Ionenfallen, und konzentrierten uns dabei auf jene Fälle, in denen die Resonanzstärke maximal wird. Nach unseren Rechnungen wird man eine experimentelle Energieauflösung von weniger als 1 eV für das Kontinuumselektron benötigen, um NEEC beobachten zu können.

Die Photonen aus den verschiedenen Kanälen der elektronischen Rekombination sind im totalen Querschnitt ununterscheidbar. Darum stellt RR einen omnipräsenten Hintergrund für mögliche NEEC-Experimente dar. Wir haben die Rolle von RR im NEEC-Rekombinationsmechanismus studiert und präsentieren Abschätzungen für den Betrag des Interferenzterms der beiden Prozesse. Solch ein Interferenzeffekt ist sehr interessant, da er zwei sehr verschiedene Übergangsprozesse verknüpft. In RR spielt nur der elektronische Teil eine Rolle, während für NEEC der Kern in einen angeregten Zustand übergeht. Der Interferenzeffekt wird aufgrund der geringen Breite des Kernzustands im Vergleich zu RR- und NEEC-Beiträgen als klein vorhergesagt.

Durch den RR-Hintergrund und den kleinen Effekt von NEEC wird die experimentelle Vermessung von NEEC eine echte Herausforderung für die derzeitigen Messgenauigkeiten und -methoden. Mit Hilfe der Winkelverteilungen der emittierten Photonen könnte man RR-Prozesse gegenüber NEEC-Prozessen unterdrücken. Darum haben wir Winkelverteilungen für Photonen aus einem $E2$-Zerfalls der Kerns nach Anregung durch NEEC berechnet. Der $E2$-Übergang des Kerns hat eine quadrupelförmige Ausstrahlung mit Maxima bei 45° und 135°, während im Falle von RR der dominierende $E1$-Übergang eine $\sin^2(\theta)$-Abhängigkeit der Winkelverteilung besitzt. Wir haben die Verhältnisse von RR zu NEEC für verschiedene Emissionswinkel abgeschätzt.

Die Diskussion der derzeitigen experimentellen Möglichkeiten zur Messung von NEEC konzentrierte sich auf Experimente mit Ionenbeschleunigern und EBITs (Electron Beam Ion Trap). Hochgeladene Ionen und eine gute Energieauflösung für die Elektronen sind zwingend notwendig um NEEC erfolgreich messen zu können. Da man derzeit in einem EBIT die benötigte Energieauflösung nicht erreichen kann, werden neue Konzepte zur Messung von NEEC benötigt. Diese zielen auf eine Reduktion des RR-Hintergrunds ab, um den Effekt schließlich beobachten zu können. Nach unseren Abschätzungen würde die momentane Meßgenauigkeit bei der Gesellschaft für Schwerionenforschung (GSI) ausreichen, um NEEC auch im Experiment analysieren zu können.

Appendix A

The magnetic Hamiltonian

In this Appendix we show that the term $QH_{nr}RG_0RH_{er}P$ can be approximated by $QH_{magn}P$, where we introduced the Hamiltonian

$$H_{magn} = -\frac{1}{c}\vec{\alpha}\int d^3r_n \frac{\vec{j}_n(\vec{r}_n)}{|\vec{r}_e - \vec{r}_n|}\ , \tag{A.1}$$

describing the magnetic interaction of the nuclear and electric currents due to the exchange of a transverse photon. The replacement is valid in the case when the frequency of the virtual photon is negligible, or, in other terms, when its wavelength is large compared to the typical linear size of the total system.

In this derivation we use the second quantized forms

$$\begin{aligned} H_{er} &= -\sum_{ab}\sum_{\vec{k}\sigma}\sqrt{\frac{2\pi c}{k}}c_a^\dagger c_b \\ &\times \int d^3r_e \phi_a^*(\vec{r}_e)\vec{\alpha}\left(\vec{\epsilon}_{\vec{k}\sigma}a_{\vec{k}\sigma}e^{i\vec{k}\cdot\vec{r}_e} + \vec{\epsilon}^*_{\vec{k}\sigma}a^\dagger_{\vec{k}\sigma}e^{-i\vec{k}\cdot\vec{r}_e}\right)\phi_b(\vec{r}_e) \end{aligned} \tag{A.2}$$

and

$$\begin{aligned} H_{nr} &= -\sum_{st}\sum_{\vec{k}'\sigma'}\sqrt{\frac{2\pi}{ck'}}\beta_s^\dagger\beta_t \\ &\times \int d^3r_n \vec{j}_n^{st}(\vec{r}_n)\left(\vec{\epsilon}_{\vec{k}'\sigma'}a_{\vec{k}'\sigma'}e^{i\vec{k}'\cdot\vec{r}_n} + \vec{\epsilon}^*_{\vec{k}'\sigma'}a^\dagger_{\vec{k}'\sigma'}e^{-i\vec{k}'\cdot\vec{r}_n}\right) \end{aligned} \tag{A.3}$$

of the electromagnetic interaction Hamiltonians. For convenience, we use here the plane wave expansion of the electromagnetic fields. The photon is characterized by the discrete wave number $\vec{k}$ ($\vec{k}'$) and the polarization $\sigma(\sigma') = 1, 2$, and $\vec{\epsilon}_{\vec{k}\sigma}$ ($\vec{\epsilon}_{\vec{k}'\sigma'}$) stands for the polarization vector. The ϕ_a form a complete set of one-electron states, and the $c_a^\dagger$ (c_b) are electronic creation (annihilation) operators. The $\beta_s^\dagger$ and β_t are the mode operators of the nuclear collective model like in Eq. (1.10). Here we only label these operators by one index for simplicity. The nuclear current is denoted by $\vec{j}_n^{st} = \langle s|\vec{j}_n|t\rangle$. It describes a transition from state t to s and it is the nuclear analogue of the electronic transition current $-\phi_a^*\vec{\alpha}\phi_b$ in Eq. (A.2).

Substituting these operators into the matrix element of $QH_{nr}RG_0(z)RH_{er}P$, we obtain

$$\sum_r \frac{\langle q|H_{nr}|r\rangle\langle r|H_{er}|\alpha\varepsilon\rangle}{z-E_r+i\epsilon} = \sum_r \sum_{abst} \sum_{\vec{k}\vec{k}'} \sum_{\sigma\sigma'} \frac{2\pi}{\sqrt{k\vec{k}'}}$$
$$\times \frac{1}{z-E_r+i\epsilon} \langle q|\beta_s^\dagger \beta_t \int d^3r_n \vec{j}_n^{st}(\vec{r}_n)\cdot\vec{\epsilon}_{\vec{k}'\sigma'} a_{\vec{k}'\sigma'} e^{i\vec{k}'\cdot\vec{r}_n}|r\rangle$$
$$\times \langle r|c_a^\dagger c_b \int d^3r_e \phi_a^*(\vec{r}_e)\vec{\alpha}\cdot\vec{\epsilon}^*_{\vec{k}\sigma} a^\dagger_{\vec{k}\sigma} e^{-i\vec{k}\cdot\vec{r}_e}\phi_b(\vec{r}_e)|\alpha\varepsilon\rangle\,. \tag{A.4}$$

Note that only the photon creation term of (A.2) and the photon annihilation term of (A.3) contributes. We introduce the notations

$$M^e_{ab}(\vec{k},\sigma) = -\sqrt{\frac{2\pi c}{k}} \int d^3r_e \phi_a^*(\vec{r}_e)\vec{\alpha}\cdot\vec{\epsilon}^*_{\vec{k}\sigma} e^{-i\vec{k}\cdot\vec{r}_e}\phi_b(\vec{r}_e)\,, \tag{A.5}$$

$$M^n_{st}(\vec{k}',\sigma') = -\sqrt{\frac{2\pi}{ck'}} \int d^3r_n \vec{j}_n^{st}(\vec{r}_n)\cdot\vec{\epsilon}_{\vec{k}'\sigma'} e^{i\vec{k}'\cdot\vec{r}_n} \tag{A.6}$$

for the electronic and nuclear interaction matrix elements and take into account that the same transversal photon is emitted by the electron and absorbed by the nucleus, i.e., $\vec{k}=\vec{k}'$, $\sigma=\sigma'$. The sum over the discrete values of $\vec{k}$ can be transformed into an integral according to

$$\sum_{\vec{k}} \to \frac{1}{(2\pi)^3}\int d^3k\ , \tag{A.7}$$

considering that the quantization volume is equal to unity. Thus (A.4) can be condensed as

$$\sum_r \frac{\langle q|H_{nr}|r\rangle\langle r|H_{er}|\alpha\varepsilon\rangle}{z-E_r+i\epsilon} = \tag{A.8}$$
$$\sum_r \sum_{abst} \sum_\sigma \frac{1}{(2\pi)^3}\int d^3k \langle q|\beta_s^\dagger\beta_t a_{\vec{k}\sigma}|r\rangle\langle r|c_a^\dagger c_b a^\dagger_{\vec{k}\sigma}|\alpha\varepsilon\rangle \frac{M^e_{ab}(\vec{k},\sigma)M^n_{st}(\vec{k},\sigma)}{z-E_r+i\epsilon}\,.$$

Evaluating the above expression at $z=\varepsilon_b^e+\varepsilon_t^n$, which is equal to the sum of the initial state electron and nuclear energies, only the state for which $E_r=\varepsilon_a^e+\varepsilon_t^n+ck$ holds has to be considered in the sum over the states r. Taking into account the property

$$\sum_\sigma (\vec{a}\cdot\vec{\epsilon}_{\vec{k}\sigma})(\vec{b}\cdot\vec{\epsilon}_{\vec{k}\sigma}) = \vec{a}\cdot\vec{b} - \frac{(\vec{a}\cdot\vec{k})(\vec{b}\cdot\vec{k})}{k^2} \tag{A.9}$$

of the transversal polarization vectors which holds for any pair of vectors $\vec{a}$ and $\vec{b}$, we arrive to

$$\sum_r \frac{\langle q|H_{nr}|r\rangle\langle r|H_{er}|\alpha\varepsilon\rangle}{z-E_r+i\epsilon} = \sum_{abst} \frac{1}{(2\pi)^3}\int d^3k \langle q|\beta_s^\dagger\beta_t c_a^\dagger c_b|\alpha\varepsilon\rangle \frac{M_{abst}(\vec{k})}{\varepsilon_b^e-\varepsilon_a^e-ck+i\epsilon}\,. \tag{A.10}$$

$M_{abst}(\vec{k})$ denotes the product of electronic and nuclear matrix elements summed over the polarization directions:

$$M_{abst}(\vec{k}) = \sum_{\sigma} M^e_{ab}(\vec{k},\sigma) M^n_{st}(\vec{k},\sigma) = \frac{2\pi}{k} \int d^3 r_e \phi^*_a(\vec{r}_e)$$
$$\times \int d^3 r_n e^{i\vec{k}(\vec{r}_n - \vec{r}_e)} \left(\vec{j}^n_{st}(\vec{r}_n) \cdot \vec{\alpha} - \frac{(\vec{j}^n_{st}(\vec{r}_n) \cdot \vec{k})(\vec{\alpha} \cdot \vec{k})}{k^2} \right) \phi_b(\vec{r}_e) \ . \quad \text{(A.11)}$$

Applying the identity

$$\frac{1}{w + i\epsilon} = \mathcal{P} \frac{1}{w} - i\pi\delta(w) \ , \quad \text{(A.12)}$$

where $\mathcal{P}$ implies the principal value integration, the real part of (A.10) turns into

$$\lim_{\epsilon \to 0} \frac{1}{2} \sum_{abst} \int d^3 k \langle q|\beta^\dagger_s \beta_t c^\dagger_a c_b|\alpha\varepsilon\rangle M_{abst}(\vec{k}) \quad \text{(A.13)}$$
$$\times \left(\frac{1}{\varepsilon^e_b - \varepsilon^e_a - ck + i\epsilon} + \frac{1}{\varepsilon^e_b - \varepsilon^e_a - ck - i\epsilon} \right) =$$
$$- \lim_{\epsilon \to 0} \frac{1}{2c} \sum_{abst} \int d^3 k \langle q|\beta^\dagger_s \beta_t c^\dagger_a c_b|\alpha\varepsilon\rangle M_{abst}(\vec{k})$$
$$\times \left(\frac{1}{k - K - i\epsilon} + \frac{1}{k - K + i\epsilon} \right) .$$

Here we introduced the notation $K = (\varepsilon^e_b - \varepsilon^e_a)/c$ for the wavenumber of the photon exchanged between the electron and the nucleus and renamed ϵ/c to ϵ for simplicity. Eq. (A.13) can be rewritten as

$$\frac{1}{2} \sum_{abst} \langle q|\beta^\dagger_s \beta_t c^\dagger_a c_b|\alpha\varepsilon\rangle \int d^3 r_e \phi^*_a(\vec{r}_e) V(\vec{r}_e; K) \phi_b(\vec{r}_e) \quad \text{(A.14)}$$

in terms of the effective potential

$$\begin{aligned} V(\vec{r}_e; K) \ = \ & -\frac{1}{c} \frac{1}{(2\pi)^2} \int d^3 r_n \\ & \lim_{\epsilon \to 0} \int \frac{d^3 k}{k} \left[\vec{j}^{st}_n(\vec{r}_n) \cdot \vec{\alpha} - \frac{(\vec{j}^{st}_n(\vec{r}_n) \cdot \vec{k})(\vec{\alpha} \cdot \vec{k})}{k^2} \right] \\ & \times e^{i\vec{k}(\vec{r}_n - \vec{r}_e)} \left(\frac{1}{k - K - i\epsilon} + \frac{1}{k - K + i\epsilon} \right) . \end{aligned} \quad \text{(A.15)}$$

In the following we only consider the first term in the square brackets containing the expression $\vec{j}^{st}_n \cdot \vec{\alpha}$. It describes the magnetic interaction of the electronic and nuclear currents. The remaining term originates from a possible time dependence of the magnetic interaction and is customarily neglected in the literature since the typical radiation wavelengths are large compared to atomic or nuclear sizes:

$$Kr = \frac{2\pi r}{\lambda} \ll 1 \, . \quad \text{(A.16)}$$

Therefore, we approximate the effective potential V by the magnetic potential

$$V(\vec{r}_e;K)_{magn} = -\frac{1}{c}\frac{1}{(2\pi)^2}\int d^3r_n \lim_{\epsilon\to 0}\int \frac{d^3k}{k}\vec{j}_n^{st}(\vec{r}_n)\cdot\vec{\alpha}$$
$$\times e^{i\vec{k}(\vec{r}_n-\vec{r}_e)}\left(\frac{1}{k-K-i\epsilon}+\frac{1}{k-K+i\epsilon}\right).$$

The angular integration can be performed by inserting $d^3k = k^2 dk d\theta d\varphi$ for the volume element in the k-space. Introducing the notation $r_{ne} = |\vec{r}_n - \vec{r}_e|$, we obtain

$$V(\vec{r}_e;K)_{magn} = -\frac{1}{c}\frac{1}{(2\pi)^2}\vec{\alpha}\int d^3r_n\vec{j}_{st}^{n}(\vec{r}_n)\lim_{\epsilon\to 0}\int k dk\sin\theta d\theta d\varphi$$
$$\times e^{ikr_{ne}\cos\theta}\left(\frac{1}{k-K-i\epsilon}+\frac{1}{k-K+i\epsilon}\right) =$$
$$-\frac{1}{c}\frac{1}{2\pi}\vec{\alpha}\int d^3r_n\vec{j}_{st}^{n}(\vec{r}_n)\lim_{\epsilon\to 0}\int_0^\infty k dk\left(\frac{1}{k-K-i\epsilon}+\frac{1}{k-K+i\epsilon}\right)$$
$$\times\int_0^\pi \sin\theta d\theta\left(\cos(kr_{ne}\cos\theta)+i\sin(kr_{ne}\cos\theta)\right) =$$
$$-\frac{1}{c}\frac{1}{\pi}\vec{\alpha}\int d^3r_n\vec{j}_{st}^{n}(\vec{r}_n)\frac{1}{r_{ne}}$$
$$\times\lim_{\epsilon\to 0}\int_0^\infty dk\left(\frac{1}{k-K-i\epsilon}+\frac{1}{k-K+i\epsilon}\right)\sin(kr_{ne}). \tag{A.17}$$

In accordance with the approximation (A.16), we assume the wave number K to be negligible and the integral over k can be performed by using the sine integral formula [Bro05]

$$\int_0^\infty dx\frac{\sin(x)}{x} = \frac{\pi}{2}. \tag{A.18}$$

Finally, the magnetic potential $V_{magn}(\vec{r}_e;0)$ in the long-wavelength approximation turns out to be

$$V_{magn}(\vec{r}_e;0) = -\frac{1}{c}\vec{\alpha}\int d^3r_n\frac{\vec{j}_{st}^{n}(\vec{r}_n)}{|\vec{r}_n-\vec{r}_e|}. \tag{A.19}$$

This is equal to the magnetic Hamiltonian in (A.1). It can also be shown that the imaginary part associated with the Dirac delta term in (A.12) vanishes if the frequency $cK = \varepsilon_b^e - \varepsilon_a^e$ of the exchanged photon goes to zero: performing the integral over $\vec{k}$ in this term similarly to (A.17) yields an expression proportional to $\sin(Kr_{ne})$.

Appendix B

Magnetic transitions in the nuclear collective model

In this Appendix we derive the nuclear magnetic multipole moment $M_{\ell m}(t)$ using the collective model presented in Section 2.1. We show that $M_{\ell m}(t) = 0$ in the first order in the collective coordinates $\alpha_{\ell m}(t)$. The magnetic multipole operator is defined as [Sch55]

$$M_{\ell m}(t) = -\frac{i}{c}\sqrt{\frac{\ell}{\ell+1}} \int d^3 r r^\ell \vec{Y}^m_{\ell\ell}(\theta,\varphi) \cdot \vec{j}_n(\vec{r},t) \ , \tag{B.1}$$

where $\vec{j}_n(\vec{r},t)$ is the current density operator of the nucleus. The motion of the nuclear matter is associated with the motion of the surface. Considering the velocity of the nuclear matter $\vec{v}_n(\vec{r},t)$, the nuclear current can be written as

$$\vec{j}_n(\vec{r},t) = \rho_n(\vec{r},t)\vec{v}_n(\vec{r},t) \ . \tag{B.2}$$

The incompressibility of the nuclear matter requires that

$$\nabla \cdot \vec{v}_n(\vec{r},t) = 0 \ , \tag{B.3}$$

and we assume that the flow of the nuclear fluid is irrotational,

$$\nabla \times \vec{v}_n(\vec{r},t) = 0 \ . \tag{B.4}$$

The irrotational flow model, although not justified quantitatively, is often used in nuclear physics and it provides a convenient limiting case to which more detailed pictures of nuclear dynamics can be compared. For irrotational flow the velocity field can be expressed in terms of a potential

$$\vec{v}_n(\vec{r},t) = \nabla\Phi(\vec{r},t) \ . \tag{B.5}$$

The assumed incompressibility of the nuclear matter in Eq. (B.3) then delivers the Laplace equation for the potential,

$$\Delta\Phi(\vec{r},t) = 0 \ . \tag{B.6}$$

In spherical coordinates the general solution of the above equation, regular at the origin, is given by

$$\Phi(\vec{r},t) = \sum_{\lambda\mu} A_{\lambda\mu}(t) r^{\lambda} Y_{\lambda\mu}(\theta,\varphi) \ , \tag{B.7}$$

with the coefficients $A_{\lambda\mu}(t)$ that are determined from the boundary condition

$$\frac{\partial}{\partial t} R(\theta,\varphi,t) = v_r\big|_{r=R(\theta,\varphi,t)} = \frac{\partial}{\partial t}\Phi(\vec{r},t)\bigg|_{r=R(\theta,\varphi,t)} \ . \tag{B.8}$$

Here we use the parameterization of the nuclear surface expressed in Eq. (2.1) and v_r is the radial component of the nuclear velocity $\vec{v}_n(\vec{r},t)$. The boundary condition expresses the equality of the radial component of the velocity on the surface to the velocity of the time-dependent surface itself. In principle the components should be evaluated along the surface normal, but as we assume small deformations of the nuclear surface in the first-order approximation in $\alpha_{\ell m}(t)$, this deviates only slightly from the radial direction. A more accurate calculation would require an additional condition that the surface always consists of the same particles,

$$\frac{dF}{dt} = \frac{\partial F}{\partial t} + \vec{v}_n(\vec{r},t)\cdot\nabla F = 0 \ , \tag{B.9}$$

when

$$F = r - R_0\Big(1 + \sum_{\ell m} \alpha^*_{\ell m}(t) Y_{\ell m}(\theta,\varphi)\Big) = 0 \ . \tag{B.10}$$

In the first order in the collective coordinates $\alpha_{\lambda\mu}(t)$, we obtain the coefficients $A_{\lambda\mu}(t)$ from the boundary condition (B.8)

$$A_{\lambda\mu}(t) = \frac{1}{\lambda} R_0^{2-\lambda} \dot{\alpha}^*_{\lambda\mu}(t) \ . \tag{B.11}$$

The potential can then be written as

$$\Phi(\vec{r},t) = \sum_{\lambda\mu} \frac{1}{\lambda} R_0^{2-\lambda} \dot{\alpha}^*_{\lambda\mu}(t) r^{\lambda} Y_{\lambda\mu}(\theta,\varphi) \ , \tag{B.12}$$

which leads us to the surface velocity

$$\vec{v}_n(\vec{r},t) = \sum_{\lambda\mu} \frac{1}{\lambda} R_0^{2-\lambda} \dot{\alpha}^*_{\lambda\mu}(t) \nabla\left(r^{\lambda} Y_{\lambda\mu}(\theta,\varphi)\right) \ . \tag{B.13}$$

To evaluate the gradient in the above equation we make use of the following relation [VMK88]

$$\begin{aligned} \nabla\Big(f(r) Y_{\ell m}(\theta,\varphi)\Big) \ &= \ -\sqrt{\frac{\ell+1}{2\ell+1}}\left(\frac{d}{dr} - \frac{\ell}{r}\right) f(r)\vec{Y}^m_{\ell\ell+1}(\theta,\varphi) \\ &\quad +\sqrt{\frac{\ell}{2\ell+1}}\left(\frac{d}{dr} + \frac{\ell+1}{r}\right) f(r)\vec{Y}^m_{\ell\ell-1}(\theta,\varphi) \ , \end{aligned} \tag{B.14}$$

so that the nuclear velocity reads

$$\vec{v}_n(\vec{r},t) = \sum_{\ell m} \sqrt{\frac{2\ell+1}{\ell}} R_0^{2-\ell} \dot{\alpha}^*_{\ell m}(t) r^{\ell-1} \vec{Y}^m_{\ell\ell-1}(\theta,\varphi) \ . \tag{B.15}$$

The nuclear current $\vec{j}_n(\vec{r},t)$ in the first-order approximation in the collective coordinates is the product of the velocity in the above equation and the static nuclear charge density in Eq. (2.17),

$$\vec{j}_n(\vec{r},t) = \sum_{\ell m} \frac{3Z}{4\pi R_0^{\ell+1}} \dot{\alpha}^*_{\ell m}(t) \sqrt{\frac{2\ell+1}{\ell}}\, \Theta(R_0-r) r^{\ell-1} \vec{Y}^m_{\ell\ell-1}(\theta,\varphi) \ . \tag{B.16}$$

Due to the orthogonality properties of the vector spherical harmonics,

$$\int_0^\pi \int_0^{2\pi} \sin\theta \, d\theta \, d\varphi \, \vec{Y}^m_{j\ell}(\theta,\varphi) \cdot \vec{Y}^{m'}_{j'\ell'}(\theta,\varphi) = \delta_{jj'}\delta_{\ell\ell'}\delta_{mm'} \ , \tag{B.17}$$

the magnetic multipole moment written using the nuclear current in Eq. (B.16) vanishes,

$$\begin{aligned} M_{\ell m}(t) &= -\frac{i}{c}\sqrt{\frac{\ell}{\ell+1}} \sum_{\lambda\mu} \frac{3Z}{4\pi R_0^{\lambda+1}} \dot{\alpha}^*_{\lambda\mu}(t) \sqrt{\frac{2\lambda+1}{\lambda}} \\ &\quad \times \int d^3r r^{2\ell-1} \Theta(R_0-r) \vec{Y}^m_{\ell\ell}(\theta,\varphi) \cdot \vec{Y}^\mu_{\lambda\lambda-1}(\theta,\varphi) \\ &= 0 \ . \end{aligned} \tag{B.18}$$

The higher-order terms of the nuclear current $\vec{j}_n(\vec{r},t)$ in the collective coordinates $\alpha_{\ell m}$ have non-zero contributions to the magnetic multipole moments, which are however expected to be very small.

Appendix C

Calculation of matrix elements involving spherical tensors

In this Appendix we use the special properties of the spherical tensor operators to derive the general expression of the electronic matrix elements

$$\mathcal{M} = \langle n_d \kappa_d m_d | f(r) \vec{\alpha} \cdot \vec{Y}^M_{JL}(\theta, \varphi) | \varepsilon \kappa m \rangle \tag{C.1}$$

which occur in the expression of the NEEC magnetic rates in Section 2.3 and in the calculation of the interference and RR terms in the total cross section in Chapter 4. Here $f(r)$ stands for an arbitrary radial function, $\vec{\alpha}$ is the vector of the Dirac matrices $(\alpha_x, \alpha_y, \alpha_z)$ and $\vec{Y}^M_{JL}(\theta, \varphi)$ is the vector spherical harmonic, defined as

$$\vec{Y}^M_{JL}(\theta, \varphi) = \sum_{\nu q} C(L\ 1\ J; \nu\ q\ M) Y_{L\nu}(\theta, \varphi) \vec{\epsilon}_q\ . \tag{C.2}$$

The index q takes the values $0, \pm 1$ and the spherical vectors $\vec{\epsilon}_q$ are given by

$$\begin{aligned} \vec{\epsilon}_+ &= -\frac{1}{\sqrt{2}}(\vec{e}_x + i\vec{e}_y)\ , \\ \vec{\epsilon}_0 &= \vec{e}_z\ , \\ \vec{\epsilon}_- &= \frac{1}{\sqrt{2}}(\vec{e}_x - i\vec{e}_y)\ . \end{aligned} \tag{C.3}$$

The $\vec{\alpha}$ matrix can be written with the help of the Pauli matrices $\vec{\sigma} = (\sigma_x, \sigma_y, \sigma_z)$

$$\vec{\alpha} = \begin{pmatrix} 0 & \vec{\sigma} \\ \vec{\sigma} & 0 \end{pmatrix}\ . \tag{C.4}$$

Using the expressions (2.39) and (2.40) for the continuum and bound electronic wave functions, respectively, we can write the matrix element as

$$\begin{aligned} \mathcal{M} &= \langle n_d \kappa_d m_d | f(r) \vec{\alpha} \cdot \vec{Y}^M_{JL}(\theta, \varphi) | \varepsilon \kappa m \rangle = i \int_0^\infty dr r^2 f(r) \\ &\times \Big(g_{n_d \kappa_d}(r) f_{\varepsilon\kappa}(r) \langle l_d \frac{1}{2} j_d m_d | \vec{\sigma} \cdot \vec{Y}^M_{JL}(\theta, \varphi) | l' \frac{1}{2} j m \rangle \\ &\quad - g_{\varepsilon\kappa}(r) f_{n_d \kappa_d}(r) \langle l'_d \frac{1}{2} j_d m_d | \vec{\sigma} \cdot \vec{Y}^M_{JL}(\theta, \varphi) | l \frac{1}{2} j m \rangle \Big)\ , \end{aligned} \tag{C.5}$$

where we have used the notation $|l\frac{1}{2}jm\rangle$ for the spherical spinor functions Ω^m_κ. Furthermore, l and l' are the orbital quantum numbers for the upper and lower two component spinors of the initial continuum wave function, while for the final bound state the notations l_d and l'_d are used. For a given value κ, the following relations hold:

$$j = |\kappa| - \frac{1}{2} \ ,$$

$$l = \begin{cases} \kappa & \text{if } \kappa > 0 \ , \\ |\kappa| - 1 & \text{if } \kappa < 0 \ , \end{cases}$$

$$l' = \begin{cases} \kappa - 1 & \text{if } \kappa > 0 \ , \\ |\kappa| & \text{if } \kappa < 0 \ . \end{cases} \tag{C.6}$$

The evaluation of the matrix element $\mathcal{M}$ in (C.1) is reduced to the calculation of the angular integral given by expressions of the type

$$\langle l_1 \frac{1}{2} j_1 m_1 | \vec{\sigma} \cdot \vec{Y}^M_{JL}(\theta, \varphi) | l_2 \frac{1}{2} j_2 m_2 \rangle \ . \tag{C.7}$$

The product $\vec{\sigma} \cdot \vec{Y}^M_{JL}(\theta, \varphi)$ can be written as

$$\vec{\sigma} \cdot \vec{Y}^M_{JL}(\theta, \varphi) = \sum_{\nu q} C(L \ 1 \ J; \nu \ q \ M) Y_{L\nu}(\theta, \varphi) \sigma_q = T_{JM}(Y_L, \vec{\sigma}) \ , \tag{C.8}$$

where we have introduced the spherical composite tensor $T_{JM}(Y_L, \vec{\sigma})$ [BS71], as the product of the irreducible tensors $Y_{L\nu}$ and $\sigma_q = \vec{\sigma} \cdot \vec{\epsilon}_q$. As $Y_{L\nu}$ and σ_q have the ranks L and 1, respectively, the rank of the composite tensor is given by $J = L, L \pm 1$. The reduced matrix element of the composite tensor can be expressed in terms of the matrix elements of the component systems. We use the Wigner-Eckart theorem [BS71]

$$\begin{aligned} &\langle l_1 \frac{1}{2} j_1 m_1 | \vec{\sigma} \cdot \vec{Y}^M_{JL}(\theta, \varphi) | l_2 \frac{1}{2} j_2 m_2 \rangle = \\ &C\left(j_2 \ J \ j_1; m_2 \ M \ m_1\right) \langle l_1 \frac{1}{2} j_1 \| \vec{\sigma} \cdot \vec{Y}^M_{JL}(\theta, \varphi) \| l_2 \frac{1}{2} j_2 \rangle \ . \end{aligned} \tag{C.9}$$

Here $\langle l_1 \frac{1}{2} j_1 \| \vec{\sigma} \cdot \vec{Y}^M_{JL}(\theta, \varphi) \| l_2 \frac{1}{2} j_2 \rangle$ stands for the reduced matrix element, as defined by [BS71]. This can be further written in terms of the reduced matrix elements of the orbital and spin component systems,

$$\begin{aligned} &\langle l_1 \frac{1}{2} j_1 \| T_{JM}(Y_L, \vec{\sigma}) \| l_2 \frac{1}{2} j_2 \rangle = [2(2j_2 + 1)(2J + 1)(2l_1 + 1)]^{\frac{1}{2}} \\ &\times \begin{Bmatrix} j_1 & j_2 & J \\ l_1 & l_2 & L \\ \frac{1}{2} & \frac{1}{2} & 1 \end{Bmatrix} \langle l_1 \| Y_L \| l_2 \rangle \langle \frac{1}{2} \| \vec{\sigma} \| \frac{1}{2} \rangle \ . \end{aligned} \tag{C.10}$$

We have used here the Wigner $9j$-symbol which is a generalization of the Clebsch-Gordan coefficients arising in the coupling of four angular momenta. Various formulas relating the $9j$-symbols with the Clebsch-Gordan coefficients, the Wigner $3j$-symbols and $6j$-symbols can be found in [BS71]. The spin reduced matrix element is simple to evaluate and gives $\langle \frac{1}{2} \| \vec{\sigma} \| \frac{1}{2} \rangle = \sqrt{3}$. The orbital

part can be calculated by taking into account the orthogonality properties of the spherical harmonics,

$$\langle l_1 \| Y_L \| l_2 \rangle = (-1)^{L-l_2} \left[\frac{(2l_2+1)(2L+1)}{4\pi} \right]^{\frac{1}{2}} \begin{pmatrix} L & l_2 & l_1 \\ 0 & 0 & 0 \end{pmatrix} . \tag{C.11}$$

The relation between the Wigner $3j$-symbol used above and the Clebsch-Gordan coefficients has been given in Eq. (2.46). The reduced matrix element of the spherical tensor in Eq. (C.10) then yields

$$\langle l_1 \frac{1}{2} j_1 \| T_{JM}(Y_L, \vec{\sigma}) \| l_2 \frac{1}{2} j_2 \rangle = (-1)^{L-l_2} \begin{pmatrix} L & l_2 & l_1 \\ 0 & 0 & 0 \end{pmatrix} \begin{Bmatrix} j_1 & j_2 & J \\ l_1 & l_2 & L \\ \frac{1}{2} & \frac{1}{2} & 1 \end{Bmatrix}$$
$$\times \left[\frac{6(2j_2+1)(2J+1)(2l_1+1)(2l_2+1)(2L+1)}{4\pi} \right]^{\frac{1}{2}} . \tag{C.12}$$

Depending on the value of $J = L, L \pm 1$, the expression above can be written in a more convenient form. We discuss in the following these three cases.

- $J = L$, corresponding to magnetic transitions
  We make use of the formula [BS71]

$$[6(2c+1)(2d+1)(2e+1)]^{\frac{1}{2}} \begin{pmatrix} c & d & e \\ 0 & 0 & 0 \end{pmatrix} \begin{Bmatrix} a & b & c \\ d & e & c \\ \frac{1}{2} & \frac{1}{2} & 1 \end{Bmatrix} =$$
$$\begin{pmatrix} a & b & c \\ \frac{1}{2} & \frac{1}{2} & -1 \end{pmatrix} , \tag{C.13}$$

  that simplifies substantially the expression in Eq. (C.12). In our case the formula above becomes

$$[6(2L+1)(2l_1+1)(2l_2+1)]^{\frac{1}{2}} \begin{pmatrix} L & l_1 & l_2 \\ 0 & 0 & 0 \end{pmatrix} \begin{Bmatrix} j_1 & j_2 & L \\ l_1 & l_2 & L \\ \frac{1}{2} & \frac{1}{2} & 1 \end{Bmatrix} =$$
$$\begin{pmatrix} j_1 & j_2 & L \\ \frac{1}{2} & \frac{1}{2} & -1 \end{pmatrix} . \tag{C.14}$$

  The reduced matrix element of the spherical tensor then reads

$$\langle l_1 \frac{1}{2} j_1 \| T_{LM}(Y_L, \vec{\sigma}) \| l_2 \frac{1}{2} j_2 \rangle =$$
$$(-1)^{l_1} \sqrt{\frac{(2j_2+1)(2L+1)}{4\pi}} \begin{pmatrix} j_1 & j_2 & L \\ \frac{1}{2} & \frac{1}{2} & -1 \end{pmatrix} . \tag{C.15}$$

  The Wigner $3j$-symbol can be brought to a different form by using the formula [BS71]

$$\begin{pmatrix} a & b & c \\ \frac{1}{2} & \frac{1}{2} & -1 \end{pmatrix} =$$
$$-\frac{1}{2} \begin{pmatrix} a & b & c \\ \frac{1}{2} & -\frac{1}{2} & 0 \end{pmatrix} \frac{2b+1+(-1)^{a+b+c}(2a+1)}{\sqrt{c(c+1)}} . \tag{C.16}$$

Taking also into account that $\kappa = (l-j)(2j+1)$, we can rewrite the expression of the reduced matrix element of the spherical tensor in Eq. (C.12),

$$\langle l_1 \frac{1}{2} j_1 \| T_{LM}(Y_L, \vec{\sigma}) \| l_2 \frac{1}{2} j_2 \rangle = (-1)^{j_2 - L + \frac{1}{2}} \times \sqrt{\frac{(2L+1)(2j_2+1)}{4\pi L(L+1)}} (\kappa_2 - \kappa_1) \begin{pmatrix} j_1 & j_2 & L \\ \frac{1}{2} & -\frac{1}{2} & 0 \end{pmatrix} . \quad \text{(C.17)}$$

- $J = L + 1$, corresponding to electric transitions

  The reduced matrix element of the spherical tensor $T_{L+1M}(Y_L, \vec{\sigma})$ is

$$\langle l_1 \frac{1}{2} j_1 \| T_{L+1M}(Y_L, \vec{\sigma}) \| l_2 \frac{1}{2} j_2 \rangle = (-1)^{L-l_2} \begin{pmatrix} L & l_2 & l_1 \\ 0 & 0 & 0 \end{pmatrix} \begin{Bmatrix} j_1 & j_2 & L+1 \\ l_1 & l_2 & L \\ \frac{1}{2} & \frac{1}{2} & 1 \end{Bmatrix} \times \left[\frac{6(2j_2+1)(2L+3)(2l_1+1)(2l_2+1)(2L+1)}{4\pi} \right]^{\frac{1}{2}} . \quad \text{(C.18)}$$

  We use the simplifying formula [BS71]

$$\begin{pmatrix} c-1 & d & e \\ 0 & 0 & 0 \end{pmatrix} \begin{Bmatrix} a & b & c \\ d & e & c-1 \\ \frac{1}{2} & \frac{1}{2} & 1 \end{Bmatrix} = \begin{pmatrix} a & b & c \\ \frac{1}{2} & -\frac{1}{2} & 0 \end{pmatrix} \times \frac{(-1)^{b+e+\frac{1}{2}}[(d-a)(2a+1) + (e-b)(2b+1) - c]}{[6c(2c+1)(2c-1)(2d+1)(2e+1)]^{\frac{1}{2}}} , \quad \text{(C.19)}$$

  which allows us to reach the following expression for the reduced matrix element

$$\langle l_1 \frac{1}{2} j_1 \| T_{L+1M}(Y_L, \vec{\sigma}) \| l_2 \frac{1}{2} j_2 \rangle = (-1)^{j_2 - (L+1) + \frac{1}{2}} \sqrt{\frac{(2j_2+1)}{4\pi(L+1)}} \times (L + 1 - \kappa_1 - \kappa_2) \begin{pmatrix} j_1 & j_2 & L+1 \\ \frac{1}{2} & -\frac{1}{2} & 0 \end{pmatrix} . \quad \text{(C.20)}$$

- $J = L - 1$, corresponding to electric transitions

  The reduced matrix element of the spherical tensor $T_{L-1M}(Y_L, \vec{\sigma})$ reads

$$\langle l_1 \frac{1}{2} j_1 \| T_{L-1M}(Y_L, \vec{\sigma}) \| l_2 \frac{1}{2} j_2 \rangle = (-1)^{L-l_2} \begin{pmatrix} L & l_2 & l_1 \\ 0 & 0 & 0 \end{pmatrix} \begin{Bmatrix} j_1 & j_2 & L-1 \\ l_1 & l_2 & L \\ \frac{1}{2} & \frac{1}{2} & 1 \end{Bmatrix} \times \left[\frac{6(2j_2+1)(2L-1)(2l_1+1)(2l_2+1)(2L+1)}{4\pi} \right]^{\frac{1}{2}} . \quad \text{(C.21)}$$

We use, like in the case of $J = L + 1$, a simplifying formula [BS71]

$$\left(\begin{array}{ccc} c+1 & d & e \\ 0 & 0 & 0 \end{array} \right) \left\{ \begin{array}{ccc} a & b & c \\ d & e & c+1 \\ \frac{1}{2} & \frac{1}{2} & 1 \end{array} \right\} = \left(\begin{array}{ccc} a & b & c \\ \frac{1}{2} & -\frac{1}{2} & 0 \end{array} \right) \quad \text{(C.22)}$$

$$\times \frac{(-1)^{b+e+\frac{1}{2}}[(d-a)(2a+1)+(e-b)(2b+1)+c+1]}{[6c(c+1)(2c+1)(2c+3)(2d+1)(2e+1)]^{\frac{1}{2}}} \ ,$$

and derive the reduced matrix element of $T_{L-1M}(Y_L, \vec{\sigma})$,

$$\langle l_1 \frac{1}{2} j_1 \| T_{L-1M}(Y_L, \vec{\sigma}) \| l_2 \frac{1}{2} j_2 \rangle = (-1)^{j_2 - L + \frac{1}{2}} \sqrt{\frac{(2j_2+1)}{4\pi L}}$$

$$\times (L + \kappa_1 + \kappa_2) \left(\begin{array}{ccc} j_1 & j_2 & L-1 \\ \frac{1}{2} & -\frac{1}{2} & 0 \end{array} \right) \ . \quad \text{(C.23)}$$

By using the special properties of the spherical tensors the angular parts of the matrix element in Eq. (C.5) can be derived in a simple manner obtaining rather short formulas. For the case of magnetic transitions ($J = L$), the expression of the matrix element $\mathcal{M}$ can be written as

$$\begin{aligned} \mathcal{M}^{(m)} &= \langle n_d \kappa_d m_d | f(r) \vec{\alpha} \cdot \vec{Y}^M_{LL}(\theta, \varphi) | \varepsilon \kappa m \rangle = i(-1)^{j-L+\frac{1}{2}} \sqrt{\frac{(2L+1)(2j+1)}{4\pi L(L+1)}} \\ &\times C\,(j\ L\ j_d; m\ M\ m_d)\,(\kappa_d + \kappa) \left(\begin{array}{ccc} j_d & j & L \\ \frac{1}{2} & -\frac{1}{2} & 0 \end{array} \right) \\ &\times \int_0^\infty dr r^2 f(r) \big(g_{n_d \kappa_d}(r) f_{\varepsilon\kappa}(r) + g_{\varepsilon\kappa}(r) f_{n_d\kappa_d}(r) \big) \ . \end{aligned} \quad \text{(C.24)}$$

With the choice $f(r) = r^{-(L+1)}$, we obtain the formula used in the calculation of the NEEC rates for magnetic transitions in Eq. (2.45). Using the Bessel functions $j_L(kr)$ instead, it yields up to a constant factor the expression of the RR matrix element in Eq. (4.33).

For the electric transitions a combination of the $J = L \pm 1$ matrix elements enters the expression of the RR matrix element,

$$\begin{aligned} \mathcal{M}^{(e)} &= \sqrt{\frac{L}{2L+1}} \langle n_d \kappa_d m_d | j_{L+1}(kr) \vec{\alpha} \cdot \vec{Y}^M_{LL+1}(\theta, \varphi) | \varepsilon \kappa m \rangle \\ &\quad - \sqrt{\frac{L+1}{2L+1}} \langle n_d \kappa_d m_d | j_{L-1}(kr) \vec{\alpha} \cdot \vec{Y}^M_{LL-1}(\theta, \varphi) | \varepsilon \kappa m \rangle \ . \end{aligned} \quad \text{(C.25)}$$

Using the formulas of the reduced matrix elements of the spherical tensor $T_{L\pm1M}(Y_L, \vec{\sigma})$ in Eqs. (C.20) and (C.23) we obtain for the electric transitions

$$\begin{aligned} \mathcal{M}^{(e)} &= i(-1)^{j-L-\frac{1}{2}} C(j\ L\ j_d; m\ M\ m_d) \sqrt{\frac{2j+1}{4\pi}} \left(\begin{array}{ccc} j_d & j & L \\ \frac{1}{2} & -\frac{1}{2} & 0 \end{array} \right) \\ &\times \left[\sqrt{\frac{L+1}{L(2L+1)}} \big(L I^-_{L-1} - (\kappa_d - \kappa) I^+_{L-1} \big) \right. \\ &\quad \left. + \sqrt{\frac{L}{(L+1)(2l+1)}} \big((L+1) I^-_{L+1} + (\kappa_d - \kappa) I^+_{L+1} \big) \right] , \end{aligned} \quad \text{(C.26)}$$

with the radial integrals

$$I_L^{\pm} = \int_0^{\infty} dr r^2 j_L(kr)\big(g_{\kappa_d}(r) f_{\varepsilon\kappa}(r) \pm g_{\varepsilon\kappa}(r) f_{\kappa_d}(r)\big) \ . \tag{C.27}$$

These expressions have been used in the calculation of the RR matrix element corresponding to electric transitions in Section 4.2.

Bibliography

[AAC+95] F. Attallah, M. Aiche, J.F. Chemin, J.N. Scheurer, W.E. Meyerhof, J.P. Grandin, P. Aguer, G. Bogaert, J. Kiener, A. Lefebvre, J.P. Thibaud, and C. Grunberg, *Charge state blocking of K-shell internal conversion in ^{125}Te*, Phys. Rev. Lett. **75** (1995), 1715.

[ABH+56] K. Alder, A. Bohr, T. Huus, B. Mottelson, and A. Winther, *Study of nuclear structure by electromagnetic excitation with accelerated ions*, Rev. Mod. Phys. **28** (1956), 432.

[BBH+02] C. Brandau, T. Bartsch, A. Hoffknecht, H. Knopp, S. Schippers, W. Shi, A. Müller, N. Grün, W. Scheid, T. Steih, F. Bosch, B. Franzke, C. Kozhuharov, P.H. Mokler, F. Nolden, M. Steck, and T. Stöhlker, *High Rydberg resonances in dielectronic recombination of* Pb^{79+}, Phys. Rev. Lett. **89** (2002), 053201.

[BEG85] R. G. Barrera, G. A. Estevez, and J. Giraldo, *Vector spherical harmonics and their application to magnetostatics*, Eur. J. Phys. **6** (1985), 287.

[BEK06] T.J. Bürvenich, J. Evers, and C.H. Keitel, *Nuclear quantum optics with X-ray laser pulses*, Phys. Rev. Lett. **96** (2006), 142501.

[BGM88] J.F. Berger, D. Gogny, and Weiss M.S, *Nuclear excitation via the motion of electrons in a strong laser field*, J. Quant. Spectrosc. Radiat. Transfer **40** (1988), 717.

[BGR56] G. Breit, R.L. Gluckstern, and J.E. Russell, *Reorientation effect in Coulomb excitation*, Phys. Rev. **103** (1956), 727.

[Bha92] M. R. Bhat, *Nuclear data sheets update for A=57*, Nucl. Dat. Sheets **67** (1992), 195.

[BJO+00] E. Behar, V.L. Jacobs, J. Oreg, A. Bar-Shalom, and S.L. Hahn, *Measure for the effect of quantum interference between radiative and dielectronic recombination*, Phys. Rev. A **62** (2000), 030501(R).

[BK58] P. Brix and H. Kopfermann, *Isotope shift studies of nuclei*, Rev. Mod. Phys. **30** (1958), 517.

[BKM+03] C. Brandau, C. Kozhuharov, A. Müller, W. Shi, S. Schippers, T. Bartsch, S. Böhm, C. Böhme, A. Hoffknecht, H. Knopp, N. Grün, W. Scheid, T. Steih, F. Bosch, B. Franzke, P.H. Mokler, F. Nolden, M. Steck, T. Stöhlker, and Z. Stachura, *Precise determination of the* $2s_{1/2} - 2p_{1/2}$ *splitting in very heavy lithium-like ions utilizing dielectronic recombination*, Phys. Rev. Lett. **91** (2003), 073202.

[BKM+06] C. Brandau, C. Kozhuharov, A. Müller, K. Beckert, P. Beller, D. Bernhardt, F. Bosch, S. Böhm, F.J. Currell, J. Jacobi, H.-J. Kluge, P.H. Mokler, F. Nolden, R. Reuschl, S. Schippers, E.W. Schmidt, U. Spillmann, Z. Stachura, M. Steck, Th. Stöhlker, and A. Wolf, *Isotopic shift measurements of Li-like* $^{142}Nd^{57+}$ *–*$^{150}Nd^{57+}$ *by means of dielectronic recombination*, GSI Jahresbericht 2005 (2006).

[Bla53] J.M. Blatt, *The Beta-Decay Interaction*, Phys. Rev. **89** (1953), 83.

[Blu81] K. Blum, *Density matrix theory and applications*, Plenum, New York, 1981.

[Bre30] G. Breit, *Possible effects of nuclear spin on X-ray terms*, Phys. Rev. **35** (1930), 1447.

[Bre32] ———, *The isotope displacement in hyperfine structure*, Phys. Rev. **42** (1932), 348.

[Bro95] E. Browne, *Nuclear data sheets update for A=185*, Nucl. Dat. Sheets **74** (1995), 165.

[Bro05] I.N. Bronstein, *Taschenbuch der Mathematik*, Frankfurt am Main, 2005.

[BS71] D.M. Brink and G.R. Satchler, *Angular Momentum*, Clarendon Press, Oxford, 1971.

[BS03] H.F. Beyer and V.P. Shevelko, *Introduction to the Physics of Highly Charged Ions*, Institute of Physics Publishing, Bristol, 2003.

[BT93] I.M. Band and M.B. Trzhaskovskaya, *Internal conversion coefficients*, At. Dat. Nucl. Dat. Tabl. **55** (1993), 43.

[BTN+02] I.M. Band, M.B. Trzhaskovskaya, C.W. Nestor, P.O. Tikkanen, and S. Raman, *Dirac-Fock internal conversion coefficients*, At. Dat. Nucl. Dat. Tabl. **81** (2002), 1.

[Bur89] T. Burrows, *Nuclear data sheets for A=163*, Nucl. Dat. Sheets **56** (1989), 313.

[CHA+00] T. Carreyre, M. R. Harston, M. Aiche, F. Bourgine, J. F. Chemin, G. Claverie, J. P. Goudour, J. N. Scheurer, F. Attallah, G. Bogaert, J. Kiener, A. Lefebvre, J. Durell, J. P. Grandin, W. E.

Meyerhof, and W. Phillips, *First direct proof of internal conversion between bound states*, Phys. Rev. C **62** (2000), 024311.

[CPR89] N. Cue, J.-C. Poizat, and J. Remillieux, *Exciting the nucleus by target electron capture into atomic orbitals*, Europhys. Lett. **8** (1989), 19.

[CS95] M.H. Chen and J.H. Scofield, *Relativistic effects on angular distribution and polarization of dielectronic satellite lines of hydrogenlike ions*, Phys. Rev. A **52** (1995), 2057.

[CS04] J. A. Cameron and Balraj Singh, *Nuclear data sheets for A=40*, Nucl. Dat. Sheets **102** (2004), 293.

[Cue89] N. Cue, *Nuclear excitation by target electron capture*, Nucl. Instr. Meth. B **40/41** (1989), 25.

[Cur03] F.J. Currell, *Physics of Multiply and Highly Charged Ions*, Kluwer Academic Pub, 2003.

[Dau06] D. Dauvergne, Habilitation dissertation, Université Lyon 1, 2006.

[DGJ+89] K.G. Dyall, I.P. Grant, C.T. Johnson, F.A. Parpia, and E.P. Plummer, GRASP*: A General-purpose Relativistic Atomic Structure Program*, Comp. Phys. Comm. **55** (1989), 425.

[Edm96] A. R. Edmonds, *Angular Momentum in Quantum Mechanics*, Princeton University Press, 1996.

[EM95] J. Eichler and W.E. Meyerhof, *Relativistic Atomic Collisions*, Academic Press San Diego, 1995.

[Fan57] U. Fano, *Description of states in quantum mechanics by density matrix and operator techniques*, Rev. Mod. Phys. **29** (1957), 74.

[Fan61] ———, *Effects on configuration interaction on intensities and phase shifts*, Phys. Rev. **124** (1961), 1866.

[Fir91] R.B. Firestone, *Nuclear data sheets for A=187*, Nucl. Dat. Sheets **62** (1991), 159.

[FSS05] S. Fritzsche, A. Surzhykov, and T. Stöhlker, *Radiative recombination into high-Z few-electron ions: Cross sections and angular distributions*, Phys. Rev. A **72** (2005), 012704.

[GB29] S. Goudsmit and R.F. Bacher, *Separations in hyperfine structure*, Phys. Rev. **34** (1929), 1501.

[GGS98] M. Gail, N. Grün, and W. Scheid, *Angular distribution of radiation emitted after resonant transfer and excitation*, J. Phys. B: At. Mol. Opt. Phys. **31** (1998), 4645.

[GM96] W. Greiner and J.A. Maruhn, *Nuclear Models*, Springer Verlag Berlin Heidelberg, 1996.

[GN76] V.I. Goldanskii and V. A. Namiot, *On the excitation of isomeric nuclear levels by laser radiation through inverse internal electron conversion*, Phys. Lett. **62B** (1976), 393.

[GR58] T.A. Green and M.E. Rose, *Nuclear structure effects in internal conversion*, Phys. Rev. **110** (1958), 105.

[Hah85] Y. Hahn, *Theory of dielectronic recombination*, Adv. At. Mol. Phys. **21** (1985), 123.

[Har04] Z. Harman, *Theorie der Elektron-Elektron-Wechselwirkung in der Dielektronischen Rekombination*, Dissertation, Gießen, 2004.

[HC99] M.R. Harston and J.F. Chemin, *Mechanisms of nuclear excitation in plasmas*, Phys. Rev. C **59** (1999), 2462.

[Hel88] R. G. Helmer, *Nuclear data sheets for A=157*, Nucl. Dat. Sheets **55** (1988), 71.

[HJ89] S.L.. Haan and V.L. Jacobs, *Projection-operator approach to the unified treatment of radiative and dielectronic recombination*, Phys. Rev. A **40** (1989), 80.

[Huo91] J. Huo, *Nuclear data sheets update for A=55*, Nucl. Dat. Sheets **64** (1991), 723.

[IE00] A. Ichihara and J. Eichler, *Cross sections for radiative recombination and the photoelectric effect in the K, L and M shells of one-electron systems with 1≤ Z≤112 calculated within an exact relativistic description*, At. Data Nucl. Data Tabl. **74** (2000), 1.

[JS85] W.R. Johnson and G. Soff, *The Lamb shift in hydrogenlike atoms,* $1 \leq Z \leq 110$, At. Dat. Nucl. Dat. Tabl. **33** (1985), 405.

[KBC91] J.C. Kimball, D. Bittle, and N. Cue, *A comment on 'nuclear excitation by target electron capture'*, Phys. Lett. A **152** (1991), 367.

[KBE+94] I. Klaft, S. Borneis, T. Engel, B. Fricke, R. Grieser, G. Huber, T. Kühl, D. Marx, R. Neumann, S. Schröder, P. Seelig, and L. Völker, *Precision laser spectroscopy of the ground state hyperfine splitting of hydrogenlike* $^{209}Bi^{82+}$, Phys. Rev. Lett. **73** (1994), 2425.

[KKR99] O. Kocharovskaya, R. Kolesov, and Y. Rostovtsev, *Coherent optical control of Mössbauer spectra*, Phys. Rev. Lett. **82** (1999), 3593.

[Kol98] K. Kollmar, *Resonante Elektronenstreuung an sehr schweren hochgeladenen Ionen*, Dissertation, Gießen, 1998.

[KYS+00] S. Kishimoto, Y. Yoda, M. Seto, Y. Kobayashi, S. Kitao, R. Haruki, T. Kawauchi, K. Fukutani, and T. Okano, *Observation of nuclear excitation by electron transition in* ^{197}Au *with synchrotron X-rays and an avalanche photodiode*, Phys. Rev. Lett. **85** (2000), 1831.

[LAB+06] A. L'Hoir, L. Adoui, F. Barrué, A. Billebaud, F. Bosch, A. Bräuning-Demian, H. Bräuning, A. Cassimi, M. Chevallier, C. Cohen, D. Dauvergne, C.E. Demonchy, L. Giot, R. Kirsch, A. Gumberidze, C. Kozhuharov, D. Liesen, W. Mittig, P. Mokler, S. Pita, J.-C. Poizat, C. Ray, P. Roussel-Chomaz, H. Rothard, J.-P. Rozet, Th. Stöhlker, M. Tarisien, E. Testa, S. Toleikis, M. Toulemonde, and D. Vernhet, *Ion slowing down and charge exchange at small impact parameters selected by channeling: Superdensity effects*, Nucl. Instr. Meth. B **245** (2006), 1.

[LJLU+05] A. Lapierre, U.D. Jentschura, J.R. Crespo López-Urrutia, J. Braun, G. Brenner, H. Bruhns, D. Fischer, A.J. González Martínez, Z. Harman, W.R. Johnson, C.H. Keitel, V. Mironov, C.J. Osborne, G. Sikler, R. Soria Orts, V. Shabaev, H. Tawara, I.I. Tupitsyn, J. Ullrich, and A. Volotka, *Relativistic Electron Correlation, Quantum Electrodynamics, and the Lifetime of the* $1s^2 2s^2 2p^2 P^0_{3/2}$ *Level in Boronlike Argon*, Phys. Rev. Lett. **95** (2005), 183001.

[LUBB+05] J.R. Crespo López-Urrutia, A. Artemyev J. Braun, G. Benner, H. Bruhns, I.N. Draganic, A.J. González Martínez, A. Lapierre, V. Mironov, J.H. Scofield, R. Soria Orts, H. Tawara, M. Trinczek, I.I. Tupitsyn, and J. Ullrich, *High precision measurements of forbidden transitions in highly charged ions at the Heidelberg EBIT*, Nucl. Instr. Meth. B **235** (2005), 85.

[MB42] H.S.W. Massey and D.R. Bates, *The negative ions of atomic and molecular oxygen*, Rep. Prog. Phys. **9** (1942), 62.

[MLUB+05] A.J. González Martínez, J.R. Crespo López-Urrutia, J. Braun, G. Benner, H. Bruhns, A. Lapierre, V. Mironov, R. Soria Orts, H. Tawara, M. Trinczek, J. Ullrich, and J.H. Scofield, *State-selective quantum interference observed in the recombination of highly charged* $Hg^{75+...78+}$ *Mercury ions in an Electron Beam Ion Trap*, Phys. Rev. Lett **94** (2005), 203201.

[Mok89] *Proposal S003: Exciting the Nucleus by Electron Capture in Axial Channeling*, GSI, Darmstadt, 1989.

[Mor73] M. Morita, *Nuclear excitation by electron transition and its application to Uranium 235 separation*, Prog. Theor. Phys **49** (1973), 1574.

[MS01] A. Müller and S. Schippers, *Dielectronic Recombination: Experiment*, ASP Conf. Series **247** (2001), 53.

[PDA+97] H.-Th. Prinz, D. Dauvergne, S. Andriamonje, K. Beckert, M. Chevallier, C. Cohen, J. Dural, H. Eickhoff, B. Franzke, H. Geissel, R. Kirsch, A. L'Hoir, P.H. Mokler, R. Moshammer, F. Nickel, F. Nolden, J.C. Poizat, H. Reich, J. Remillieux, F. Sanuy, C. Scheidenberger, D. Schmaus, M. Steck, Th. Stöhlker, and M. Toulemonde, *Probing a cooled beam of decelerated highly-charged heavy ions extracted out of the ESR by a channeling experiment*, Hyp. Inter. **108** (1997), 325.

[Pek92] L. K. Peker, *Nuclear data sheets update for A=165*, Nucl. Dat. Sheets **65** (1992), 439.

[PFFG96] F. A. Parpia, C. Froese-Fischer, and I. P. Grant, GRASP92*: A package for large-scale relativistic atomic structure calculations*, Comp. Phys. Comm. **94** (1996), 249.

[PHS06] A. Pálffy, Z. Harman, and W. Scheid, *Theory of nuclear excitation by electron capture for heavy ions*, Phys. Rev. A **73** (2006), 012715.

[PMGS89] G. Plunien, B. Müller, W. Greiner, and G. Soff, *Nuclear polarization contribution to the Lamb shift in heavy ions*, Phys. Rev. A **39** (1989), 5428.

[PMGS91] G. Plunien, B. Müller, W. Greiner, and G. Soff, *Nuclear polarization in heavy ions and superheavy quasiatoms*, Phys. Rev. A **43** (1991), 5853.

[RD00] M. Ryšavý and O. Dragoun, *On the reliability of the theoretical internal conversion coefficients*, J. Phys. G:Nucl. Part. Phys. **26** (2000), 1859.

[Rei94] C. W. Reich, *Nuclear data sheets for A=155*, Nucl. Dat. Sheets **71** (1994), 709.

[RFAP78] F. Rösel, H.M. Fries, K. Alder, and H.C. Pauli, *Internal conversion coefficients for all atomic shells*, At. Dat. Nucl. Dat. Tabl. **21** (1978), 91.

[RNT01] S. Raman, C. Nestor, and P. Tikkanen, *Transition probability from the ground state to the first-excited* 2^+ *state of even-even nuclides*, At. Dat. Nucl. Dat. Tabl. **78** (2001), 1.

[RS80] P. Ring and P. Schuck, *The Nuclear Many-Body Problem*, Springer Verlag New York, 1980.

[Sch55] C. Schwartz, *Theory of hyperfine structure*, Phys. Rev. **97** (1955), 380.

[Sch02] S. Schippers, *Experimente zur Photorekombination atomarer Ionen an Schwerionenspeicherringen*, Habilitation dissertation, Gießen, 2002.

[Sha94] V.M. Shabaev, *Quantum electrodynamic theory of recombination of an electron with a highly charged ion*, Phys. Rev. A **50** (1994), 4521.

[SHH+02] T. Schenkel, A.V. Hamza, J.P. Holder, K. Krämer, J.W. McDonald, A. Persaud, and D.H. Schneider, *Extraction of highly charged ions from the electron beam ion trap at LBNL for applications in surface analysis and materials science*, Rev. Sci. Instr. **73** (2002), 663.

[Shi88] V. S. Shirley, *Nuclear data sheets for A=173*, Nucl. Dat. Sheets **54** (1988), 589.

[SHSG04] R. Schiopu, Z. Harman, W. Scheid, and N. Grün, *Isotope shifts of dielectronic resonances for heavy few-electron ions*, Eur. Phys. J. D **31** (2004), 21.

[SJSF06] A. Surzhykov, U.D. Jentschura, T. Stöhlker, and S. Fritzsche, *Radiative electron capture into high-Z few-electron atoms: Alignment of the excited ionic state*, Phys. Rev. A **73** (2006), 032716.

[SML+92] W. Spies, A. Müller, J. Linkemann, A. Frank, M. Wagner, C. Kozhuharov, B. Franzke, K. Beckert, F. Bosch, H. Eickhoff, M. Jung, O. Klepper, W. König, P.H. Mokler, R. Moshammer, F. Nolden, U. Schaaf, P. Spädtke, M. Steck, P. Zimmerer, N. Grün, W. Scheid, M.S. Pindzola, and N.R. Badnell, *Dielectronic and radiative recombination of lithiumlike gold*, Phys. Rev. Lett. **69** (1992), 2768.

[SYBE00] V. M. Shabaev, V. A. Yerokhin, T. Beier, and J. Eichler, *QED corrections to the radiative recombination of an electron with a bare nucleus*, Phys. Rev. A **61** (2000), 052112.

[TN03] M.B. Trzhaskovskaya and V.K. Nikulin, *Radiative recombination of an electron with multiply charged Uranium ions*, Opt. Spectrosc. **95** (2003), 580.

[VMK88] D.A. Varshalovich, A.N. Moskalev, and V.K. Khersonskii, *Quantum Theory of Angular Momentum*, World Scientific Singapore, 1988.

[WG03] A. Wolf and G. Gwinner, *Recombination measurements at ion storage rings*, Hyp. Inter. **146-147** (2003), 5.

[WGL+00] A. Wolf, G. Gwinner, J. Linkemann, A.A. Saghiri, M. Schmitt, D. Schwalm, M. Grieser, M. Beutelspacher, T. Bartsch, C. Brandau, A. Hoffknecht, A. Müller, S. Schippers, O. Uwira, and

D. Savin, *Recombination in electron coolers*, Nucl. Instrum. Meth. Phys. Res. A **441** (2000), 183.

[YHHI01] N. Yamanaka, A. Haga, Y. Horikawa, and A. Ichimura, *Nuclear polarization in hydrogenlike heavy ions*, Phys. Rev. A **63** (2001), 062502.

[YK93] Zhu-Shu Yuan and J.C. Kimball, *First-priciples calculation of the cross sections for nuclear excitation by electron capture of channeled nuclei*, Phys. Rev. C **47** (1993), 323.

[YSBE00] V. A. Yerokhin, V. M. Shabaev, T. Beier, and J. Eichler, *Interelectronic-interaction effect on the radiative recombination of an electron with a heavy He-like ion*, Phys. Rev. A **62** (2000), 042712.

[Zak01] S. Zakowicz, *Dielektronische Rekombination bei hochgeladenen schweren Ionen unter Emission von zwei Photonen*, Diplomarbeit, Gießen, 2001.

[ZC02] A.A. Zadernovsky and J.J. Carroll, *Non-radiative triggering of long-lived nuclear isomers*, Hyp. Inter. **143** (2002), 153.

[ZGS90] P. Zimmerer, N. Grün, and W. Scheid, *Auger rates for dielectronic recombination cross sections with highly charged relativistic heavy ions*, Phys. Lett. A **148** (1990), 457.

[ZGS97] M. Zimmermann, N. Grün, and W. Scheid, *Photo recombination on highly charged few-electron Uranium ions*, J. Phys. B **30** (1997), 5259.

[Zim92] P. Zimmerer, *Relativistische Theorie für die Dielektronische Rekombination bei sehr schweren hochgeladenen Ionen*, Dissertation, Gießen, 1992.

[ZLUU03] Y. Zou, J.R. Crespo López-Urrutia, and J. Ullrich, *Observation of dielectronic recombination through two-electron-one-photon correlative stabilization in an electron-beam ion trap*, Phys. Rev. A **67** (2003), 42703.

[ZSG04] S. Zakowicz, W. Scheid, and N. Grün, *Dielectronic recombination into hydrogen-like heavy ions with emission of two photons*, J. Phys. B **37** (2004), 131.

List of Tables

List of Figures

Acknowledgments

It is my pleasure to mention here all the people that have contributed in one way or another to this work.

I would like to thank my doctoral supervisor, Prof. Werner Scheid, for the great opportunity to join the Institute for Theoretical Physics in Gießen. He assigned me a very interesting topic and supported me in every aspect of my work, physics matters as well as technical or administrative details. Without his careful guidance my doctoral study couldn't have been completed in such a short time. I would also like to acknowledge the financial support that I benefited from, which allowed me to present the results of my work at many international conferences. On a personal level, I thank Prof. Scheid for always giving me the best advice and for supporting my professional future.

Special thanks go to my friend and collaborator Dr. Zoltán Harman. He was the one who passed over to me the atomic physics heritage of our group, FORTRAN codes and the skills in handling the GRASP packages. I want to thank him for our fruitful discussions and continuous work together. His physics knowledge as well as his friendly and familiar manner have been a very important support in my work.

I would like to acknowledge the valuable help of Prof. Rostislav Jolos from the Joint Institute for Nuclear Research in Dubna, which has been often a guest of our institute during my time in Gießen. The discussions with him on nuclear models helped me in many stages of my work. I am grateful to Prof. Jolos for proof-reading the nuclear physics chapter of this work.

I acknowledge stimulating discussions with Dr. Andrey Surzhykov regarding the density matrix formalism and our collaboration on the topic of angular distribution of the radiation emitted in NEEC.

Writing the section about experimental observation of NEEC wouldn't have been possible without the valuable contribution of several specialists. I would like to thank PD Stefan Schippers for fruitful discussions regarding NEEC experimental aspects and for taking the time to answer to my questions on many occasions. His friendly attitude and his advice were most helpful. Special thanks go to Prof. Paul Mokler who was so kind to guide me on a tour of the accelerator facility at the GSI and to explain step by step the physics involved. I also owe him my knowledge about past attempts to measure NEEC at the GSI. Prof. Hiro Tawara agreed at very short notice to read the 'experimental' section of my thesis and his valuable suggestions were most welcome. I thank him for his continuous interest in my work and for not giving up the idea of measuring NEEC at the Heidelberg EBIT. I would also like to thank Dr. Denis

Dauvergne for offering me precious unpublished information about the NEEC experiment that took place at GANIL.

The writing of this thesis was a demanding project and would have been impossible in such a short time without the help of many colleagues and friends involved in proof-reading and improving the style of the text. I would like to thank my fellow colleagues Jan Scholz, Oliver Melchert and Michael Genkin for their willingness to invest time in hunting typos. Zoltán Harman and Zoltán Gagyi-Pálffy proof-read in several occasions at very short notice parts of this work. Oliver Buß was the one to help me with writing the German summary in authentic German. My special thanks go to Francisc Aaron and to my mother Magda Bălănescu for their valuable comments on the text. To our computer specialists Manuel Hölß, Jan Scholz and Zoltán Gagyi-Pálffy I owe many thanks for solving every computer problem that crossed my way.

The friendly and relaxed atmosphere at the Institute for Theoretical Physics has been beneficial to me personally and influenced the quality of my work. I would like to thank Prof. Scheid, our secretary Susanne Gretschel and all my colleagues for contributing through their kind and friendly way of being to the pleasant working ambient.

Last but not least, I would like to thank my mother for introducing me at an early age to the fascinating world of physics and for continuously inspiring me towards a scientific career.